POLITECNICO

MILANO 1863

SCUOLA DI INGEGNERIA INDUSTRIALE
E DELL'INFORMAZIONE

Model to investigate the interference induced by NGSO constellations on GSO system ground stations

TESI DI LAUREA MAGISTRALE IN
TELECOMMUNICATION ENGINEERING - INGEGNERIA DELLE
TELECOMUNICAZIONI

Author: **Enrico Polo**

Student ID: 945866
Advisor: Prof. Lorenzo Luini
Co-advisors: Luis Emiliani
Academic Year: 2021-22

Abstract

In this thesis, a model to investigate how a NGSO constellation impacts on the communication between a ground station and a GSO satellite is presented. Initially, a simulator is built with the purpose of thoroughly analysing the yearly evolution of the fixed-satellite service for a specific site, given the orbital data of the NGSO constellation interfering with the GSO communications. The rain attenuation, the major atmospheric impairment for the high frequency bands considered such as *Ka*, *Q* and *V*, is also accounted for by examining 200 km × 200 km rain maps produced by the rain field generator *ST-MultiEXCELL* for events lasting one full year. The simulated data are thus stored and investigated, allowing to define the long-term statistics of the system parameters. The statistical distributions for each parameter are then exploited in order to build a statistical model capable of generating new samples of the parameters of interest. Additionally, the relationships among the parameters, such as the rain attenuation concurrently affecting the links towards the GSO and NGSO satellites and the avoidance angle, defined to reduce the interference induced by the NGSO satellites on the GSO ones, are also presented and discussed. Finally, the model shows how the system design can be greatly facilitated once the simulated data are collected and stored, allowing to easily evaluate how the system performance changes by tuning some of the system parameters, for example the avoidance angle threshold α and the number of NGSO satellites interfering with the GSO communication.

Keywords: NGSO constellation, GSO, interference, avoidance angle, rain attenuation, *ST-MultiEXCELL*

Abstract in lingua italiana

In questa tesi viene affrontato il problema relativo all'interferenza causata da costellazioni NGSO su comunicazioni attive tra una stazione di terra ed un satellite GSO. Viene dunque presentato un modello per analizzare suddetto scenario e comprendere quanto significativo possa essere l'impatto dell'interferenza causata dai satelliti NGSO sul sistema di comunicazione GSO. Inizialmente, viene descritta l'implementazione di un simulatore realizzato con lo scopo di analizzare l'evoluzione del sistema satellitare per un sito specifico, considerando i dati orbitali della costellazione NGSO interferente con le comunicazioni relative al satellite GSO. A causa delle alte frequenze a cui lavorano questi sistemi, principalmente nelle bande Ka, V e Q, è necessario anche tener conto dell'attenuazione dovuta alla pioggia, principale responsabile di attenuazione atmosferica per frequenze oltre i 10 GHz. L'attenuazione da pioggia viene calcolata esaminando le mappe di pioggia generate dal software *ST-MultiEXCELL*, le quali descrivono l'andamento del *rain rate* per un'area geografica di dimensioni 200 km × 200 km. Quindi, i dati ottenuti tramite simulazioni vengono conservati, in questo modo è possibile, analizzando l'evoluzione del sistema per un periodo sufficientemente lungo, esaminare le statistiche dei parametri caratterizzanti del sistema. Inoltre, è possibile utilizzare le distribuzioni statistiche dei vari parametri per implementare un modello statistico capace di generare nuovi valori per i suddetti parametri senza il bisogno di ricorrere nuovamente a lunghe e complesse simulazioni. L'analisi statistica dei dati ottenuti, rende anche possibile evidenziare eventuali correlazioni tra i parametri d'interesse. Infine, il modello presentato dimostra come la fase di progettazione del sistema possa essere significativamente facilitata sfruttando le informazioni ottenute durante la fase di simulazione. È infatti possibile osservare come varino le prestazioni del sistema modificando alcuni dei parametri, come ad esempio il numero di satelliti della costellazione interferenti o l'angolo minimo che deve essere rispettato tra la direzione di puntamento dell'antenna di un satellite NGSO e la congiungente tra la stazione di terra e il satellite GSO con cui sta comunicando.

Parole chiave: costellazione NGSO, GSO, interferenza, angolo di separazione, attenuazione da pioggia, *ST-MultiEXCELL*

Contents

1 | Introduction

Satellite based communications nowadays represent the main alternative to terrestrial transmissions. These systems are particularly appealing for sites difficult to reach through terrestrial infrastructure, either because of the harsh environment or for the implementation costs being too expensive. Satellite systems became a reality during the second half of the 20th century, when substantial progresses in the field of rocketry were achieved. The very first launch of a satellite into orbit happened in the 1957 with the SPUTNIK I, which established the beginning of the Space Age. While the SPUTNIK was deployed by the Soviet Union for research purposes, this achievement encouraged many attempts to make use of artificial satellites for a wider spectrum of objectives, including communications.

Throughout the 1960s the first commercial communication satellites were deployed in the geostationary orbit, one of the three main orbital altitudes. GEO satellites operate at an altitude of 35,760 km above ground, they share the characteristic of appearing at a fixed spot in the sky by an observer on Earth. Indeed, at that particular altitude, the satellites revolve around the planet with an angular velocity equal to the one of the Earth. Therefore, the implementation of GEO satellites allows ground stations to constantly point at the same direction in the sky, without the need to fix the orientation of their antennas to optimally receive the signal. The other two main orbital altitudes chosen for satellite systems are the *Medium Earth Orbit* (MEO), going from 10,000 to 20,000 km and the *Low Earth Orbit* (LEO) at much lower altitude, between 160 and 2,500 km above Earth. MEO and LEO, together with *Highly Elliptical Orbit* (HEO), are also known as *Non-Geostationary Orbit* (NGSO) systems, in fact they are not continuously visible by ground observers because their angular velocity does not match that of the Earth. For these systems, in order to guarantee continuity of transmission, a network of satellites is required, so that they are able to share information and allow communications from Earth with at least one visible satellite at all times.

Lower altitude orbits are particularly fascinating when considering services requiring low latency, such as voice, video and certain data communications. For this reason, in the last decade important private companies such as SpaceX picked an interest on constellations

of satellites working at LEO and VLEO (*Very Low Earth Orbit*). In 2015, Elon Musk announced that SpaceX would start to implement their own constellation of satellites, with the purpose of providing global internet access [1]. The long-term stated goal was to "rebuild the internet in space" with "a majority of long-distance internet traffic going over this network". This project aimed to bring internet coverage even to the poorest areas, in which service is not normally guaranteed, as well as to increase the quality of communications in high-density areas. These objectives can indeed be achieved thanks to the properties of low-altitude orbital constellations, which, with respect to an equivalent GSO transmission, can provide a much shorter round-trip time and a lower free space loss since the signal travels for a shorter path. These features are very promising to obtain low-latency and low-energy-requiring transmissions.

Since SpaceX's constellation announcement, whose name was lately trademarked as "Starlink", the company has planned to achieve two sub-constellations, one implemented at LEO, comprising 4,425 satellites operating in the *Ka* and *Ku* band, and another one at VLEO with 7,518 satellites operating in the *V* band. These high values of frequencies, though, cause the signal to be heavily affected by hydrometeors, such as clouds and rain, which all become significantly impactful for values of frequency above 10 GHz. The atmospheric attenuation, hence, needs to be thoroughly investigated when designing a satellite based system.

Furthermore, as stated, NGSO constellations will play a prominent role in the near future and satellites implemented in these orbits will considerably grow in numbers. Therefore, it is vital to guarantee that their transmissions do not interfere with signals coming from GSO satellites. To protect GSO communications, one of the main adopted methods is to silence the NGSO satellites closest to the line of sight between the operating GSO satellite and the ground station. In order to do so, a specific angle is defined, denominated as the *avoidance angle*, evaluated from the LOS between the GSO and the Earth station. All NGSO satellites contained in the cone with vertex coinciding with the Earth station and aperture equal to the avoidance angle are thus forbidden from transmitting when the GSO is operating. However, all those satellites falling outside of the cone will maintain their communications active, potentially causing interference to the Earth station receiving data from a GSO satellite.

The first aim of this thesis is to build a simulator able to calculate the attenuation caused by rain on the path that connects a generic ground site to a satellite, given their latitudes, longitudes and altitudes. *Chapter 2* addresses the role played by rain on the performance of the satellite system, followed by a description of the rain field generator *ST-MultiEXCELL*, which made possible the generation of yearly rain events to implement, analyse and study

the impact of rain attenuation on a given site. Finally, the method implemented to build the rain attenuation simulator is described.

Chapter 3 extends the newly implemented simulator to evaluate the rain attenuation for a constellation of NGSO satellites. In this way, it is possible to simulate a scenario where the ground station is interacting with a GSO satellite while an NGSO constellation is interefering with the commmunication.

Finally, *Chapter 4* focuses on the final purpose of the thesis, that is the development of a statistical generator obtained from the data generated by the implemented simulator. For this aim, the results obtained with the simulator are analysed and the method adopted for the modelling phase is thoroughly described. The novelty introduced by this model consists in randomly generating, with a proper distribution, samples of rain attenuation affecting the path between Earth station and an NGSO satellite, given the rain attenuation affecting the GSO path and the avoidance angle of the NGSO satellite. This model therefore, once calibrated, allows the generation of new results in a much faster way than to simulate the whole scenario once again.

2 | Rain Attenuation Simulator

This chapter contains a brief introduction about atmospheric impairments impacting satellite communications, with particular focus on the effect of rain attenuation on satellite transmissions. Following, a model to generate realistic rain events is presented and described: *ST-MultiEXCELL*. Finally, the remainder of the chapter addresses the development and implementation of a simulator, which analyses the rain events provided to calculate the rain attenuation impacting on the path between a ground-station and a satellite.

2.1. Atmospheric impact on satellite communications

For transmissions requiring wireless links, it is imperative to take into account the effect of the atmosphere on the transmitted signal. The Earth's atmosphere has a complex structure for which different layers called spheres can be identified. The layers that mainly affect the propagation of a radio signal are the ionosphere and the troposphere. The former is a region strongly ionized and, for frequency below 30 MHz [2], it acts as a reflector and attenuator. When the carrier frequency increases, the effect caused by the ionosphere weakens, beyond 3 GHz in particular, as commonly happens for satellite communications, this layer of the atmosphere becomes almost transparent to the signal. Indeed, at these high frequencies, the troposphere becomes the primary source of impairment. This region is the lowest layer of the atmosphere. Transmission impairments in the troposphere are mainly due to hydrometeors, i.e. particles of water in any state, such as rain, hail, snow and also droplets in clouds and fog. For transmissions involving frequencies higher than 10 GHz, hydrometeors become the most crucial element to take into consideration in the system design. Thus, for satellite communications, which normally operate between 10 and 30 GHz, it is vital to properly evaluate how much this impairment can impact the radio wave signal.

2.2. Rain Attenuation Effects

Among all hydrometeors, rain is the most impactful on the quality and performance of Earth-space communications operating above 10GHz [3]. At these values of frequency, in fact, the wavelength of the radio wave becomes comparable with the diameter of a rain drop, which normally ranges between 0.1 and 8 mm, and, as a result, the signal will be more affected by this obstacle. A radio wave impinging on a single rain drop, will experience a loss of energy primarily due to absorption, for which part of the energy is converted to heat, and scattering, which causes the reflection of the energy in every direction. This loss of energy, caused by the combination of both absorption and scattering, constitutes the rain attenuation.

To properly evaluate the rain attenuation it is important to remark some important properties of the system. Firstly, the incident power decays exponentially when the impinging wave propagates through the volume of rain. Secondly, the drops are considered to be spherical, so an equivalent diameter is defined, to preserve the equivalent volume of the drop. Lastly, each rain drop causes an independent and additive effect to that of the other drops.

Considering these premises, the attenuated power of the wave obtained after crossing the rain volume can be defined as:

$$P_{att} = P_i \, e^{-kL} \tag{2.1}$$

where P_i is the power of the incident wave, P_{att} is the power attenuated at the end of the rain volume crossed, L is the length of the rain volume crossed and k is the attenuation coefficient for the rain volume, which can be expressed as:

$$k = \rho \, Q_t \tag{2.2}$$

ρ is the number of drops per volume and Q_t is the attenuation cross-section of the drop, expressed in units of area. The attenuation cross-section can be interpreted as the equivalent area of a receiving antenna [2], represented by the single water drop, which is subtracting power from the incident wave, whose power density is S_i:

$$P_{att} = S_i \, Q_t \tag{2.3}$$

Q_t can be further developed when considering both contributions to attenuation generated by absorption and scattering, each associated to their own attenuation cross-section:

$$Q_t = Q_{abs} + Q_{sc} = Q_t(r, \lambda, m) \tag{2.4}$$

The attenuated power can be likewise divided into an absorbed and a scattered component:

$$P_{abs} = S_i \, Q_{abs} \tag{2.5a}$$

$$P_{sc} = S_i \, Q_{sc} \tag{2.5b}$$

To evaluate the components of Q_t depending on absorption and on scattering, it is necessary to consider the complex context depicted in *Figure 2.1*, where a plane wave with propagation constant β_0 is impinging on a water drop which scatters part of the power across the space as a spherical wave. The relation between the incident and scattered electric field can be expressed as:

$$\vec{E}_{sc} = \frac{e^{-j\beta_0 r}}{j\beta_0 r} \, S(\theta, \phi, \psi) \, \vec{E}_{in} \tag{2.6}$$

where r is the distance from the center of the drop to wherever the scattered field $\vec{E}_{sc}$ is observed from and $S(\theta, \phi, \psi)$ is a 2×2 matrix denominated as the *scattering matrix*. The elements S_{ij} of $S(\theta, \phi, \psi)$ are known as *scattering amplitudes* and are unitless once the matrix is divided by the term $j\beta_0$. These elements depend on the shape, dimension and refractive index of the water drop, as well as on the angles of view of the particle as illustrated in *Figure 2.1*.

The attenuation cross-section is strongly related to the the scattering amplitudes, which can be calculated with different methods. If the drop can be assumed to be spherical, a mathematical solution can be applied, given by the *Mie's algorithm*, however, since it requires an infinite summation, it can cause problems in the practical case due to the unavoidable truncation during calculations. There exists an approximation of this solution known as the *Rayleigh approximation*, which in addition to the spherical shape condition also requires the diameter of the drop to be much lower than the wavelength of the wave internal to drop itself. The Rayleigh approximation represents a very simple closed form alternative solution, though the condition on the diameter of the drop is typically not respected in the case of rain, for which the diameter of the drop is comparable to the wavelength and definitely not much lower than. To evaluate the scattering amplitudes for

a general scenario, with no condition on the shape and diameter of the drop, numerical approximations are commonly implemented and are nowadays very reliable. Some examples of these numerical approximations are the *Method of Moments*, the *Point Matching Technique* and the *T-Matrix* approach, the latter in particular has proven to produce very accurate results and is natively implemented in many software environments.
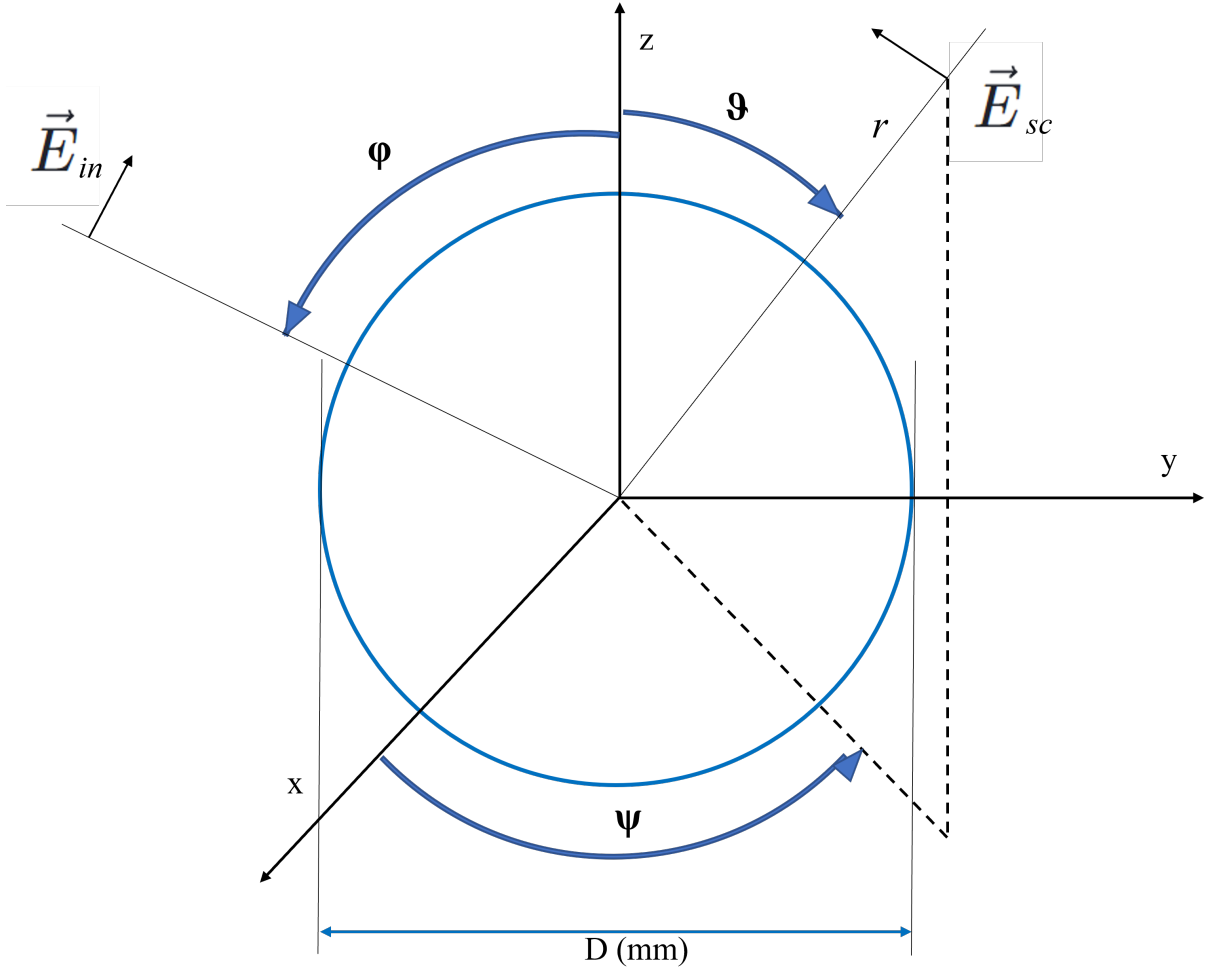

Figure 2.1: Plane wave impinging on a water drop and being scattered as spherical.

Realistically, rain drops do not share the same radius, therefore, the attenuation coefficient k must be integrated to account for all possible drop size:

$$k = \int Q_t(r, \lambda, m)\eta(r) \, dr \tag{2.7}$$

where $\eta(r)$ is considered as the number of drops per unit of volume with a diameter in the interval between r and $r + dr$.

The rain attenuation evaluated in dB is:

$$A[dB] = 10\,log_{10}\left(\frac{P_i}{P_{att}}\right) \tag{2.8}$$

Considering (*2.1*) and changing the base of the logarithm to the natural one, it is easy to obtain the following expression for the rain attenuation:

$$A[dB] = 4.343\,kL \tag{2.9}$$

The total attenuation caused by the rain volume can also be seen as:

$$A[dB] = \int_0^L \alpha\,dl \tag{2.10}$$

where alpha is the specific attenuation of the rain volume expressed in $\frac{dB}{km}$. The integration is thus taken over the whole linear path crossed by the radio wave through the rain volume.

From (2.7) and (2.9) it is also noteworthy to observe how the specific attenuation can be defined as:

$$\alpha\left[\frac{dB}{k}\right] = 4.343 \int Q_t(r,\lambda,m)\eta(r)\,dr \tag{2.11}$$

which is quite an interesting result since it associates the specific attenuation to the size of the drop, the wavelength of the impinging wave, the attenuation cross-section and the drop distribution in the considered volume.

Furthermore, the Drop Size Distribution η can be expressed as a function of the rain rate through an exponential form:

$$\eta(r) = N_0\,e^{-[cR^{-d}]r} \tag{2.12}$$

Where N_0, c and d are all empirical constants, while R is the rain rate measured in mm/h and r is the radius of the rain drop.

Lastly, combining (2.11) and (2.12) the attenuation caused by rain on the path can be expressed with the formula dependent of the rain rate:

$$A\,[dB] = 4.343 \int_0^L \left[N_0 \int Q_t(r, \lambda, m)\, e^{-[cR^{-d}]r}\, dr \right] dl \qquad (2.13)$$

where the integration over dl indicates the propagation path of the radio wave crossing the rain volume. However, this expression is not easy to adopt in the general case due to the variability of the drop size distribution which can depend on the link, on the height and even on the specific event. Therefore, researchers focused their efforts into finding a more practical and general form, attempting through empirical methods to find an alternative to the complex analytical result.

2.3.   ITU-R standard to calculate Rain Attenuation

Comparing empirical measurements with results obtained with the theoretical equations reported in (2.2), a compact and elegant approximation for the specific attenuation was proposed:

$$\alpha \left[\frac{dB}{km} \right] \cong a\, R^b \qquad (2.14)$$

This expression approximates well the behaviour of the specific attenuation, while simply being function of the rain rate R and the constants a and b which are dependent on frequency, temperature, wave polarization and elevation angle of the communication link. These constants were initially obtained empirically for a limited number of frequencies, however the whole expression was also analytically demonstrated by Olsen, Rogers and Hodge, who managed, in their work, to present values for a and b for the frequencies ranging from 1 to 1000 GHz [4]. Additionally, ITU-R latest Recommendation P.838-3 contains a tabulate of the values that a and b can assume for each range of the parameters they depend on.

The expression (2.14) has become the most adopted formula in models to calculate the rain attenuation affecting a transmission link given the rain rate. Even ITU-R defined a standard model for the purpose of calculating rain attenuation based on (2.14) and it is presented in Recommendations P.618-8 [5], P.838-3 [6] and P.839-4 [7].

Also the procedure chosen for the development of the present rain attenuation simulator, as will be explained in *Section 2.5*, makes use of a model based on equation (2.14), resorting to Recommendations P.838-3 [6] and P.839-4 [7].
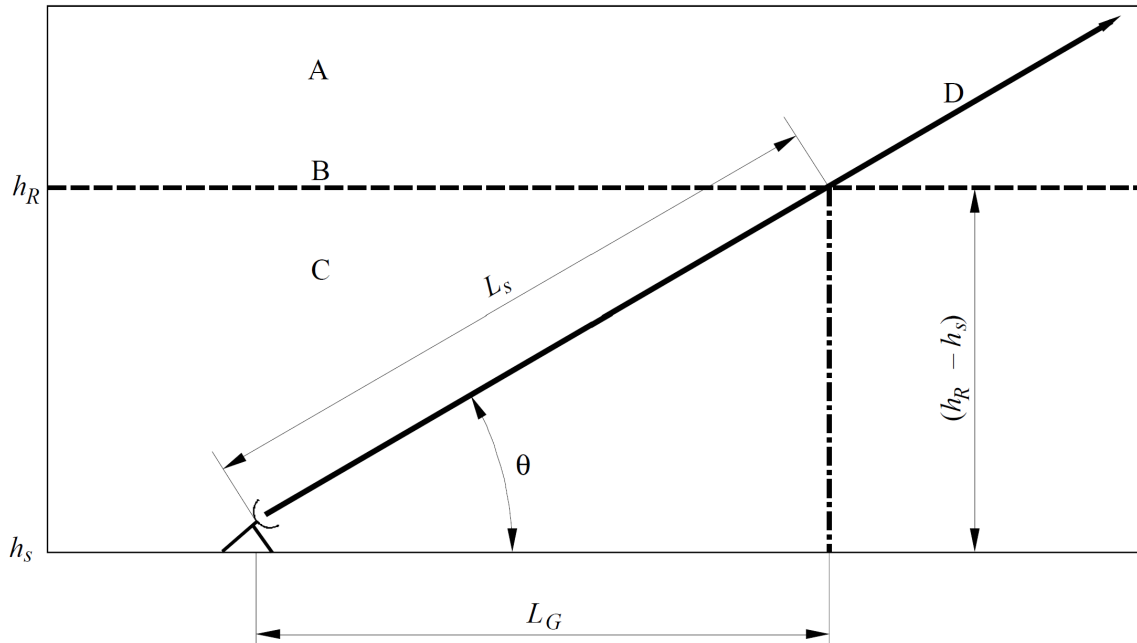
Figure 2.2: Satellite communication during rain event scenario (*source: ITU-R Recommendation P.618-8 [5]*).

Figure 2.2 depicts the typical scenario of a ground-satellite communication system. When the link is affected by rain, the attenuation impacts the quality of the transmission. The path subject to rain attenuation, though, does not correspond to the entire link from Earth to satellite, but only to the portion below the so called **rain height h_R**. In addition, a key parameter for the design of this system is the **elevation angle θ**, which, if changed, can modify the length of the path affected by rain. The elevation angle is defined as the angle formed between the line of sight of the link and the tangent to the local horizon.

The first step to calculate the rain attenuation is therefore to identify the altitude from which the rain starts to fall. While the rain rate can change significantly on the horizontal direction, it tends to remain constant on the vertical one until the altitude defined as the 0°C isotherm height, below which water assumes liquid form. Above this altitude, a transition region known as the **melting layer** is encountered, characterized by the presence of large particles resembling snowflakes mixed with water. Beyond the melting layer only ice particles are found, from which it is expected very low attenuation as the ice tends to change the refractive index in a way that it becomes transparent to the radio wave and it can thus be neglected, at least up to about 70 GHz. The water-snow mixture in the melting layer affects the incident radio wave in the same way large droplets would do, so it is crucial to also keep into consideration this transition layer when evaluating the height for which the link is affected by rain attenuation. The melting layer is thus

accounted for by equivalently increasing the 0°C isotherm height by 0.36km, as expressed in the ITU-R model in Recommendation 839-4 [7].

Once the rain height is identified, also accounting for the melting layer, the **slant path**, i.e. the portion of the link extending from the ground station to the rain height, can be evaluated as:

$$L_s = \frac{h_R}{sin(\theta)} \tag{2.15}$$

Even though rain rate remains approximately constant when investigating the vertical direction, this is not true for the horizontal one. In reality, rain fields are characterized by a very strong space and time variability and they can be described by complex structures, denominated as rain cells, to which analytical forms can be associated to define how the rain rate varies in the horizontal direction. An example of a handful analytical expression to describe a rain cell is the exponential one, where the rain rate assumes a peak value at the center of the cell and decreases quickly when moving away from it.

$$R(\rho) = R_M \, e^{-\frac{\rho}{\rho_0}} \tag{2.16}$$

In equation (2.16), R_M represents the peak rain rate value at the center of the cell, ρ is the considered distance from the center, while ρ_0 is an equivalent radius which regulates how quickly the rain rate decreases when getting further away from the peak.

The information that the rain rate varies primarily only on the horizontal direction, becomes particularly useful when calculating the rain attenuation. Indeed, it is possible to derive from the slant path its projection on the ground $L_G = L_S \, cos(\theta)$ and evaluate the specific attenuation for it through equation (2.14). The total attenuation is calculated integrating the specific attenuation over the ground path and dividing the result by $\cos\theta$ to take into account the relation between slant and ground path.

$$\alpha \left[\frac{dB}{km} \right] \cong a \, R^b \tag{2.17a}$$

$$A_G = \int_0^{L_G} \alpha(x) \, dx \tag{2.17b}$$

$$A_S = \int_0^{L_S} \alpha(l) \, dl = \frac{A_G}{\cos\theta} \tag{2.17c}$$

where x corresponds to the horizontal direction while l to the direction of propagation.

In particular, l is obtained from x through the relation $l = \frac{x}{cos(\theta)}$.

2.4. Rain Field Models

As stated in section 2.3, the obtained formula (2.14) is very practical to calculate the attenuation induced by rain. The only information needed in this case is about the rain rate of the considered site. The constants a and b, in fact, can be extracted from the tabulate of ITU-R Recommendation P.838-3 [6] depending on the operative parameters of the system. Information on the rain rate can extracted from rain maps generated by rain field models, which are the topic of interest of this section.

The objective of these models is to generate rain fields with characteristics as close as possible to those of the real ones. In particular, the most important features that a model should reflect are the local rainfall statistics, the correlation in space and in time.

Through the years, several rain field models of different nature were proposed, each providing advantages, but with inherent flaws [8]. Numerical models are able to accurately reproduce the physical characteristics of the full meteorological environment, yet the calculations to achieve the desired resolution in space and time result too long to be adopted in efficient simulators. Another kind of researched models are the Stochastic ones, which successfully reflect the local rainfall statistics and achieve satisfying evolution in space and time, however the rain rate in this case has a fixed statistical distribution and it experiences always the same rainfall spatial correlation. On the other hand, Fractal models exploit self similarity properties of rain fields, but the events generated are based on input parameters which are difficult to retrieve from local data. Moreover, Statistical models are also noteworthy, they are flexible and applicable at global scale, though the calibration phase typically requires rain gauge time series and also the integration time turns out to be much longer than the desired 1 minute. Lastly, one more significant rain field model is based on the generation of synthetic rain cells defined by analytic expressions.

2.4.1. EXCELL and MultiEXCELL

As stated in [9]: "*a rain cell is defined as any connected region of space composed of points where the rain rate exceeds a given intensity threshold*". These structures, therefore, aim to describe the rain profile of the local statistics, in such a way that the variation of the rain rate on the horizontal direction can be described by an analytic expression. In *Section 2.3*, a kind of rain cell was already introduced based on an exponential profile. The same expression of (2.16) is the one adopted for generating rain cells in the model

EXCELL [9]. The advantage of EXCELL is that it makes possible to derive the rain cells' occurrence probability based on the 1-minute integrated rainfall statistics P(R) of the considered site. This model, however, is only able to generate and consider isolated cells, inevitably limiting its applicability to the small-scale.

In order to obtain a large-scale model, capable of generating realistic rainfall processes over a wide area, it is necessary to consider aggregation of rain cells into clusters. This, in fact, was the objective that encouraged the development of MultiEXCELL [10]. This rain field model is able to reflect the realistic spatial features of the rain fields even in the large-scale scenario by combining rain cells into aggregates. Indeed, MultiEXCELL succeeds in preserving the spatial correlation of the rainfall process by accurately defining the main properties of single rain cells, such as their area and their average rain rate, as well as characterizing their aggregation process, i.e. defining the distances between cells in a single cluster, the number of cells that aggregate together and the distance between clusters themselves. This information was extracted from the data collected at the experimental station of Spino d'Adda, near Milano, Italy, in which long-term measurements were carried out from 1988 to 1992 with the aim of creating an extensive database of rain events to analyse and model. Moreover, a key parameter studied by this model for the generation of spatially correlated processes is the fractional area of the map covered by rain η_P. This information is extracted from radar data and compared to results available from global long-term Numerical Weather-Predition data sets, specifically *ERA-40*.

The main flaw related to MultiEXCELL, however, is its lack of time correlation. Even if it successfully generates rain fields with realistic space correlation, the model is not capable of describing the time evolution of the system. Therefore, a new model was developed with the aim of characterizing the temporal correlation of rainfall processes: *ST-MultiEXCELL* [8].

2.4.2. ST-MultiEXCELL

As stated, *ST-MultiEXCELL* is a model developed to introduce time correlation in rainfall processes. It inherits the features of MultiEXCELL, such as being able to generate spatial correlated rain fields with statistics successfully reproducing the local complementary cumulative distribution function of the rain rate P(R).

A fundamental element to describe the time correlation of the rain fields, is the characterization of the temporal evolution of the fractional rainy area η_P already described in subsection 2.4.1 and the rainy area η, which is defined as the area in which the rain rate

exceeds a certain threshold (for this model 0.5 mm/h). The evolution of η and η_P depends on the duration of the event and on its type. In fact, two main kinds of rainfall processes can be identified, the first being *stratiform rain*, characterized by a larger covered area, lower rain rate (typically below 10 mm/h [3]) and long duration, while *convective rain* is commonly associated to high rain rates, more spatially localized and of shorter duration. These events must obviously be characterized by different a temporal evolution, such as reducing the size of the cell when the rain is more intense and viceversa. In order to achieve this result, *ST-MultiEXCELL* takes advantage of the data extracted from Numerical Weather Prediction data sets (ERA-40), which is already conveniently organized in 6-h slots allowing an accurate analysis of the time correlation of rainfall processes.

To reflect the realistic case even more truthfully, this Cellular model, besides the structural evolution of the cells, also considers a realistic movement of the perturbations across the map, based on the intensity of the wind v and the direction in which it blows θ. These values are also extracted from the ERA-40 database, corresponding to the local site considered.

ST-MultiEXCELL is thus able to generate rain events, as in precipitation processes evolving in time, for geographical maps of 200 km $\times$ 200 km with a 1 km $\times$ 1 km spatial distribution, as can be observed in *Figure* 2.3. Each rain event lasts for 6 hours and it has a time resolution of 1 minute, therefore consisting of a total of 359 maps per event. Each pixel of the map contains the instantaneous Rain Rate value in $\frac{mm}{h}$, making it possible to easily calculate the attenuation with equation (2.14). Comparing the results obtained from the model with respect to local measurements carried out in Spino d'Adda, it was demonstrated that *ST-MultiEXCELL* manages to preserve the statistics of the local rainfall process P(R) while still overcoming the limitation of *MultiEXCELL* of lacking temporal correlation when generating synthetic rain fields.
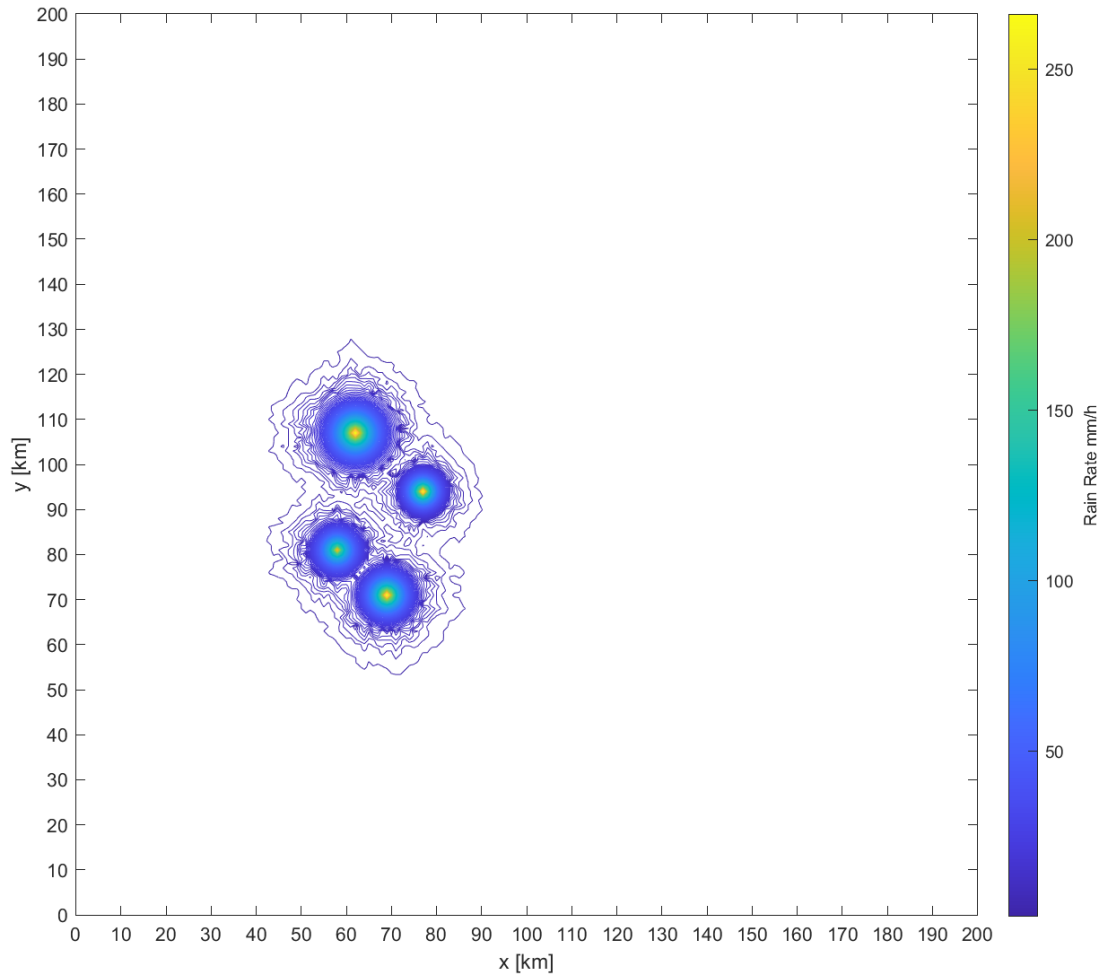
Figure 2.3: Contour plot of typical rain map generated by *ST-MultiEXCELL* at a fixed time t in a map of 200 km x 200 km.

2.5.   Rain Attenuation Simulator

This section describes how the information presented in this chapter can be used to develop a simulator capable of calculating the rain attenuation affecting an Earth-space link. More specifically, the objective of this section is to study the impairment caused by rain on a satellite communication, either for downlink or uplink, between a Ground Station and a generic satellite.

2.5.1.   Required Inputs and Initialization Phase

Figure 2.4 depicts a typical scenario elaborated by the simulator in which a satellite link is affected by rain. The rain field considered is a 3D representation of the same one already reported in *Figure 2.3*. Different points of view of the same 3D scenario are also

presented *Figure* 2.5 *a)* and *b).* The red cube represents the ground station, which is positioned by the simulator at the centre of the map. In this particular example, the rain height is fixed to 4.5 km, thus the path concerned by rain attenuation is only the portion of the link crossing the rain field below this altitude. The red line represents the aerial link between the Earth station and the satellite, while the green line coincides with the projection on the ground of the intersection between the satellite link and the plane at rain height. Finally, the black line, connecting the mentioned projection and the ground station, corresponds to the projection of path below rain height L_G.

The simulator requires as input the latitude, longitude and altitude of both the ground station and the considered satellite to accordingly calculate the azimuth ψ and elevation angle θ of the link between the two ends. Exploiting the geographical information on the ground site, the simulator also calculates the local rain height by resorting to the method described in Recommendation P.839-4 of ITU-R [7] (whose script was implemented by Carlo Riva, Professor at Politecnico di Milano). Once the rain height is evaluated, it is possible to calculate the length of the projection on the ground of the slant path by taking advantage of the knowledge on the elevation angle of the link:

$$L_G = \frac{h_r}{\tan \theta} \tag{2.18}$$

In order to define the right direction of the link, the simulator makes use of the information on the azimuth. As shown in *Figure* 2.6, this procedure initially takes into account a segment with length equal to L_G directed to the North, this line is subsequently rotated clockwise by an angle equal to the azimuth, making it coincide perfectly with the ground projection of the slant path.

The final input required by this simulator is the rain map providing information about the rain fields for a fixed moment in time. The maps analysed during the development of the simulator were generated by *ST-MultiEXCELL* with the same procedure already discussed in *Section 2.4.2*. Once again, the maps describe a geographic area of 200 km × 200 km with a spatial resolution of 1 km × 1 km and a time resolution of 1 minute. These maps in the practical case correspond to 200 × 200 matrices, where each cell contains the instantaneous value of the rain rate in mm/h related to the pixel of area 1 km × 1 km in that fixed time. A rain event generated by *ST-MultiEXCELL* covers a period of 6 hours, therefore, given the time resolution of 1 minute, it consists of 359 rain maps. The simulator takes the time resolution one step ahead. By interpolating two consecutive maps in time, calculating the arithmetic average of the corresponding values, it is in fact able to achieve a temporal resolution between rain events of 30 seconds instead

of 1 minute. In this way, a new maps is interposed between each couple of rain maps in the event, ultimately increasing the number of rain maps in the 6 hours slot up to 717. This operation provides a smoother evolution of the events in time, allowing the rainfall processes to be analysed in a more precise way.
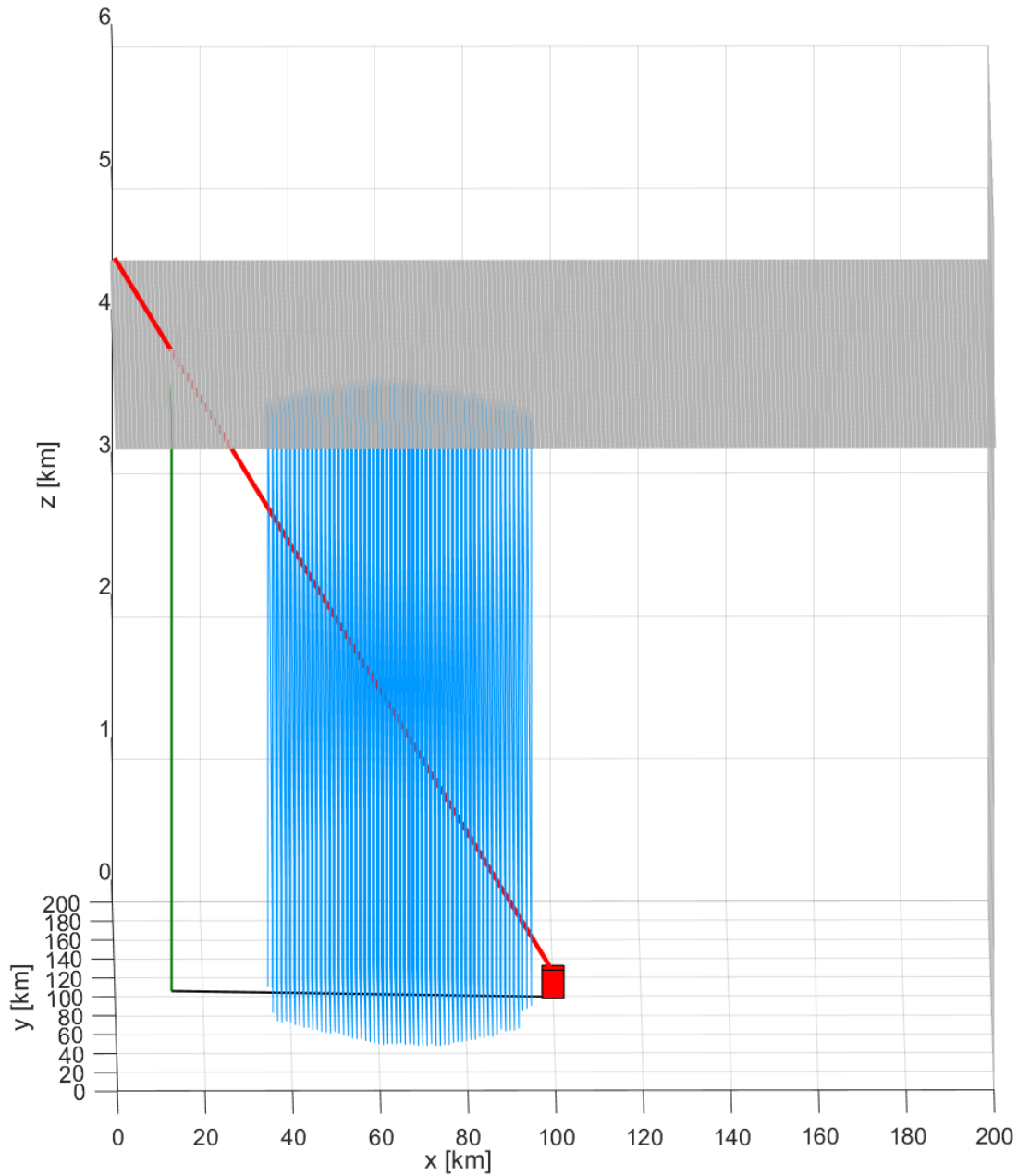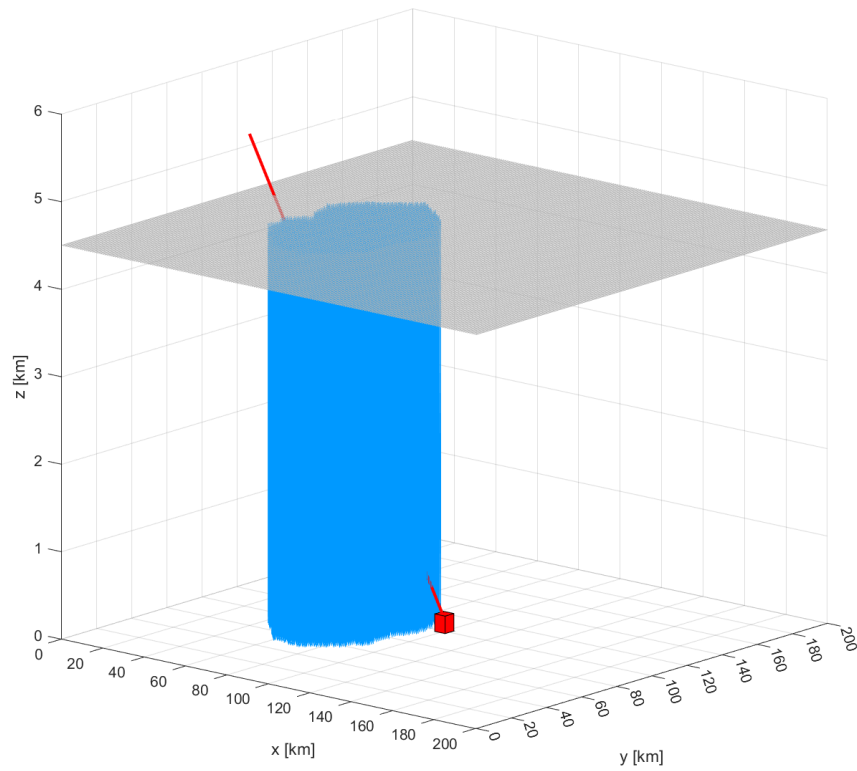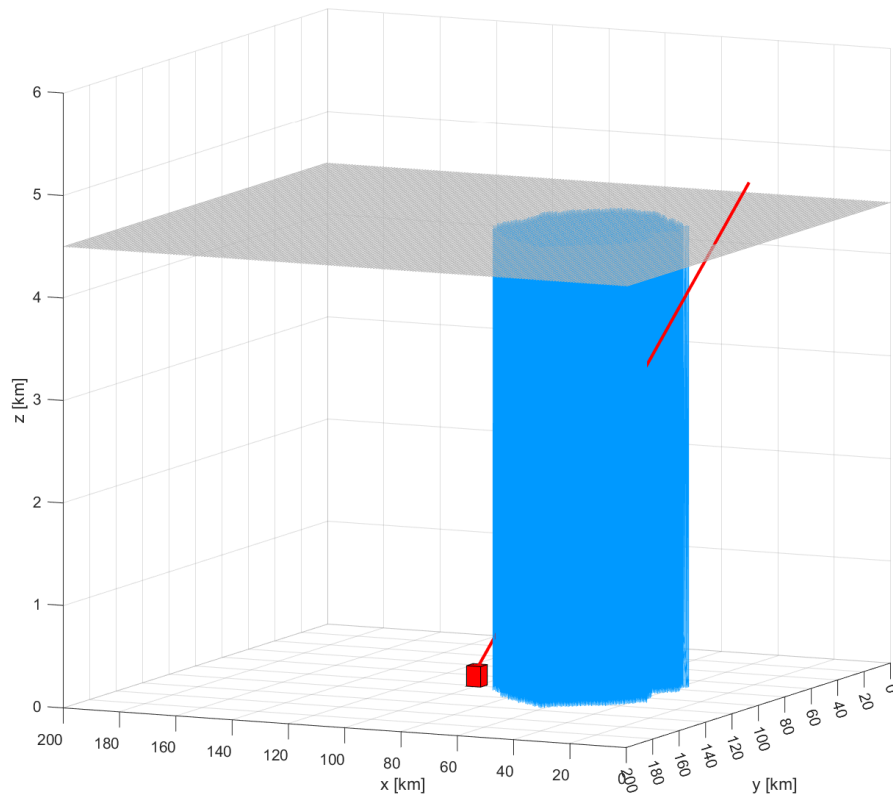

Figure 2.4: Profile of ground-satellite link affected by rain.

(a) Satellite link from the front.

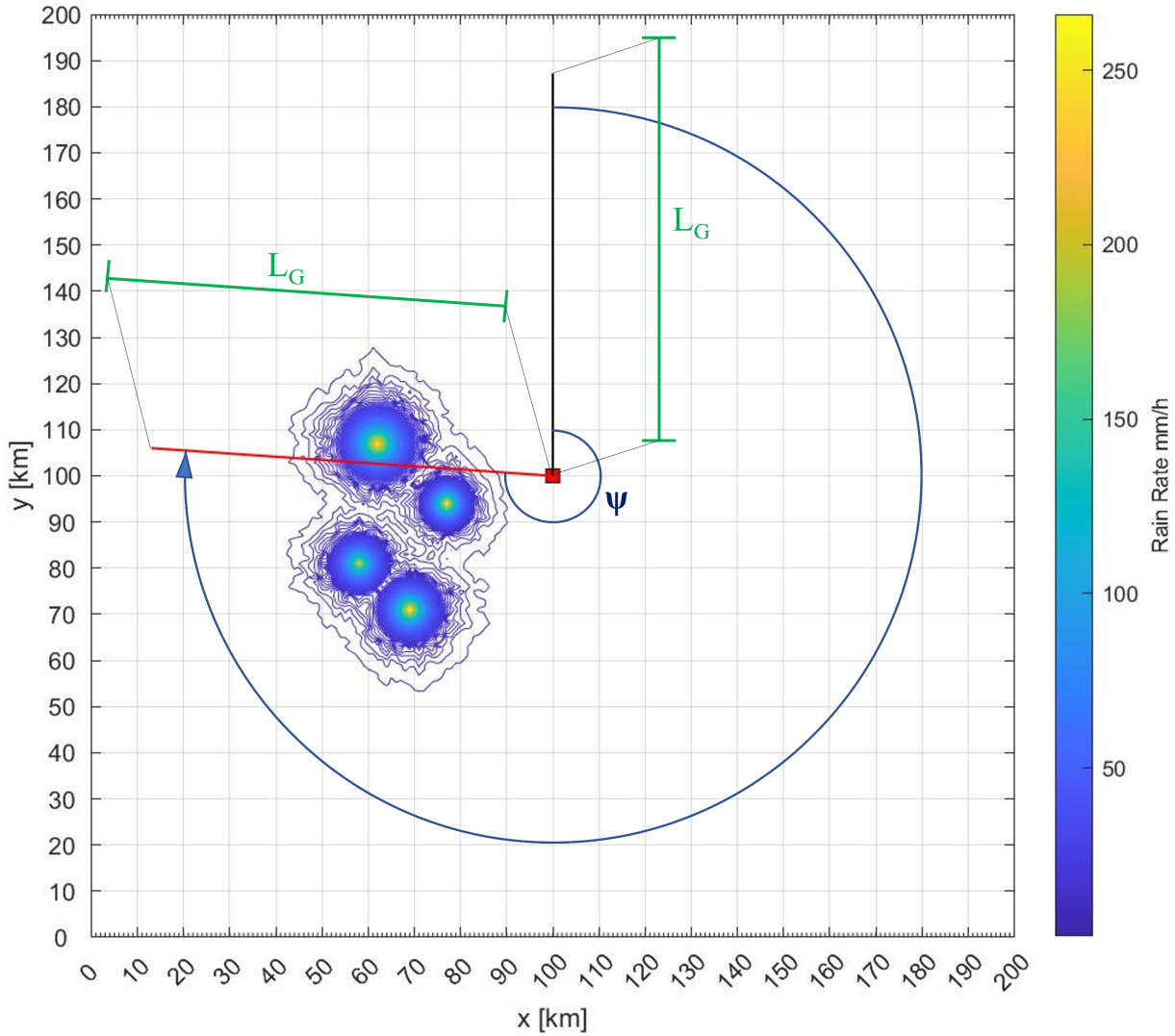(b) Satellite link from the back.

Figure 2.5: 3D view of rain affecting satellite link.

Figure 2.6: View from above of the rain map considered by the simulator.

2.5.2.   Calculation of the rain attenuation

Once the initialization phase is over, the simulator has access to the length of the ground projection of the slant path L_G, the direction of the satellite link and the rain map containing the instantaneous rain field values for every pixel corresponding to 1 km $\times$ 1 km of the 200 km $\times$ 200 km map.

The method followed by the simulator to calculate the rain attenuation affecting the path refers to the standard of the ITU-R examined in *Section* 2.3. In this realistic case, the rain rate is not constant in the horizontal direction, therefore every value it assumes along the path must be taken into consideration when applying equation (2.14). In order to do so, the procedure takes advantage of the cells of the rain map, each containing a

corresponding value of the rain rate. The first step is therefore to identify the cells crossed by the link, so that the total rain rate can be characterized.

The simulator makes use of a right-hand spatial reference system based on a plane tangent to the local site, where one coordinate is related to the East direction, one to the north and one to the normal to the ground. In this way it is possible to refer to the rain map as if it was directly related to the real site. The ground station is positioned at the center of the map in coordinates (x_0, y_0) and it serves as one of the ends of the segment representing the ground projection of the slant path. The other end is found through the information obtained during initialization phase. Initially, the coordinates considered for the other end of the segment are simply $(x_{north} = x_0, y_{north} = y_0 + L_G)$. This point, thereafter, undergoes a clockwise rotation around the ground station of an angle equal to the azimuth ψ. This final position, (x_f, y_f), coincides with the projection on the ground of the intersection between the link and the rain height.

Now that the ground projection of the slant path is fully defined between the coordinates (x_0, y_0) and (x_f, y_f), the cells that are crossed by this segment can be identified by simply evaluating the intersections of the segment with the grid of the rain map.

Figure 2.7 depicts the method implemented to select the right pixels. The example takes into consideration a link where the initial point is at $(x_0 = 68.5, y_0 = 102.5)$ and the final point at $(x_f = 61.5, y_f = 107.5)$. This choice of coordinates was merely intended for a representation of the model, it does not affect in any way the procedure. Firstly, the two ends of the segment are considered (2.7 *a)*), then, the intersections of the segment with the grid of the rain map (recalling that the spatial resolution is 1 km × 1 km) are identified (2.7 *b*). This step is carried out by simply calculating the Cartesian equation of the line passing through the two points and determining the values for which it crosses the grid. The next step requires to evaluate the medium points between each consecutive intersections of the line with the grid (2.7 *c*). These same medium points lie exactly in the pixels crossed by the link, their coordinates therefore can be used to identify the crossed cells of the rain map matrix in a univocal way (2.7 *d*).

At this point, an auxiliary matrix is created with the same dimension of the rain matrix describing the rain map (200×200). This new matrix will have all its values equal to 0, except for the ones corresponding to the pixels of the rain map crossed by the link. In these cells, the auxiliary matrix, hereafter referred to as the *distances matrix*, will store the length of the portions of the link crossing that specific area, as illustrated in *Figure 2.8*.

(a) Ground projection of slant path

(b) Intersections with the map grid

(c) Medium points between intersections

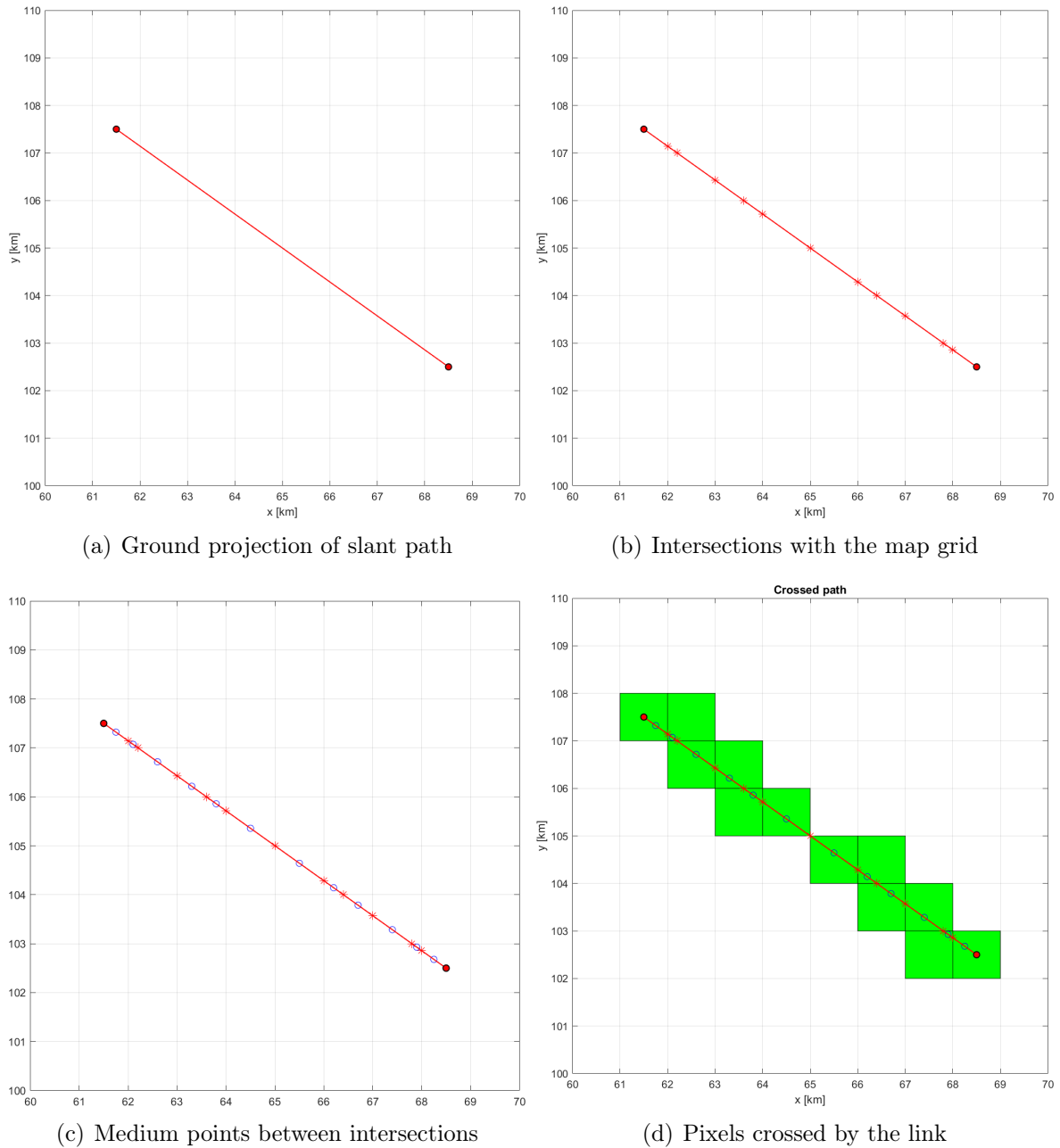(d) Pixels crossed by the link

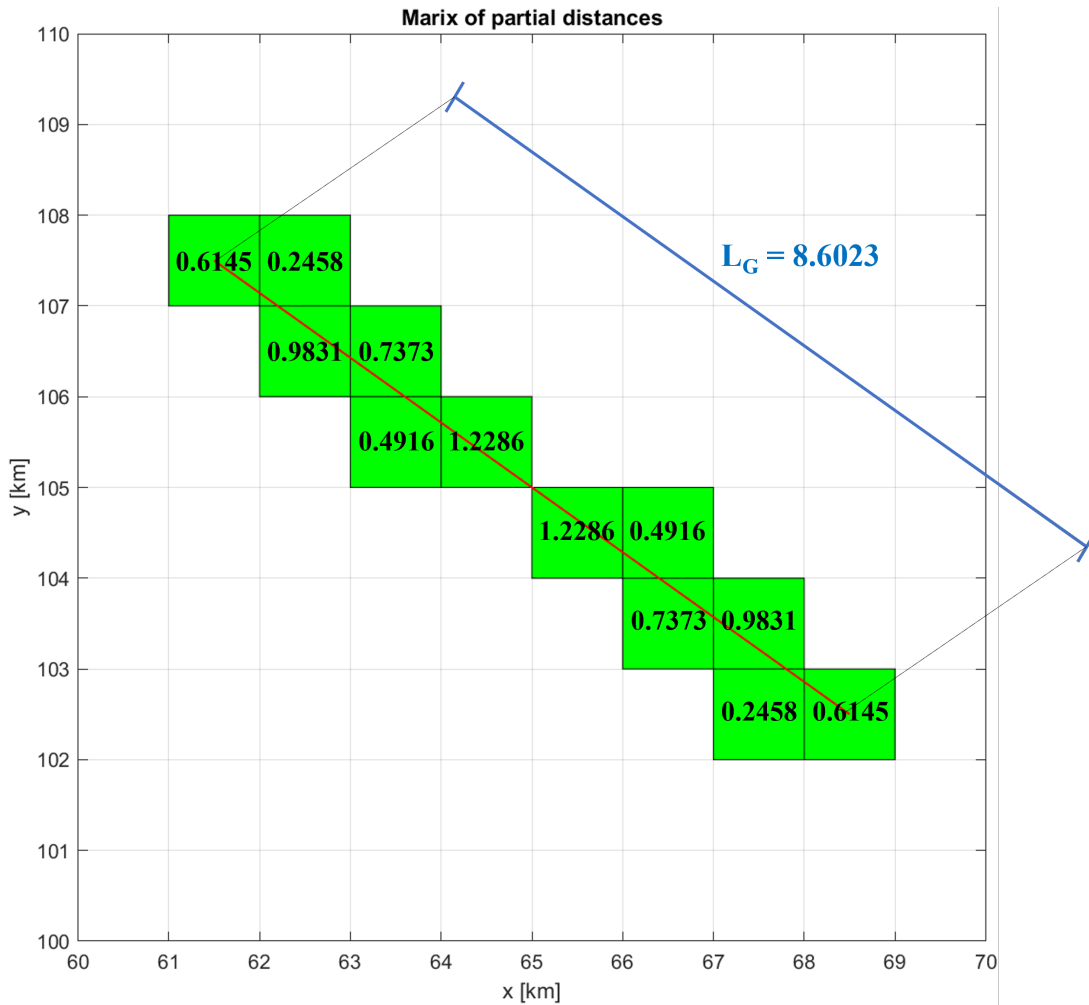Figure 2.7: Procedure to identify the pixels crossed by the link.

Figure 2.8: The only non-zero values of the distances matrix, storing the lengths of the portions of the link crossing those pixels.

The next step requires to calculate the specific attenuation $\left[\frac{dB}{km}\right]$ from the rain rate. Equation (2.14) was exploited to achieve this goal. Since the simulator makes use of a 200×200 matrix with cells containing values of rain rate, it is possible to derive a corresponding value of specific attenuation for each of these cells. To achieve this result the simulator evaluates the coefficients a and b of equation (2.14) as indicated in ITU-R Recommendation P.838-3 [6], whose script was once again implemented by Professor Carlo Riva. Said script requires as input the information on the frequency and wave polarization of the radio wave, as well as the elevation angle of the link. Once a and b are known, the calculation of the specific attenuation for each cell of the rain matrix is trivial. Indeed, since each cell already contains the corresponding rain rate value in [mm/h], it is enough to elevate every element of the matrix to the exponent b and multiply the newly obtained matrix by a. In this way, the matrix representing the rain rate values for each pixel is

converted to an equivalent one this time expressing the specific attenuation.

The final step to calculate the total attenuation caused by rain on the link requires the integration of the specific attenuation $\alpha(l)$ along the slant path L_S, as reported in (2.17c). In the case of the simulator, obviously the rain rate is not described by a continuous function, since this information is acquired from the elements of prior-generated matrices. Therefore the integration along the slant path can be developed into a discrete summation:

$$
\begin{aligned}
A_S &= \int_{L_S} \alpha(l)\, dl \\
&= \int_{L_G} \alpha(x)\, \frac{dx}{cos(\theta)} \\
&= \frac{1}{cos(\theta)} \sum_{i=1}^{N} \alpha_i(x)\, \Delta x_i
\end{aligned}
\tag{2.19}
$$

Where Δx_i is the length of the portion of the link crossing pixel i while N is the number of pixels crossed. In addition, $\sum_{i=1}^{N} \Delta x_i = L_G$.

For this calculation, the *distances matrix* proves to be particularly useful. This matrix, in fact, stores exactly the value of Δx_i in the corresponding cells. Exploiting the element-by-element multiplication between the distances matrix and the specific attenuation matrix, the obtained result will be a 200×200 matrix with all elements equal to 0 except for the ones corresponding to the pixels crossed by the link, which will store the value $\alpha_i(x)\Delta x_i$. To calculate the total rain attenuation affecting the link according to (2.19) it is enough to sum all the elements of the newly obtained matrix and dividing the result by $cos(\theta)$ to convert the result from ground projection to slant path.

3 | NGSO constellation simulator

3.1. Fundamentals of Satellite Communications

In this section a background on satellite based systems is presented, specifically describing how satellites are deployed in different orbits in the field of telecommunications. The information presented will serve as an introduction to the final section of the chapter, which will present the extension of the simulator described in *Chapter 2* to consider a specific constellation of satellites instead of a generic single one.

3.1.1. Ground and Space segments

A communication satellite system mainly consists of two major segments: the **space segment** and the **ground segment** [3]. The former comprises the orbiting satellite, or the network of satellites, as well as the *TTC&M* (*Tracking, Telemetry, Control and Monitoring*) ground facility, which provides management and control instructions to the satellites in order to maintain them in the prior-established orbit. These TTC&M link are separated from the usual communication links, however they can still operate in the same bands. A single TTC&M ground facility can manage to maintain several satellites in orbit by directly establishing specific links with each one of them. On the other hand, the ground segment, which does not include the TTC&M ground facility, is located on the Earth's surface and it represents the other end of the communication link with the satellite. The nature of the ground segment depends on its movement during transmission. A **fixed** terminal is designed to not change its location since its installation, an example can be terminals built on top of buildings to receive broadcast signals. **Transportable** terminals do not move during transmissions with the space segment, however they can be transported to different locations when inactive, for example if mounted on top of a truck. Finally, **mobile** terminals can communicate with the satellite even when in motion.

A communication satellite typically acts as a relay between two ground stations placed on Earth. In this case, the wireless link between the first station and the satellite is called **uplink**, while the one from the satellite to the receiving station is the **downlink**. The

satellite is equipped with a *transponder* used to receive, amplify and possibly process the incoming signal to then relay it to the designated ground station. In addition to the transponder electronics, the satellite also makes use of reception and transmission antennas.

Two more key parameters involved in satellite communications, have already been mentioned in *Chapter 2*, are the **elevation angle (θ)** and the **azimuth (ψ)**. The former is the angle formed between the local horizon and the line of sight between the ground station and the satellite, while the latter is defined as the angle characterizing the clockwise rotation applied to a line parallel to the North to coincide with the projection of the satellite link on the ground.

3.1.2. Satellite Orbits

Satellites can be deployed at different altitudes above Earth's surface, the orbits they follow when revolving around the planet are of vital importance for the design of the system, depending on the desired application. For example, as the altitude of a satellite increases so does the area that it covers, however the latency of the signal gets more severe since it travels on a longer path.

Kepler's Laws, which apply to the interactions of two bodies under the effect of the gravitational force, are to be considered when studying the properties of different orbits. The three laws, as reported in [3], can be interpreted for the case of artificial satellite as:

- **Kepler's First Law**: "the path followed by a satellite around the Earth will be an ellipse, with the center of mass of Earth as one of the two foci of the ellipse."

- **Kepler's Second Law**: "for equal time intervals, the satellite sweeps out equal areas in the orbital plane."

- **Kepler's Third Law**: "the square of the periodic time of orbit is proportional to the cube of the mean distance between the two bodies."

The first law defines the shape of the orbit as elliptical. This ellipse can be further characterized by the **eccentricity**, which determines how squeezed its shape is, and by the **inclination angle**, which defines the angle between the Earth's equatorial plane and the orbital one.

As a main consequence of Kepler's second law, the satellites orbit around the Earth at different velocities depending on its position, they will travel faster when approaching the closest position to the Earth (perigee) and slower when they are at the furthest (apogee).

Kepler's third law is particularly interesting when evaluating the altitude at which a satellite would need to be launched in order to achieve the desired orbit period. The law can in fact be be expressed as:

$$T^2 = \frac{4\pi^2}{\mu} a^3 \tag{3.1}$$

where T is the orbit period in s, $\mu = 3.986005 \times 10^5 \frac{km^3}{s^2}$ is the Kepler's constant and a is the distance between the two bodies in km.

When considering a circular orbit, the distance between the two bodies is equal to the radius of the orbit $a=r$. Thence, inverting equation (3.2), the following expression can be obtained:

$$r = \left(\frac{\mu}{4\pi^2}\right)^{\frac{1}{3}} T^{\frac{2}{3}} \tag{3.2}$$

which is a very important result since it directly relates the orbit radius, r, to the orbit period, T, allowing system designer to choose a proper altitude for the satellite given its application.

3.1.3. Geosynchronous Orbit

An orbit of particular interest is the one for which the orbit period matches the rotation period of the Earth, corresponding to one mean sidereal day. Moreover, if this orbit is also characterized by a spherical shape, thus an eccentricity equal to 0, and it lies on the equatorial plane, with an inclination angle equal to 0, then the satellite moving along this orbit would appear motionless at a fixed spot in the sky by any observer on Earth. This is a very promising scenario, since, for such a satellite, ground stations would not need any tracking in order to optimally communicate with the space segment.

Such an obit exists and it is denominated as the ***Geostationary Earth Orbit*** (**GEO**). Its orbit radius can be calculated through (3.1), accounting for an orbit period of T=86,164.09 s:

$$
\begin{aligned}
r &= \left(\frac{\mu}{4\pi^2}\right)^{\frac{1}{3}} T^{\frac{2}{3}} \\
&= \left(\frac{3.986005 \times 10^5}{4\pi^2}\right)^{\frac{1}{3}} 86,164.09^{\frac{2}{3}} \\
&= 42,164.17 km
\end{aligned} \tag{3.3}
$$

It is possible to obtain the orbit altitude by subtracting the Earth radius at the equatorial plane from the previous result:

$$
\begin{aligned}
h_{orbit} &= r_{orbit} - r_{earth} \\
&= 42,164.17 - 6378 \\
&= 35,786 \ km
\end{aligned}
\tag{3.4}
$$

The circular orbit at altitude 35,786 km over the equator is known as Geostationary Earth Orbit, however this orbit is only ideal. In the real case, it is complex and inefficient to achieve the properties stated, such as eccentricity and inclination angle exactly equal to 0. Indeed, a large amount of fuel would be required to maintain the right position of the satellite. In the realistic scenario, an orbit very similar to the one described is implemented, however with an inclination angle and eccentricity both slightly greater than 0. To differentiate the ideal case from the real one, the deployed orbit is called *Geosynchronous Earth Orbit* (**GSO**).

One of the main advantages of GSO is that at that altitude satellites can see almost one third of the Earth, meaning that the deployment of three GSO satellites placed 120° apart is enough to bring coverage to the global scale. Another favorable characteristic of GSO satellites is that, since they are perceived from the ground as almost fixed in the sky, they require minimal tracking by the ground stations.

On the other hand, GSO communications also have some inherent flaws caused by the elevated altitude. The signal relayed by the satellite, in fact, has to travel a very long path, leading to significant two-way delays (about 260 ms [3]), and large path losses. Furthermore, the number of satellites that can operate in the GSO orbit is limited, since the plane in which they are deployed in, the equatorial plane, is unique. Thus, there is a need for allocation of the geostationary orbit locations, which is regulated by the ITU.

3.1.4.   Non - Geosynchronous Orbit

All orbits for which the angular velocity of the satellite is not equal to the rotational velocity of the Earth are denominated as *Non - Geosynchronous Earth Orbits* (**NGSO**). The most common NGSO are the *Low Earth Orbits* (**LEO**), the *Medium Earth Orbits* (**MEO**) and the *Highly Elliptical Orbits* (**HEO**).

Satellites operating at LEO are typically deployed at altitudes between 160 km and 2500 km. To remain in orbit given this low altitude, satellites require a higher velocity with respect to the GSO case. Indeed, they are not visible at all times by observers on Earth

because they do not appear as motionless objects fixed in the sky. These satellites are actually visible only for 8 to 10 minutes before they cross the horizon. For this reason, one of the major disadvantage associated to LEO satellites is their inability to continuously cover a certain area, since they keep sweeping across the sky. In order to achieve a continuous global scale, a network of LEO satellites, called *constellation*, must be deployed, so that they can inter-communicate to exchange information and provide continuity of service. The costs for the implementation of multiple satellites is compensated by their relative small size and the less amount of energy required to launch them into orbit. On the other hand, LEO satellites can offer important advantages thanks to their low altitude. Since the signal has to travel a relatively short path, it is less affected by path loss and two-way latency, the delay in fact of ∼10 ms. LEO satellites proved to be a fundamental alternative whenever GSO satellites could not manage to reach designated areas. In fact, an obstruction on the line of sight between the space and the ground segments can heavily affect the communication between the two ends and, since the GSO satellites are fixed, this impairment is likely to never be resolved. With a constellation of LEO satellites it is possible to overcome this limitation since they continuously move across the sky, also providing coverage to latitudes unreachable by GSO satellites.

MEO is similar to LEO, however the orbital altitude is higher, typically among 10,000 km and 20,000 km. In this case the delay is in the order of ∼100 ms and they provide an observation time from Earth up to 2 hours. The features of this orbit are particularly interesting for applications involving remote sensing, navigation, position determination, as well as meteorology. One of the most notable service deployed at MEO is the *Global Positioning System* (GPS) which is provided by a constellation of up to 24 satellites at 20,184 km of altitude.

Finally, HEO are employed to reach latitudes that GSO satellites do not manage to cover and that may require longer contact periods than the ones offered by LEO. The highest latitude that GSO can serve in fact is of about 70°, either North or South. HEO are designed to not have circular orbits but rather exploits elliptical shapes with higher eccentricity. In order to provide service also to the latitudes most difficult to reach, the design of a HEO takes advantage of Kepler's Second Law, for which satellites travel the slowest when approaching the apogee, to increase the service period for these latitudes. In particular, the apogee altitude can be similar to that of the GSO case while the perigee's is closer to that of a LEO. For this reason the delay time in HEO can vary, ranging from ∼10 ms up to ∼260 ms.

3.1.5.   Spatial Reference Systems

In order to work with satellite links, it is imperative to define a reference system capable of identifying in a univocal way points in the space. The most intuitive is most likely a Cartesian coordinate reference system which makes use of three space coordinates x,y and z to identify the position of a point. There are actually different possible models representing a Cartesian reference system, the simplest is the ***Earth-Centered Inertial*** (**ECI**) which puts the origin of the system in the center of mass of the Earth while the axes are fixed with the stars. This last statement means that the system translates together with the Earth, however the planet's rotation around its axis causes locations on the surface to constantly change their position in the reference system. This limit can be overcome by adopting a different reference system, ***Earth-Centered Earth Fixed*** (**ECEF**) [11], which, in addition to the origin of the system coinciding with the Earth's center of mass, also considers the three axes fixed with the Earth, with the z-axis piercing through the North-Pole, the x-axis lying on the equatorial plane and intersecting the prime meridian, while the y-axis is orthogonal to the x to maintain the right-hand reference system, as depicted in *Figure* 3.1.
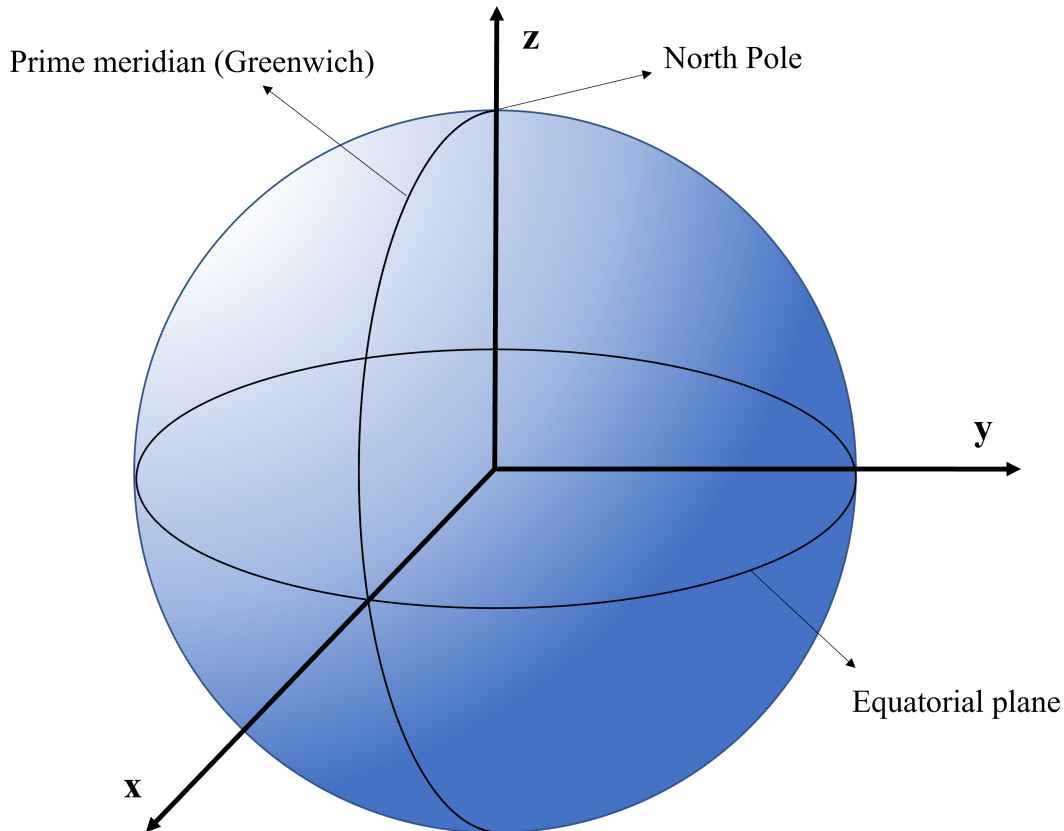
Figure 3.1: Earth Centered, Earth Fixed reference system.

The ECEF reference system is very practical for calculating line of sight links between two separate positions, however, it fails to reflect the bending properties of the Earth's surface, making it difficult to evaluate the position of points located on the surface or even to calculate distances between two points on the bended surface. For this reason there exists an alternative to the ECEF Cartesian reference system which also takes into account Earth's ellipsoidal shape: the ***Ellipsoidal Reference System***. This system identifies the position of a point on Earth's surface by making use of angles defined between reference planes, which are an horizontal plane coinciding with the equatorial plane and a vertical plane including the Earth's rotation axis and passing through the prime meridian. The angle between the considered point on the ellipsoid surface and the horizontal plane is called *latitude*, while the angle between the point and the vertical plane is called *longitude*. As a third parameter to pinpoint the position on the surface in a univocal way, the *altitude* is also employed, which defines the height of the point above the Earth's surface. There exist several reference ellipsoids that can be used in this reference system, however, among all, there is one globally accepted known as the "WGS84". This is the same reference model used by important services such as GPS.

In satellite communications both the ECEF and the ellipsoidal (geodetic) reference systems are used, the latter is more practical to store information about the positions of objects in space while the former is typically employed for calculations between relative positions.

3.2.   The Future of Satellite Networks

3.2.1.   Applications of Satellite Systems

In *Section 3.1* the main features of different orbits were presented. It is clear that due to different physical properties associated to each orbit, the right altitude at which a satellite is supposed to be launched must be chosen accordingly to the desired application.

The main advantage of GSO communication satellites can be found in the extremely large coverage area and in the fixed position with respect to the ground, allowing to constantly monitor the same region. However, as previously stated, the elevated altitude of these satellites causes the signal they relay to degrade more due to space loss and also to experience a higher delay. For these reasons, the GSO satellites should be deployed for applications that do not require low latency. Such applications commonly include broadcasting of television and radio signals, as well as weather observation [12] thanks to their continuous monitoring of specific areas.

On the other hand, for lower-altitude orbits the path the signal has to travel from and to the ground station is much shorter, resulting in smaller path losses and shorter delays. These orbits are exploited for services requiring low latency and also allow lower transmit power to compensate for the losses. LEO is particularly interesting for its proximity to the Earth's surface. Communications satellites deployed in this orbit are used for low-latency-requiring applications, such as bi-directional voice, video and data transmissions. Moreover, LEO constellations can represent a solution to the exponentially increasing data traffic that risks to saturate terrestrial networks [13]. Traditional terrestrial networks, due to bandwidth limits, also experience a limited backhaul capacity, another issue which can be potentially solved by the implementation of a dense constellations of LEO satellites, providing high-capacity backhaul. Recent internet reports carried out by *Cisco*, in fact, show that the IP traffic is growing steadily every year and this trend does not seem to change in the close future, as can be observed in *Figure 3.2.*
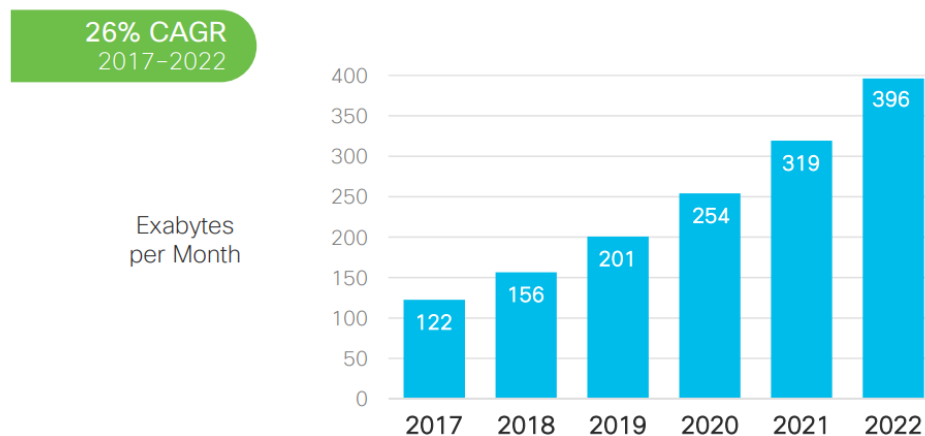
Figure 3.2: Growth of IP internet traffic between 2017-2022. Source: Cisco VNI Global IP Traffic Forecast, 2017-2022.

All these factors, are picking the interest of important private companies and satellite operators to deploy their own constellations at LEO. Furthermore, as already stated, the costs for launching a satellite into orbit greatly decrease with the altitude, therefore, even considering that a whole constellation is necessary to achieve continuous global coverage, the investments for its implementation would not be excessively high.

3.2.2. SpaceX and Starlink

Among the private companies fascinated by LEO constellations, SpaceX is particularly noteworthy. SpaceX is an American aerospace private company founded in 2002 by Elon Musk, with the objective of reducing the costs related to spaceflights to the point of making them an affordable reality [14]. The company manufactures important launch vehicles like the *Falcon 9* and the *Falcon Heavy*. SpaceX was the first private company to ever achieve extremely important results, such as successfully launching and recovering a spacecraft from Earth orbit or even sending a crewed spacecraft and docking it with the International Space Station.

Since the company's main sector is related to launch rockets and spacecrafts manufacturing, it is no surprise that in time it became interested in developing its very own constellation of satellites. It was in 2015 that Elon Musk presented the project to deploy this constellation [1], which would be later denominated as *Starlink*. The main goal presented at the time was to provide global internet access, even to the areas normally unreachable by standard networks, as well as to enhance the quality of communications in high density areas. The company also aimed to eventually redirect the majority of backhaul data into the network satellites [1], as a solution to the ever increasing data traffic which risks to saturate terrestrial networks. The global internet access can in fact become a reality thanks to the constellation of satellites continuously moving across the sky and therefore covering every area while still overcoming LOS obstacles. Moreover, employing this constellation at low altitudes results in lower delays and less powerful amplifiers mounted on the satellites, reducing the implementation costs even further.

The project of the NGSO constellation deployed by SpaceX operating at V-band consists of two main sub-constellations: the first is deployed at LEO, with altitudes between 1,110 and 1,325 km, operating in the *Ku, Ka* bands and counting 4,425 satellites , while the second is implemented at *Very Low Earth Orbit* (VLEO) with 7,518 satellites operating in the *V* band [15]. These sub-constellations' main parameters are described in *Table* 3.1 and *Table 3.2*.

These two sub-constellations cooperate together to provide a coverage which is both dense as well as concentrated. The LEO sub-constellation, in fact, exploits its higher altitude to provide coverage to users in broader areas, while the VLEO constellation manages to concentrate its bandwidth for areas where the demand is higher, also allowing for more satellite diversity options. Indeed, even these high-frequency bands were chosen with the aim of both meeting the broadband demand, especially in areas hard to reach with terrestrial networks, as well as guaranteeing a high-capacity connectivity at all locations.

Parameter	Initial Deployment (1,600 satellites)	Final Deployment (2,825 satellites)			
Orbital Planes	32	32	8	5	6
Satellites per Plane	50	50	50	75	75
Altitude	1,150 km	1,110 km	1,120 km	1,275 km	1,325 km
Inclination	53°	53.8°	74°	81°	70°

Table 3.1: Table describing SpaceX LEO constellation's parameters. Source: Table A.2-1 [15].

Parameter	Deployment		
Satellites per Altitude	2,547	2,478	2,493
Altitude	345.6 km	340.8 km	335.9 km
Inclination	53°	48°	42°

Table 3.2: Table describing SpaceX VLEO constellation's parameters. Source: Table A.2-2 [15].

Another important feature of the satellites implemented in the NGSO constellation by SpaceX is the ability to ajust their EIRP density according to the steer angle, defined as the angle formed between the boresight and the user beam, as illustrated in the graph of *Figure 3.3*. This feature is added with the objective of maintaining a constant value of Power Flux Density on the surface covered by the satellite. The values for both the EIRP density and the PFD are indicated in *Table 3.3*.

	at slant	at nadir
EIRP density [dBW/Hz]	-39.79	-44.20
EIRP in 1MHz [dBW/MHz]	20.21	15.80
Distance to Earth [km]	558.42	335.90
Spreading loss [dB]	-125.93	-121.52
PFD in 1MHz [dB(W/m^2/1MHz]	-105.72	-105.72

Table 3.3: Table describing EIRP and PFD values for VLEO sub-constellation. Source: Table A.7-2 [15].
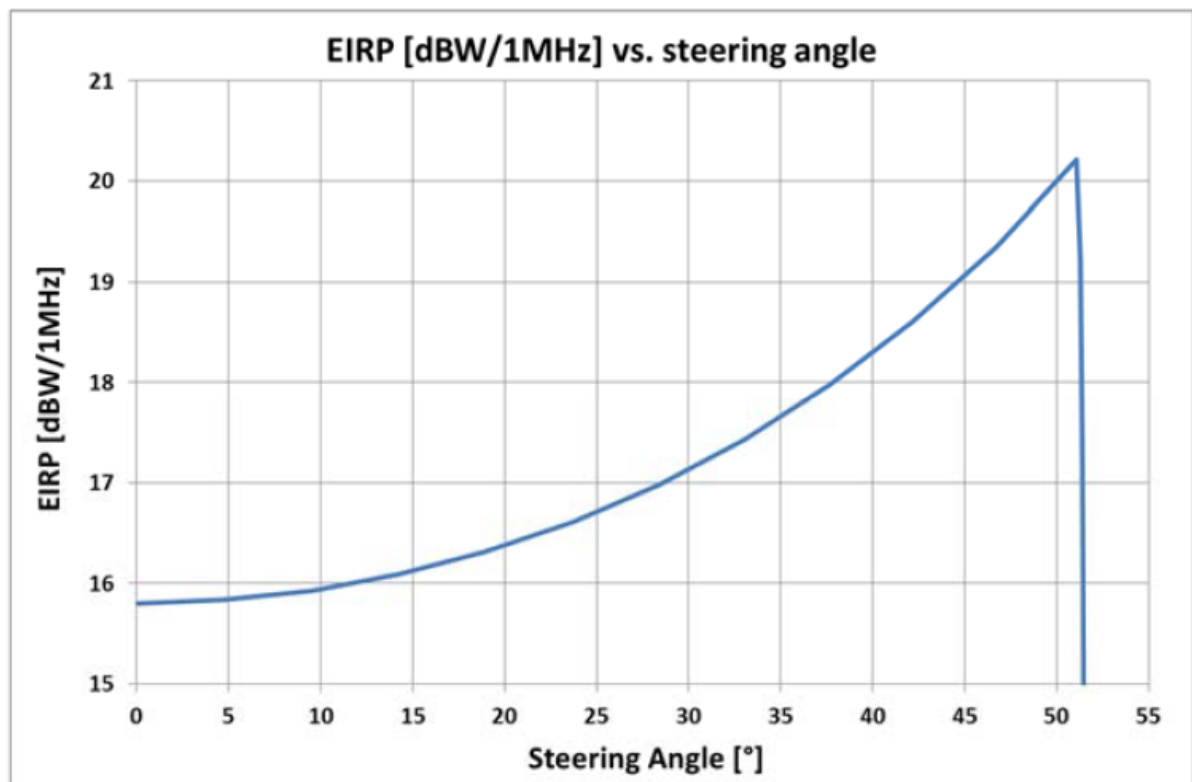
Figure 3.3: VLEO constellation's EIRP density vs steering angle. Source: Table A.7-2 [15].

The SpaceX VLEO sub-constellation, in particular, is also the one considered for the development of the model presented in this thesis.

3.2.3. Protection of GSO Communications

As previously stated, NGSO satellites will play a prominent role in the near future of telecommunications. Private companies have already started to launch their own satellites to develop new private constellations, which will inevitably become evermore dense. The high population of LEO satellites is raising awareness about the interference these NGSO communications can cause on GSO transmissions when the two systems operate at the same frequency band, even if partially. Surely, it will not be possible to completely cancel these interferences, however mitigation techniques are already being deployed to keep them under control to permit the GSO and NGSO systems to share the same frequency bands during operation. Current enforced regulations include coordination mechanisms between GSO and NGSO satellites, as well as hard limits on the aggregate emissions from NGSO space stations operating in the fixed-satellite service at the same frequency bands used by the GSO satellite system. [16] [17].
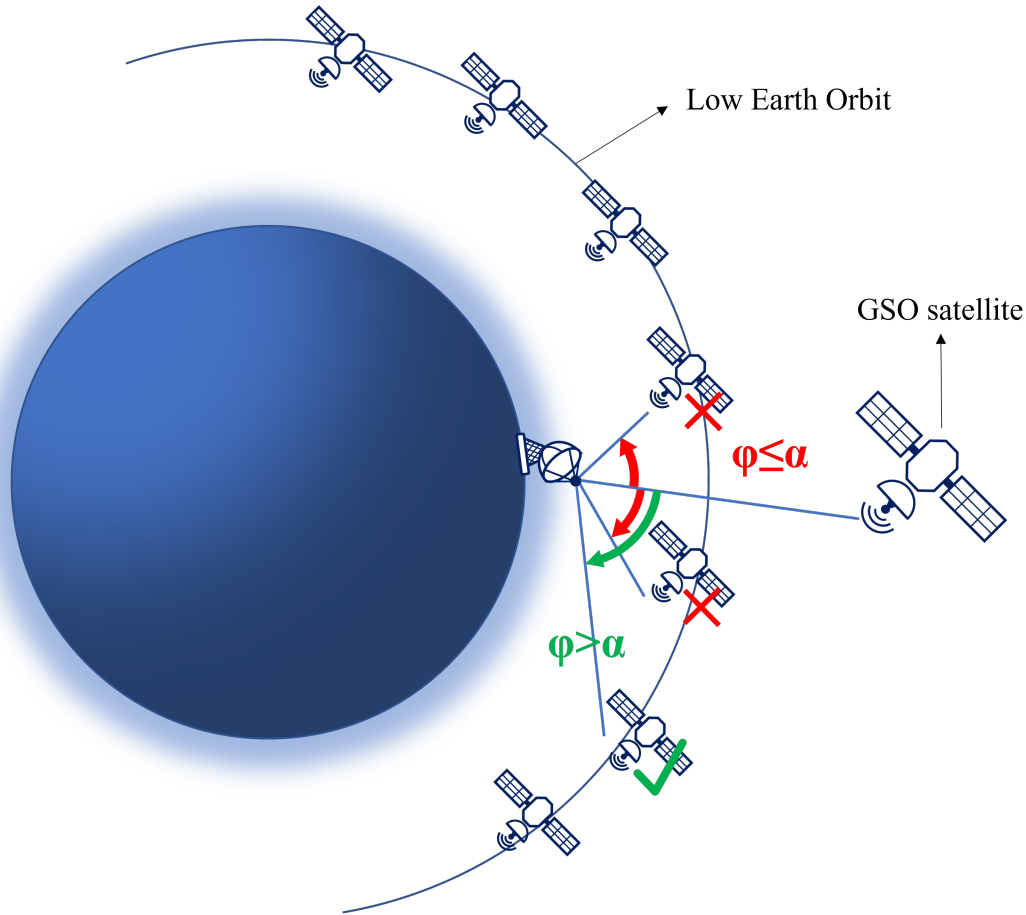
Figure 3.4: Coordination between NGSO constellation and GSO communications to ground station.

Figure 3.4 depicts the coordination mechanism between GSO and NGSO satellites triggered when the two systems operate in the same frequency band [18]. This method consists in preventing communications from NGSO satellites when they are too close to the line of sight of the GSO satellite communicating with a ground station. The worst case scenario, in fact, would be if a NGSO satellite transmits exactly along the line of sight between the GSO satellite and the ground station. However, even at a slightly shifted angle the interference could still be significant due to the coupling of significant side-lobes between the signals [19]. The angle formed between the line of sight of NGSO satellite-ground station and line of sight of GSO satellite-ground station, is commonly defined in literature as the *avoidance angle* or also *separation angle*, it is indicated in *Figure 3.4* as the angle ϕ. Whenever ϕ is lower or equal to a threshold hereafter indicated as α, the considered NGSO satellite must shut down its transmissions. The threshold α is established for every constellation by the satellite operators which deploys it.

However, the illustrated technique does not completely cancel interferences. Only the

NGSO satellites contained in the cone with vertex coinciding with the ground station and aperture equal to the threshold α will cease to transmit. All the satellites outside of the cone will maintain their communication active, inevitably causing interference with the GSO transmission to some extent. Therefore, it is instructive to study a scenario in which a fixed number of satellites with separation angle greater than the established threshold α are transmitting simultaneously with a GSO satellite.

3.3. Extension of the Simulator for NGSO Constellations

In this section the simulator implemented in *Chapter 2* will be extended to consider an input constellation of satellites with known geodetic coordinates: latitudes, longitudes and altitudes. This result are achieved thanks to the collaboration undertaken with *SES S.A.*, which provided the orbital data containing information over the geodetic coordinates of SpaceX VLEO sub-constellation.

The orbital data provided correspond to the 7,518 satellites in the same VLEO constellation reported in *Table 3.2*. For these satellites, a period of 5 days is spanned, with a resolution of 10 seconds. On the other hand, the rain events generated through *ST-MultiExcell* cover a whole year, meaning that 1460 slot events of 6 hours are available. One of the most interesting objective of a simulator for this case is to associate to every rain map the positions of the satellites of the considered constellation for the same instant of time. Since rain events are analysed with a temporal resolution of 30 seconds, the orbital data is also rearranged to consider only instants of time multiple of 30 seconds. For simplicity, the 5 days orbital data were reiterated from the beginning once fully analysed, therefore, in a year, 73 iterations of the same orbital data are considered. This choice does not actually impact on the correct application of the model. The simulator in fact, has the purpose to analyse long term simulated data, therefore 5 days are more than enough to exhaust all possible positions of LEO satellites orbiting in their inclination plane.

The first step in the procedure of the simulator is to load the orbital data of the constellation, as well as the geodetic coordinates of both the ground station and the considered GSO satellite. These coordinates, as expressed in *Section 3.1.5*, are related to a reference ellipsoid, which describe the shape of the Earth. In the case of the presented simulator, the chosen ellipsoid is the *WGS84*, the most widely accepted one. The orbital data, in the practical case, correspond to a matrix of dimensions 7,518×3×14,401, in which each row is associated to one of the 7,518 satellites orbiting in LEO, the columns describe

the latitude, longitude and altitude respectively of the selected satellite, while the third dimension refers to the evolution in time of the constellation for every 30 seconds.

Following, the coordinates are converted from geodetic to ECEF. As stated in *Section 3.1.5*, this reference system is indeed the most practical for calculations involving lines of sight of objects in space. After the conversion, what is obtained is a set of Cartesian coordinates (x, y, z), which can be exploited for standard calculations of Euclidean geometry. In this way, to each point of the space is associated a vector with its origin fixed in the center of mass of the Earth. It is very practical to also consider relative positions as vectors, for example the vectors extending from the ground station to each satellite is calculated by subtracting the initial point from the final one $(x_{sat}\text{-}x_{gs},\ y_{sat}\text{-}y_{gs},\ z_{sat}\text{-}z_{gs},)$
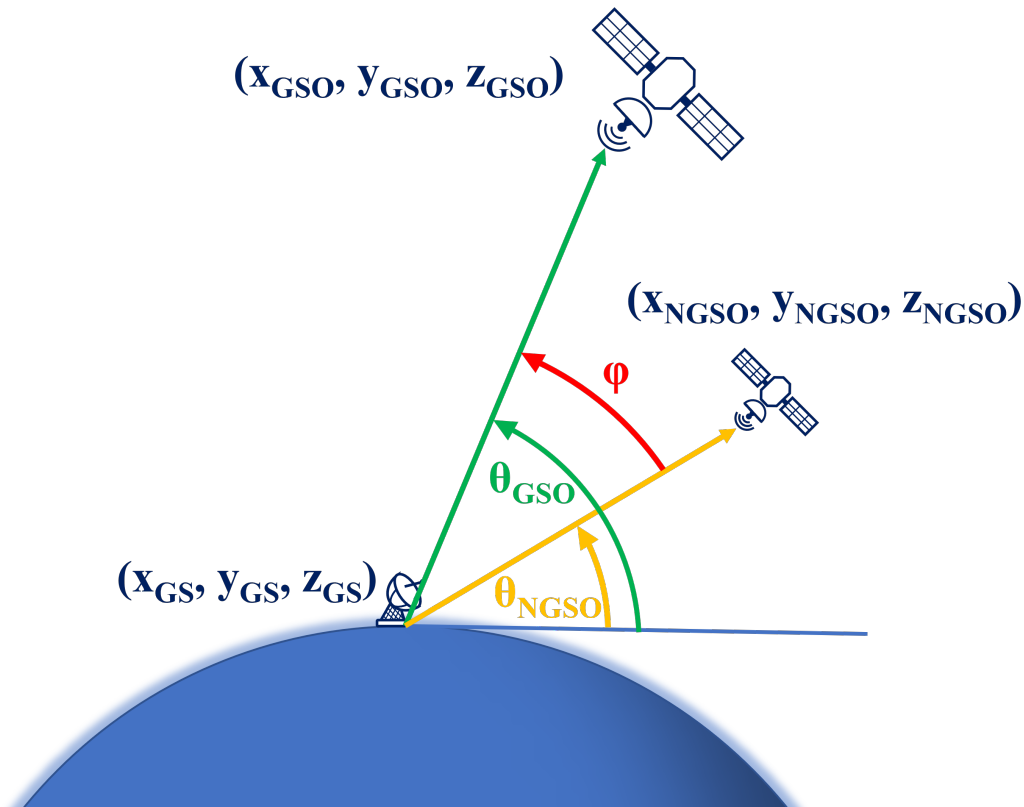
Figure 3.5: Vectors and angles in ECEF reference system.

As shown in *Figure 3.5*, the relative-position vectors are a convenient way not only to consider slant paths between the ground station and the satellite, but also to evaluate angles in space. Specifically, the angle between two vectors is calculated by inverting the dot product between them:

$$\mathbf{a} \cdot \mathbf{b} = ||a|| \, ||b|| \, cos(\Theta)$$
$$cos(\Theta) = \frac{\mathbf{a} \cdot \mathbf{b}}{||a|| \, ||b|} \tag{3.5}$$
$$\Theta = \cos^{-1} \left(\frac{\mathbf{a} \cdot \mathbf{b}}{||a|| \, ||b|} \right)$$

At the next step, the simulator selects one of the 7,518 satellites and considers a tuple containing the coordinates of the ground station, the GSO satellite and the NGSO satellite. The elevation angle relative to the link ground station - NGSO satellite is calculated and the satellite is marked as "in view" if the elevation angle is greater than a certain threshold, in this case set to 5°. Once it is known that the NGSO satellite is visible from the ground station, the simulator evaluates if it can also cause interference with the GSO communications. To do so, the parameter α, which was already defined in *Section 3.2.3* as the threshold of the avoidance angle, is an additional input of the model. A NGSO satellite with avoidance angle below this threshold shuts down its transmissions, therefore not causing any interference. On the other hand, if the avoidance angle is greater than α the satellite maintains the transmissions active, inevitably interfering with the GSO communications.

Therefore, the following step is to calculate the avoidance angle ϕ between the selected NGSO satellite and the GSO satellite. Subsequently, ϕ is compared with the threshold α and, if ϕ is indeed above this threshold, that in view satellite is also marked as "interfering".

This same procedure is repeated for every satellite of the NGSO constellation for the considered time instant. Once the set of interfering NGSO satellites is obtained, a final parameter plays its role. This parameter, **Nco**, is another input of the simulator and determines how many NGSO satellites in the interfering set are allowed to transmit, out of those that are in visibility of the ground station. For example, if Nco is equal to 8, then 8 satellites will be chosen from the interfering set and allowed to transmit, the remaining must refrain from transmitting. This choice is made by some criteria, which can be randomic, for which Nco satellites are chosen randomly from the set, or by minimizing the avoidance angle, according to which the Nco satellites with the lowest avoidance angles are selected from the set.

3.4.   Power Budget Simulator

At this point, the simulator possesses all the information necessary to calculate the power budget relative to the links between the ground station and each satellite. For each instant of time, the procedure described to identify the interfering NGSO satellites is repeated to find the set to consider. Moreover, the 200 km × 200 km rain map associated to the same time instant is also examined.

The simulator positions the ground station at the center of the map and initiate the procedure described in *Section 2.5.1* to define the projection of the slant path of the link onto the rain map. This step, in particular, is firstly carried out for the link towards the GSO satellite and then repeated for each of the interfering NGSO satellites. It is possible to now evaluate the rain attenuation affecting each one of the links according to the rain map.

The power budget (for this example the downlink Space-to-Earth is considered) can be calculated with knowledge of the EIRP associated to the GSO satellite and the PFD characterizing the NGSO satellites. Obviously, it is also necessary to consider the information related to the receiving antenna of the ground station. These values are evaluated together with the rain attenuation, which once again is the main source of atmospheric impairment for the considered Ka/V bands, to calculate the power received by the ground station:

$$P_{rx,GSO}[dBW] = EIRP_{GSO}[dBW] + G_{rx}[dBi] - fsl_{GSO}[dB] - Att_{rain,GSO}[dB] \quad \text{(3.6a)}$$

$$P_{rx,NGSO}[dBW] = PFD_{NGSO}\left[dB\left(\frac{W}{m^2}\right)\right] + A_{eff,GS}[dB(m^2)] - Att_{rain,GSO}[dB] \quad \text{(3.6b)}$$

where the term *fsl* stands for the *free space loss* relative to the link, which is defined as $fsl = \left(\frac{4\pi d}{\lambda}\right)^2$, G_{rx} is the receive gain of the antenna of the ground station and A_{eff} is the effective area of the receiving antenna defined as $A_{eff} = \frac{Gain_{rx}\lambda^2}{4\pi}$.

In particular, the power budget is calculated for each one of the interfering NGSO satellites and the total interfering received power is evaluated as the sum in Watt of all contributions received by the ground station:

$$P_{interfering}[W] = \sum_{i}^{Nco} 10^{\frac{P_{rx,NGSO,i}[dBW]}{10}} \quad \text{(3.7)}$$

4 | Results and Modelling Activity

4.1. Description of the Scenario

The simulator described in *Chapter 2* and *Chapter 3* allows to analyse a scenario in which a GSO satellite is communicating with a ground station while a constellation of NGSO satellites is interfering. Ultimately, it is possible to calculate the power received from both the GSO satellite and the single satellites of the NGSO constellation, also accounting for the attenuation caused by rain along the paths. For long enough simulated time periods, it is possible to collect a significant amount of data of the physical quantities of interest. For example, it is possible to study the long-term statistics of rain attenuation on the examined site. Furthermore, another important feature of the simulator is that, once the data are collected, the design of the system can be significantly facilitated. By exploiting the stored values of received power in dBW, it is possible to evaluate the system performance for different antennas and transmit power by simply subtracting the former parameter, e.g the EIRP, and add back the newly considered one. The stored simulated data can thus be conveniently exploited even for different scenarios, allowing to easily study the long term statistics of the system.

This chapter presents the results obtained after simulating the interaction between the GSO system and the NGSO one for a specific site, to show how effectively the collected data can facilitate the system design. Moreover, along with the results, the chapter also addresses a method to implement a statistical model based on the long-term statistics of rain attenuation, in order to statistically generate values of the atmospheric impairment as a more convenient alternative to running long simulations.

4.1.1. Space segment

The NGSO constellation of interest is the sub-constellation of SpaceX operating at LEO and at *V* band, whose orbital data were provided by *SES S.A.*. Specifically, the scenario analysed is a space-to-Earth communication downlink in which the GSO and the NGSO satellites both operate at 40 GHz. The main objective of the analysis of this scenario is to

investigate the interference caused by the NGSO spacecrafts when operating in the same frequency band of the GSO satellite. The NGSO constellation include 7,518 satellites, almost uniformly distributed along the orbits at altitude 345.6 km, 340.8 km and 335.9 km. The PFD adopted by the single NGSO satellites is equal to the one reported in *Table 3.3*: PFD = -105.72 dB$\left(\frac{W}{m^2\,1MHz}\right)$. Hereafter, when not differently specified, the avoidance angle threshold α is assumed to be 0.

The GSO satellite considered for the communications with the ground station is chosen so that the ground station link elevation angle is as close as possible to 30°. Its geodetic coordinates are:

- *latitude* : 39°

- *longitude* : 0°

- *altitude* : 35,786 km

The remaining key parameters to be considered for the GSO spacecraft are selected as indicated in Resolution 770 of ITU-R [20] "*Application of Article 22 of the Radio Regulations to the protection of geostationary fixed-satellite service and broadcasting-satellite service networks from non-geostationary fixed-satellite service systems in the frequency bands 37.5-39.5 GHz, 39.5-42.5 GHz, 47.2-50.2 GHz and 50.4-51.4 GHz*". More in details, referring to the space-to-Earth downlink, the parameters corresponding to the GSO satellite transmitting the signal are:

- *EIRP density* $\left[\frac{dBW}{MHz}\right]$ *(Gateway)* : 36

- *Bandwidth [MHz]* : 1

Finally, both the signals coming from the GSO and NGSO systems have a circular polarization with the same rotation direction.

4.1.2.   Ground station

The selected site for the analysed scenario is located in Spino d'Adda, near Milano, Italy. The coordinates that identify the site are:

- *latitude* : 45.4°

- *longitude* : 9.5°

- *altitude* : 0.084 km

The ground terminal is assumed to be a fixed gateway. The considered ground receive

antenna is manufactured by ©*CPI Vertex Antennentechnik GmbH*, *Figure 4.1* illustrates a drawing of the antenna and enlists its specifications, while *Figure 4.2* shows the radiation pattern. The corresponding antenna radiation pattern is the one indicated in Resolution S.580 of ITU-R, which describes the radiation diagrams to be used for antennas of Earth stations operating with GSO satellites [21]. Specifically, the main parameter of interest for the ground station is the implemented maximum receive gain, which is $G_{rx} = 59.6$ dBi for the considered frequency of 40 GHz of the simulated scenario.

Freq. Pol.	Tx	$47,85 - 48,15$GHz
	Rx	$37,85 - 38,15$GHz
	Beacon	39,4GHz, 45deg
Sidelobes	ITU 732, ITU-R S580	
Feed	2 port feed linear polarised	
G/T	@38GHz, elev. 20°, LNA 230K	33,8 dB/K
Gain	@ 48/38GHz	61,18dBi/ 59,08dBi
Pattern BW	-3dB @38GHz	0,17°
	-3dB @48GHz	0,14°
Power	< 50W operation, 250W (max)	

Figure 4.1: On the left CAD drawing of the 3m Q/V band antenna ©*CPI Vertex Antennentechnik GmbH* and on the right its specifications.
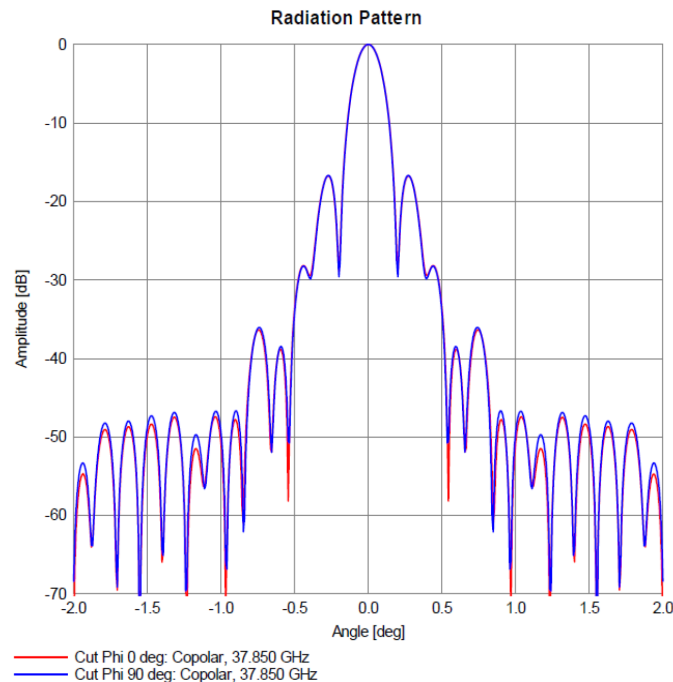
Figure 4.2: RX antenna pattern ©*CPI Vertex Antennentechnik GmbH*.

The bandwidth characterizing the receive antenna is once again indicated in Resolution 770 [20] for the case of a receiving gateway, $Bandwidth = 1$ MHz.

4.2.   Rain Attenuation simulated on GSO path

As described in *Chapter 2* and *Chapter 3*, the simulator analyses the yearly evolution of a fixed-satellite service in which a GSO satellite is communicating with the ground station while a NGSO constellation is interfering. Once the simulation is completed, the data collected provide information about many parameters of interest, mainly rain attenuation on both GSO and NGSO paths as well as the power received from each space satellite. These data can be further examined in order to study the long-term statistics of each of the parameters.

Additionally, it is important to remark that the analysed results are conditioned to the probability of having non-zero rain attenuation on the path between the ground station and the GSO satellite. Indeed, this is the most detrimental case: the ground station signal-to-noise ratio is already lowered by the presence of rain along the link and the interfering power contributes even more to its decrease.

This chapter, as stated, will thoroughly examine the relationships among system parameters. Therefore hereafter, for simplicity's sake, the rain attenuation affecting the link between the ground station and the GSO satellite will be indicated as $\boldsymbol{A_{GSO}}$, while the rain attenuation on the path extending from the ground station to a NGSO satellite will be referred to as $\boldsymbol{A_{NGSO}}$. On the other hand, the avoidance angle will be indicated as $\boldsymbol{\phi}$, as it was denominated in *Figure 3.5*.

In this section, specifically, the results obtained for the collected data of rain attenuation along the GSO satellite path, A_{GSO}, are presented and discussed. *Figure 4.3* illustrates how the long-term statistics of the data can be studied by analysing the associated *Empirical Complementary Cumulative Distribution Function* (ECCDF). This function is particularly interesting since it associates to each value *X** the corresponding *exceedance probability P(X>X*)*. The results in *Figure 4.3* definitely point out that, at 40 GHz, rain induces a significant attenuation, even exceeding 200 dB in few cases.
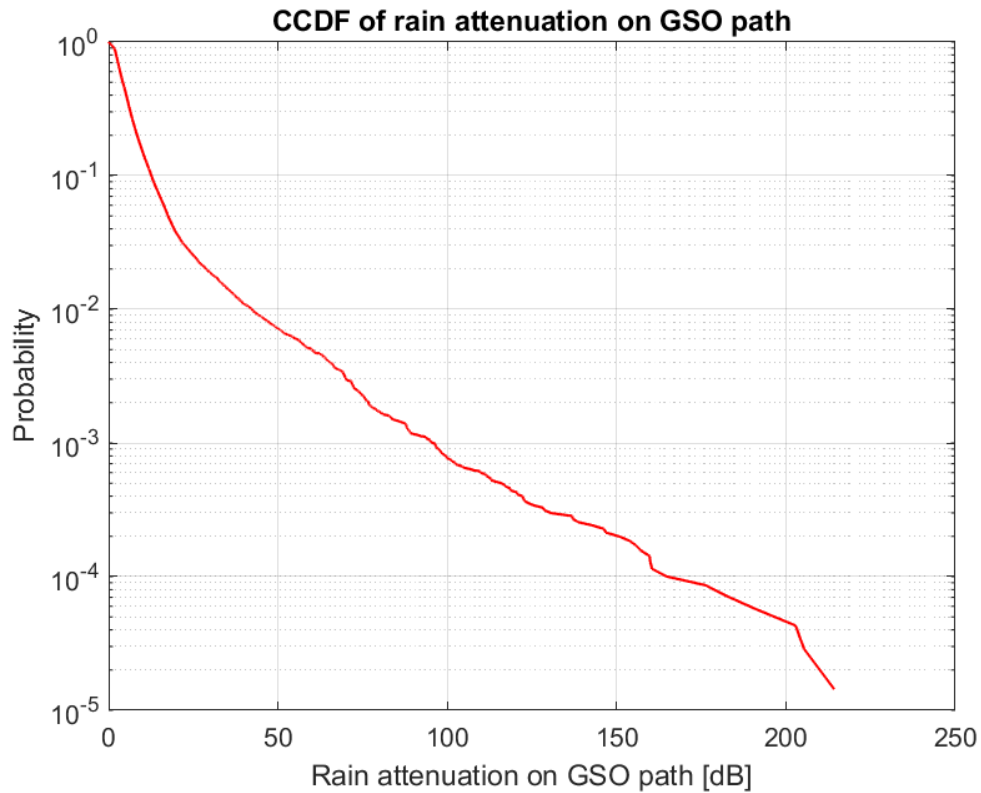
Figure 4.3: Complementary Cumulative Distribution Function of rain attenuation on GSO path.

At this point, it is interesting to study how these data are actually statistically distributed, in order to exploit this information to develop a statistical model. To this aim, as a first step, a number of possible fitting distributions can be considered. Every statistical distribution is characterized by a specific shape, which varies depending on the parameters defining the distribution itself. The parameters of the fitting distribution are identified by maximum likelihood estimation.

If there is no prior information or assumption over the possible family distribution to associate to the empirical data, it is helpful to define a quality-checking parameter that describes how accurately a specific distribution fits the data. This parameter can for example evaluate how significant the fitting error is when attempting to fit the distribution to the data. An error of this kind can simply be calculated by evaluating the squared distance for fixed values of probability between the Empirical-CCDF and the CCDF of the statistical distribution fitting the data:

$$\epsilon(P) = |X_{ECCDF}(P) - X_{CCDF}(P)|^2 \qquad (4.1)$$

where *X(P)* represents the value generating the CCDF for which the exceedance probability is equal to *P*. The error ϵ is averaged over a set of probability values and is thus associated to the corresponding statistical distribution. The same procedure is repeated so that a fitting error is associated to each distribution of the considered set and, finally, the distribution with minimal error is selected.

Figure 4.4 shows how the Empirical CCDF of the collected data can be accurately modelled with a log-normal distribution, since the two curves follow a very similar trend. Therefore, it can be claimed that the data collected corresponding to A_{GSO} is distributed almost according to a log-normal distribution.
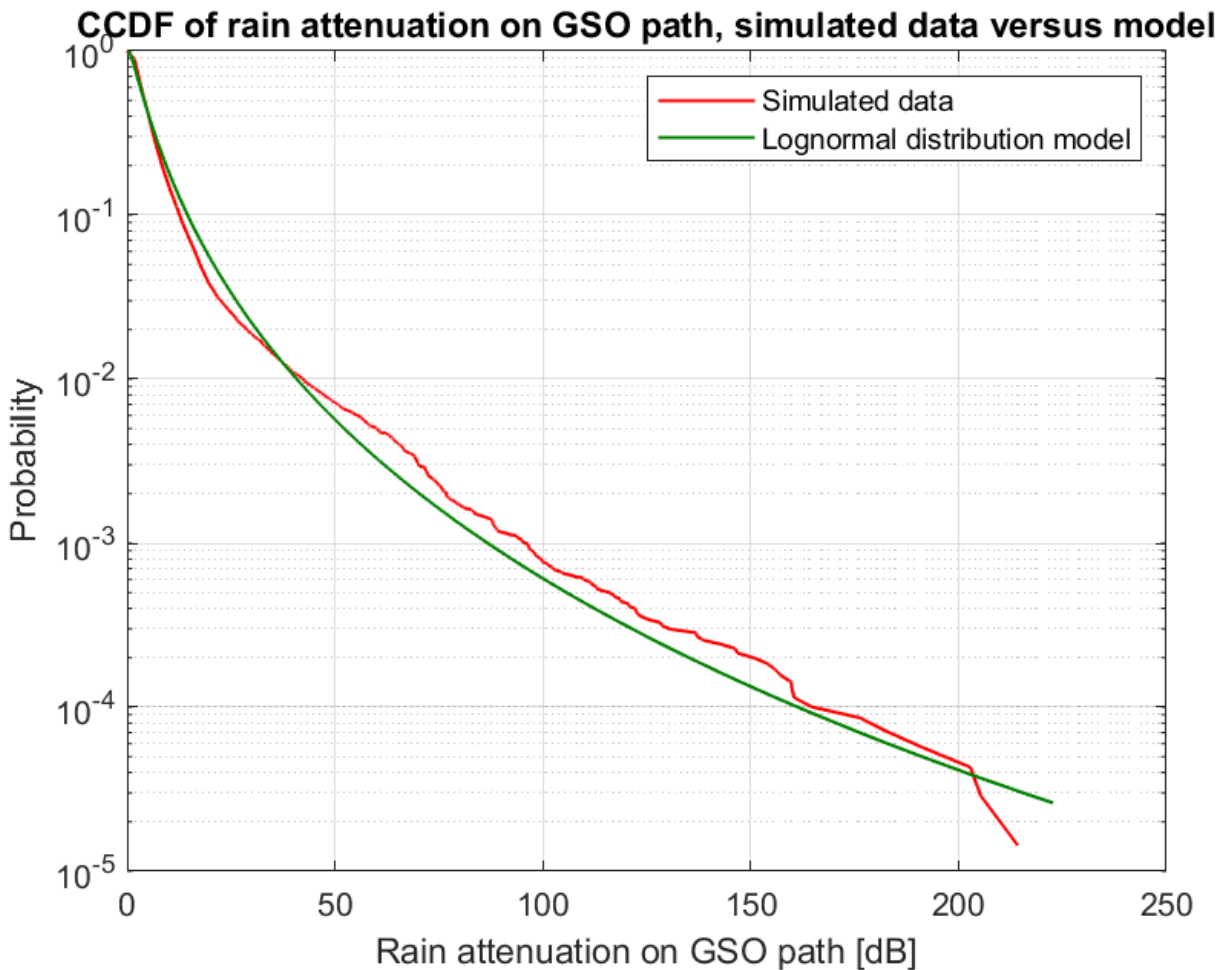
Figure 4.4: Complementary Cumulative Distribution Function of rain attenuation on GSO path for both simulated and modelled data.

This result is particularly noteworthy since it proves the correct functioning of the simulator. Indeed, in literature, the long-term statistics of the rain attenuation for mid-latitudes sites are known to be well approximated by a log-normal distribution [5] [22], with Prob-

ability Density Function defined by the expression [23]:

$$y = f_X(x|\mu, \sigma) = \frac{1}{x\,\sigma\,\sqrt{2\,\pi}}\, exp\left(\frac{-(\log x - \mu)^2)}{2\sigma^2}\right) \;\; for\; x > 0 \tag{4.2}$$

The specific values of the two parameters μ and σ used in the distribution fit, as illustrated in *Figure 4.4*, are:

- μ : 1.2336

- σ : 0.9699

4.3. Rain Attenuation simulated on NGSO path

The same procedure is thus repeated to analyse the rain attenuation affecting the links between the ground station and the NGSO satellites, A_{NGSO}. The obtained CCDF of this parameter can be observed in *Figure 4.5*.
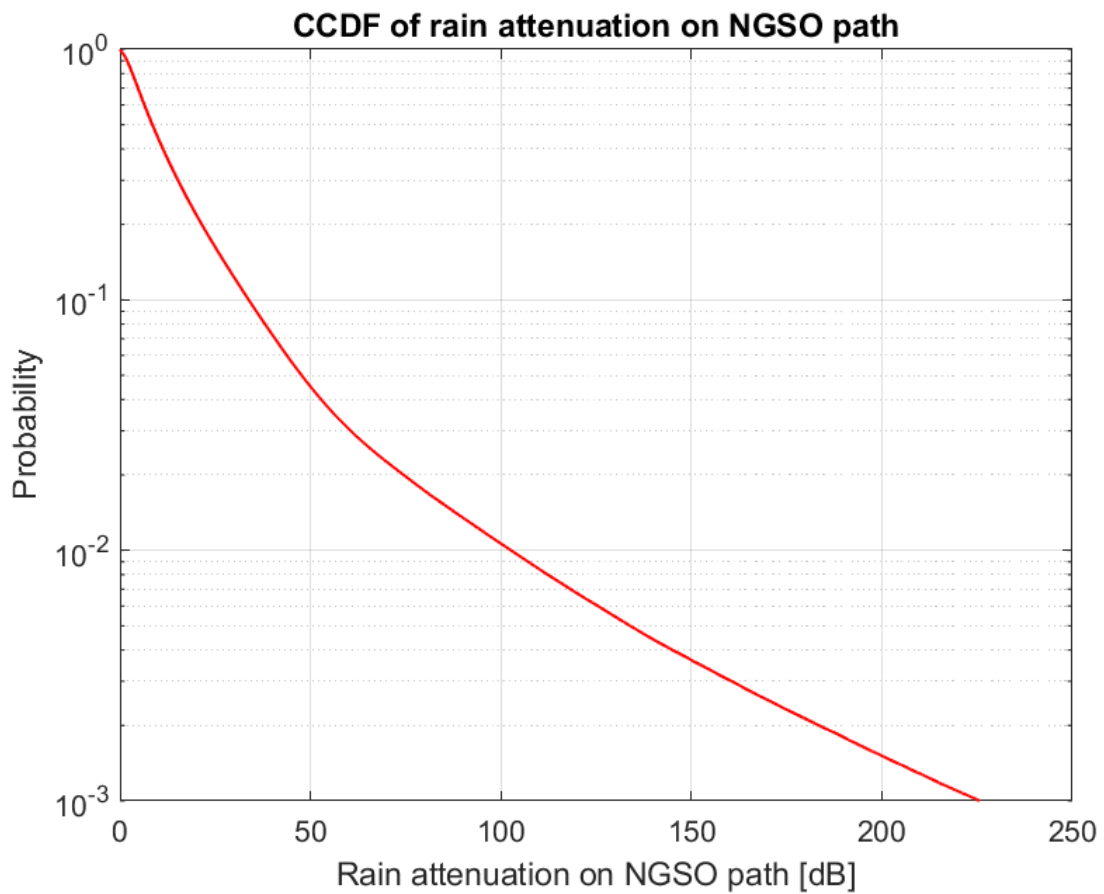
Figure 4.5: Complementary Cumulative Distribution Function of rain attenuation on NGSO path.

It is worth noticing that rain attenuation values are even higher than those obtained for the GSO link, mainly due to the low elevation angles considered when dealing with NGSO constellations. Indeed, the data collected in this case does not correspond to a scenario in which the communication satellite appears as a motionless object in the sky by the ground station. In fact, the NGSO satellites are in continuous movement, leading to constant changes in the elevation angle, azimuth and slant path of the links with the ground station. The simulator collects data for all the satellites in visibility from the ground station and potentially interfering with the GSO ground station. Therefore, the analysis of A_{NGSO} must consider the aggregation of all interfering satellites, each one characterized by different parameters. As can be observed from *Figure 4.6*, in this case the Empirical CCDF is not well approximated by a log-normal distribution, but better results can be achieved when modelling the data through a *Burr type XII* distribution fit.
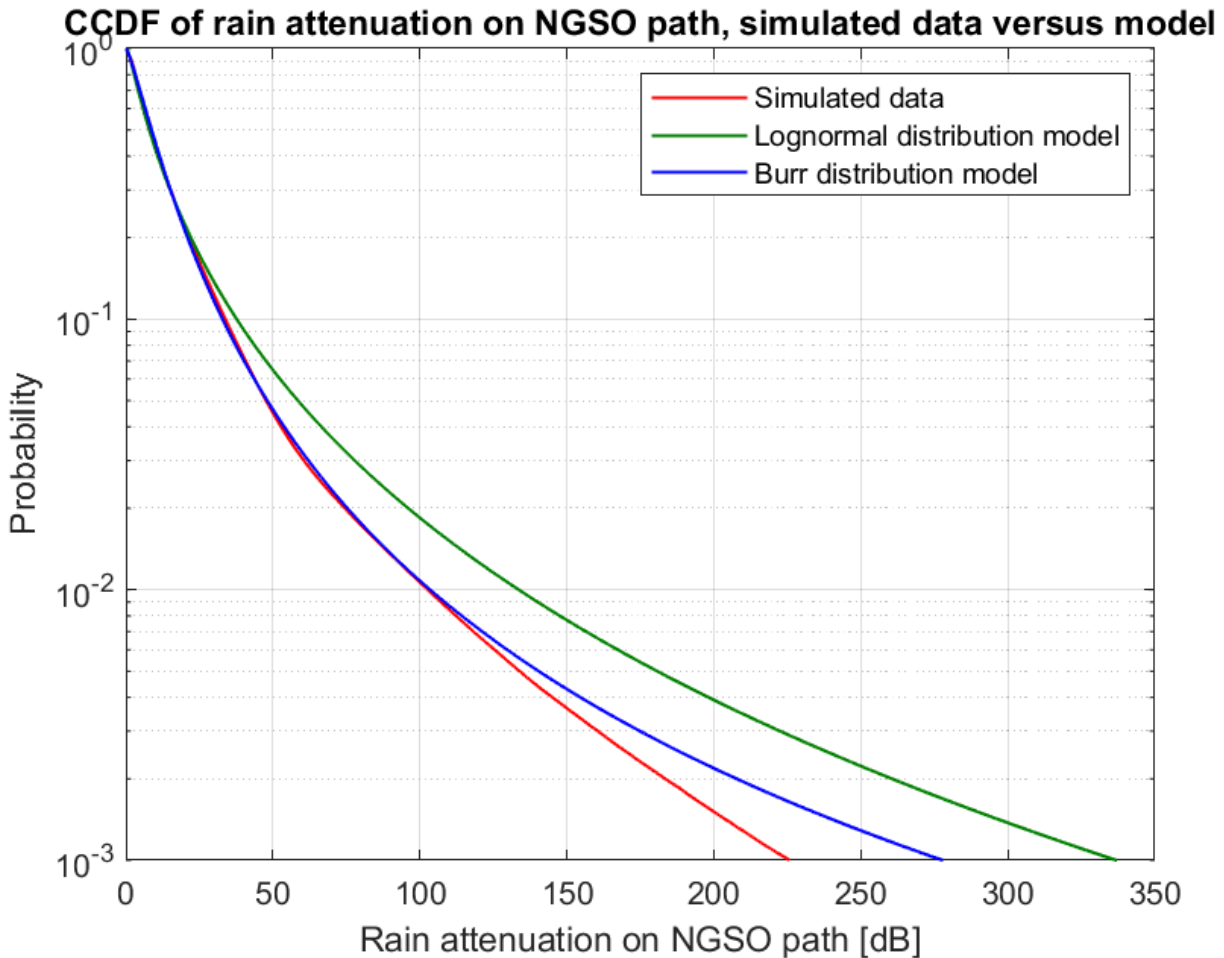
Figure 4.6: Complementary Cumulative Distribution Function of rain attenuation on NGSO path for both simulated and modelled data.

The Burr type XII distribution is defined as follows [24]:

$$f(x|\alpha, c, k) = \frac{\frac{kc}{\alpha} \left(\frac{x}{\alpha}\right)^{c-1}}{\left(1 + \left(\frac{x}{\alpha}\right)^c\right)^{k+1}}$$ (4.3)

for $x>0$, $\alpha>0$, $c>0$ and $k>0$. The corresponding fitting parameters are:

- α : 17,4316

- c : 1.2544

- k : 1.9714

Meanwhile, the parameters for the log-normal distribution fit are:

- μ : 2.0769

- σ : 1.2113

It is instructive, therefore, to study the behaviour of A_{NGSO} depending on different parameters for a more accurate model development, which will in fact be the focus of the next section.

4.4.   Correlation Analysis

In this section, results illustrating the relationship among A_{NGSO} and other system parameters are presented. One of the most useful tools exploited to analyse the relationship among these parameters is the intensity plot. An intensity plot can be interpreted as the 2D projected view of a 3D histogram, in which every vertical column of the 2D projected plane is normalized by the maximum value belonging to the column itself. In this way, it is possible to visualize, for each column, how the values distribute along the vertical direction. The colors of the intensity plot depict the density of points belonging to the specific pixel identified by an horizontal and a vertical bin; blue indicates low level of density while the maximum concentration is represented by shades of red.

Among all the system parameters, the avoidance angle ϕ, defined as the angle seen by the ground station spanning from the GSO satellite to a NGSO satellite, as in *Figure 3.5*, is of particular interest. In fact, as explained in *Chapter 3*, this parameter is used to determine if a NGSO satellite is too close to the line of sight between the ground station and the GSO satellite and, thus, if it should refrain from transmitting. To more coherently model A_{NGSO}, it is necessary to discern between the different NGSO spacecrafts and their properties. To study the relationships among the main parameters, the collected simulated data is thus organized in tuples containing A_{GSO}, A_{NGSO} and ϕ for the considered NGSO

satellite.

Figure 4.7 depicts the intensity plot of A_{NGSO} versus the corresponding avoidance angle. In the intensity plot, each column, i.e. a given limited range on the x-axis, is normalized by its maximum value and, therefore, it reflects the way the data are distributed along the vertical axis. This property is important to visualize the shape of the Probability Density Function of the values for the given column. In fact, colors tending to the red indicate a higher concentration of points, meaning that the probability for values to fall in that pixel is higher. Therefore, these plots offer important information on the statistical relationships among parameters.

From *Figure 4.7* it is possible to observe that depending on the value of the ϕ, A_{NGSO} is characterized by a different trend, which indicates a change in its PDF. This property is even more evident when comparing the above intensity plot with *Figure 4.8*, which represents once again an intensity plot, but this time of A_{GSO} versus the ϕ. This last plot shows that independently of the avoidance angle, the rain attenuation on the GSO path maintains the same distribution (in this case, log-normal), proving the independence between the two parameters. The intensity plot of *Figure 4.7*, however, shows that the analysed parameters do not appear to be independent, in fact different values of avoidance angle lead to a different distribution of the rain attenuation affecting the NGSO path. Therefore, in order to model this parameter it would be necessary to also consider its dependence on ϕ.

Intensity plot of rain attenuation on NGSO path versus avoidance angle
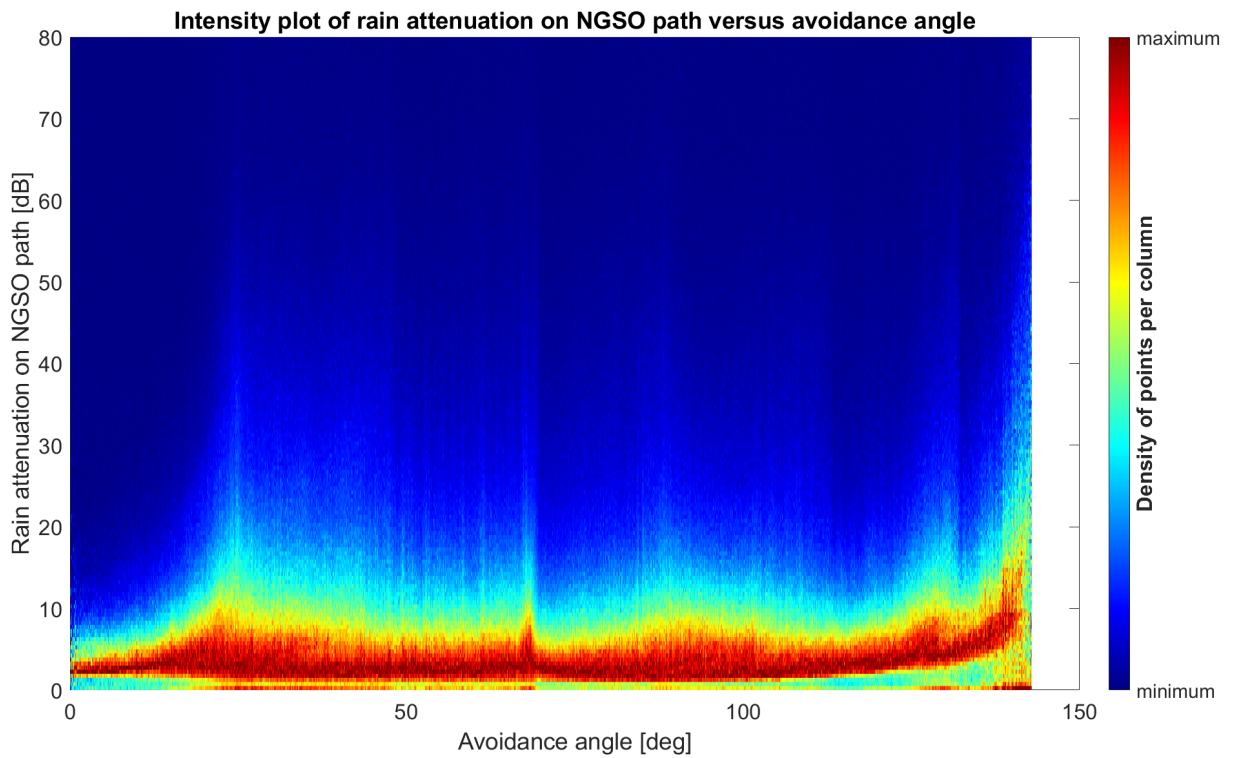
Figure 4.7: Intensity plot of rain attenuation on NGSO path versus avoidance angle.

Intensity plot of rain attenuation on GSO path versus avoidance angle
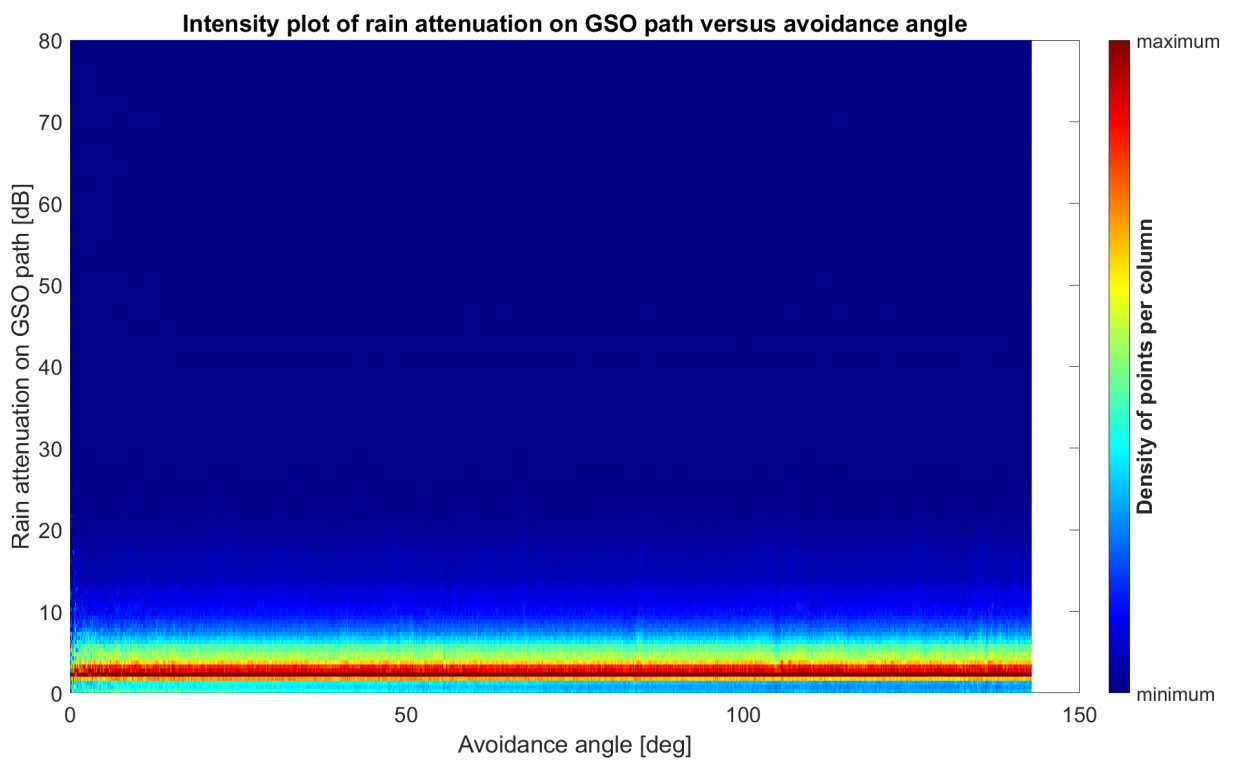
Figure 4.8: Intensity plot of rain attenuation on GSO path versus avoidance angle.

It is also noteworthy to point out that the intensity plot of *Figure 4.7* reflects in some way the geometry of the avoidance angles. Analysing the PDF of the avoidance angle, as shown in *Figure 4.9*, two peaks stand out, localized for angles around 25° and 69°, which coincide with the peaks in the corresponding intensity plot.
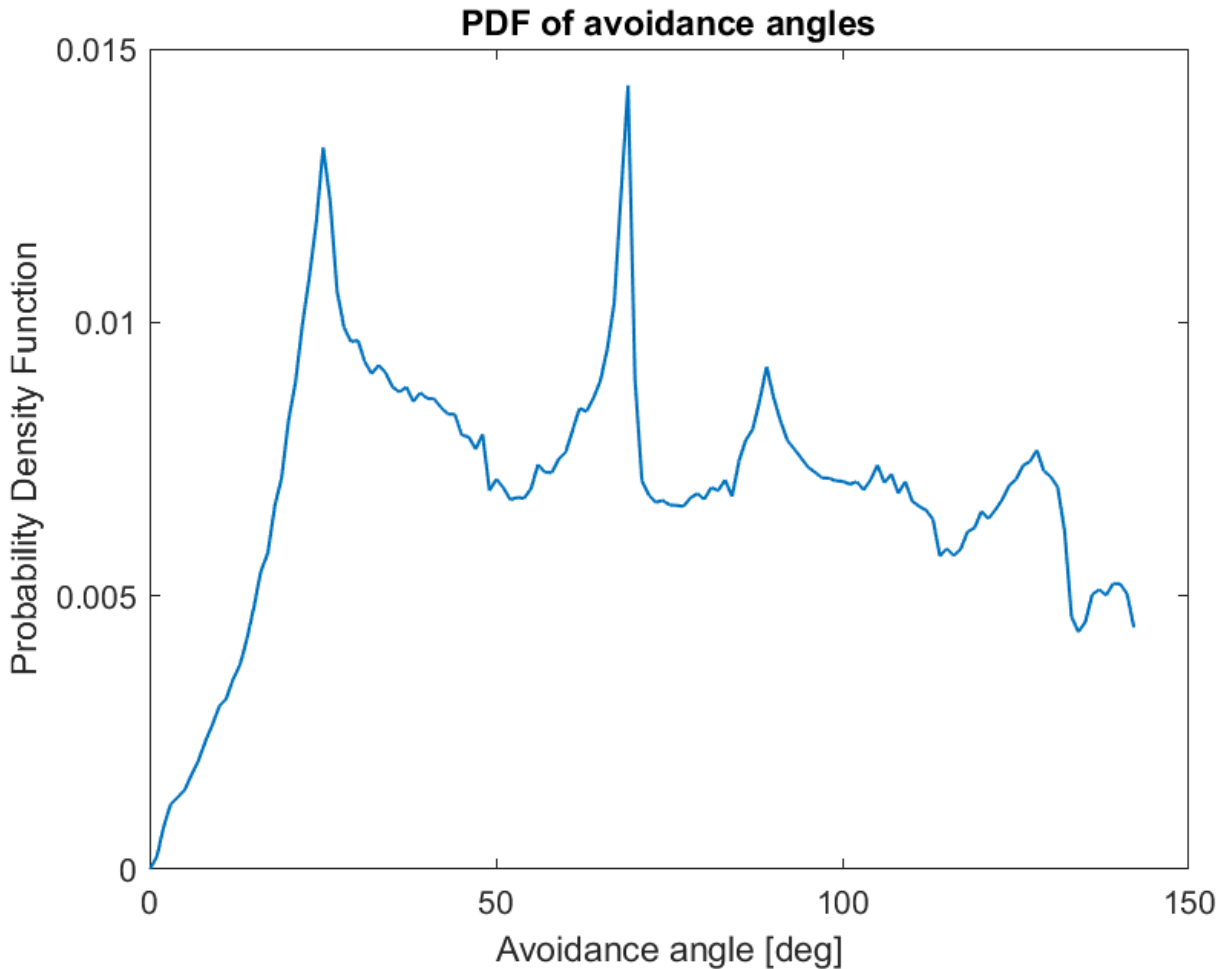
Figure 4.9: Probability Density Function of avoidance angle.

One final intensity plot, illustrated in *Figure 4.10*, shows the relationship among the attenuation affecting the GSO path and the one of the NGSO path. The trend shows that the relationship among the two parameters is fairly defined until 40∼50 dB, meanwhile beyond this value of attenuation the two parameters appear to be less correlated. This intensity plot, in particular, remarks a direct relation between the two rain attenuations. In fact, it is to be expected that if the GSO path is affected by rain the NGSO path is likely to experience the same, but less or more depending on whether the NGSO link elevation is higher or lower than the one of the GSO link, respectively. This result reflects the space correlation of rain fields and it is a key result since it proves the correlation

between A_{NGSO} and A_{GSO} up to a certain extent.
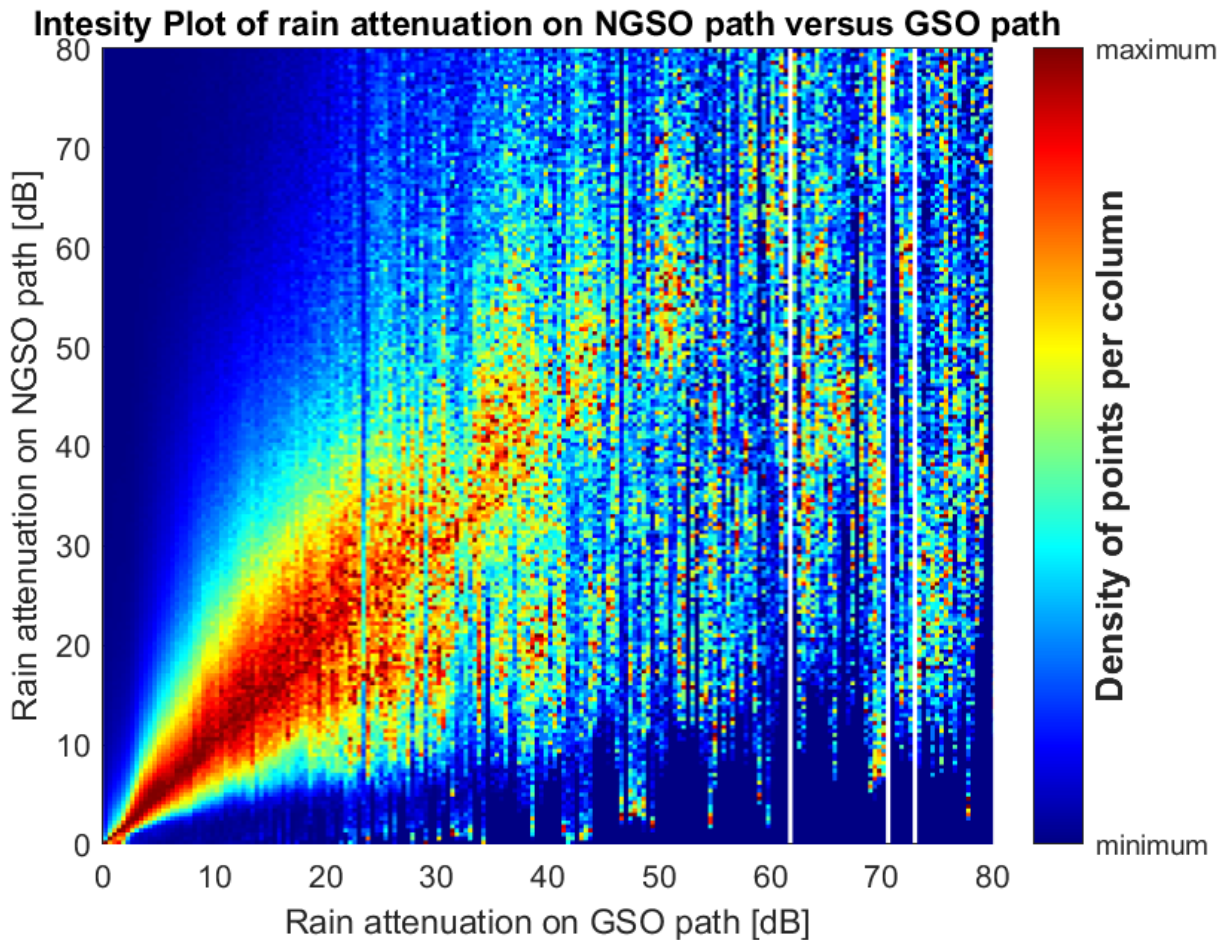
Figure 4.10: Intensity plot of rain attenuation on NGSO path versus GSO path.

4.5. Analytical Method to Generate Rain Attenuation on NGSO path

In this section, the information presented above is exploited in order to develop a statistical model to generate coherent rain attenuation affecting the link between the ground station and a generic NGSO satellite: this is, indeed, quite a complex task, which can be achieved only with simulations similar to those presented in this work, as no measurements of this kind are currently available yet. On the other hand, data collected from GSO ground stations are widely available, so a model linking statistically A_{NGSO} to A_{GSO} would allow proper interference results to be achieved in a less computationally intensive way.

4.5.1.   Model Development

As discussed in *Section 4.4*, A_{NGSO} is expected to depend on A_{GSO} as well as on the corresponding avoidance angle. When the link between ground station and GSO satellite is affected by heavy rain, the rain attenuation on the path towards a NGSO satellite should also experience a high attenuation. Moreover, the A_{NGSO} distribution obtained should reflect the trend depicted in the intensity plot of *Figure 4.7*.

This information can be summarized using probability theory. A_{NGSO}, A_{GSO} and ϕ can in fact be considered as three random variables, which assume values depending on the Probability Density Function they are characterized with. In order to coherently model A_{NGSO} accounting for A_{GSO} and the avoidance angle ϕ, it is necessary to consider the conditional probability:

$$
\begin{aligned}
P(A_{NGSO}|A_{GSO},\phi) &= \frac{P(A_{GSO},\phi|A_{NGSO})P(A_{NGSO})}{P(A_{GSO},\phi)} = \\
&= \frac{P(A_{GSO}|\phi,A_{NGSO})P(\phi|A_{NGSO})P(A_{NGSO})}{P(A_{GSO},\phi)} = \\
&= \frac{P(A_{GSO}|A_{NGSO})P(\phi|A_{NGSO})P(A_{NGSO})}{P(A_{GSO},\phi)} = \\
&= \frac{P(A_{NGSO}|A_{GSO})P(A_{GSO})}{P(A_{NGSO})}\frac{P(A_{NGSO}|\phi)P(\phi)}{P(A_{NGSO})}\frac{P(A_{NGSO})}{P(A_{GSO},\phi)} = \\
&= \frac{P(A_{GSO})P(\phi)}{P(A_{GSO},\phi)}\frac{P(A_{NGSO}|A_{GSO})P(A_{NGSO}|\phi)}{P(A_{NGSO})} = \\
&= \frac{P(A_{GSO})P(\phi)}{P(A_{GSO})P(\phi)}\frac{P(A_{NGSO}|A_{GSO})P(A_{NGSO}|\phi)}{P(A_{NGSO})} = \\
&= \frac{P(A_{NGSO}|A_{GSO})P(A_{NGSO}|\phi)}{P(A_{NGSO})}
\end{aligned}
\tag{4.4}
$$

This relation is true only if $P(A_{GSO}|\phi,A_{NGSO})$ = $P(A_{GSO}|A_{NGSO})P(\phi|A_{NGSO})$, resulting in the conditional independence between A_{GSO} and ϕ given A_{NGSO}. This conditional independence can actually be empirically tested by taking advantage of the collected data and visualizing their relation through intensity plots. The expression $P(A_{GSO}|\phi,A_{NGSO})$ = $P(A_{GSO}|A_{NGSO})$ means that the distribution of A_{GSO}, conditioned to A_{NGSO} is not affected by the change of the avoidance angle ϕ. To prove this statement, the simulated data, organized in tuples as described in *Section 4.4*, are further sub-divided into classes for fixed intervals of the avoidance angle. The values for the intervals of ϕ are selected so that to each class is associated the same number of tuples containing A_{GSO} and A_{NGSO}. An intensity plot relating both the rain attenuation is thus considered for each class of

the avoidance angle, as depicted in *Figure 4.11* and *Figure 4.12*.

These figures empirically show that for different classes of the avoidance angle, the distribution of A_{GSO} substantially does not change when conditioned to A_{NGSO}, ultimately proving the conditional independence between A_{GSO} and ϕ given A_{NGSO} and thus that the analytical method (4.4) can be used.

(a) Classes 0° - 25.1°

(b) Classes 25.1° - 38.4°

(c) Classes 38.4° - 54.6°
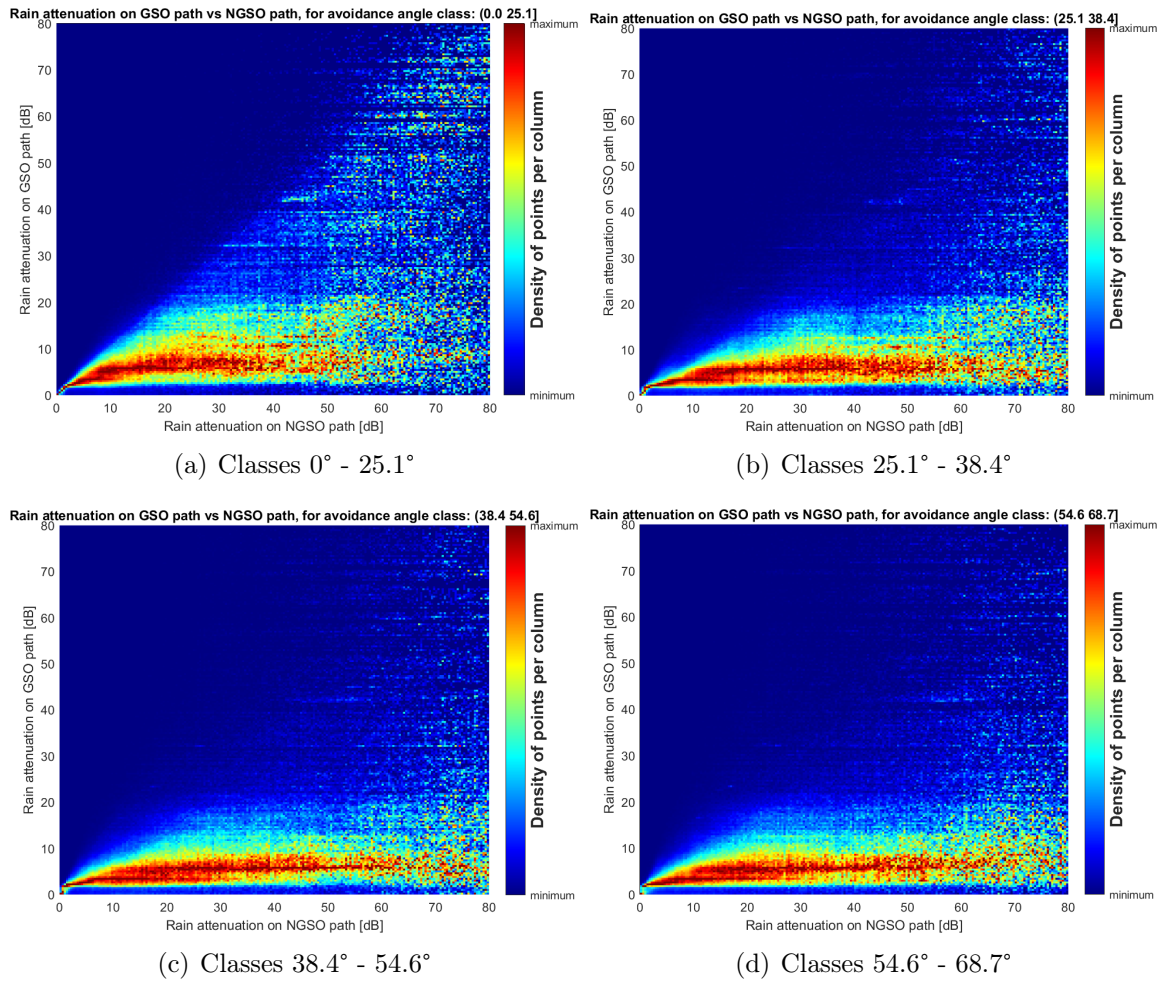
(d) Classes 54.6° - 68.7°

Figure 4.11: Intensity plots of rain attenuation on GSO path versus NGSO path for avoidance angle classes 0°-25.1°-38.4°-54.6°-68.7°.

(a) Classes 68.7° - 86.2°

(b) Classes 86.2° - 102.5°

(c) Classes 102.5° - 121.6°
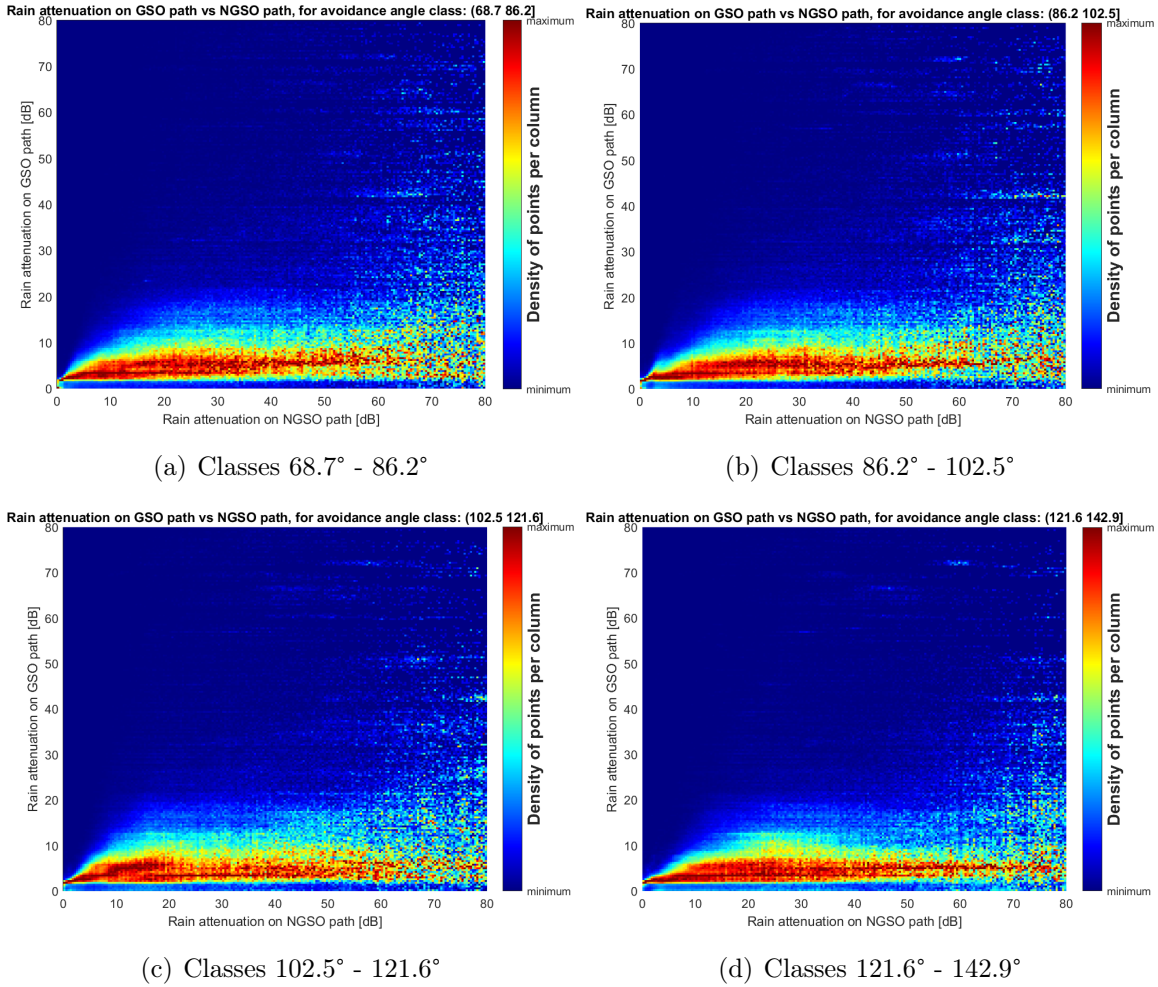
(d) Classes 121.6° - 142.9°

Figure 4.12: Intensity plots of rain attenuation on GSO path versus NGSO path for avoidance angle classes 86.2°-102.5°-121.6°-142.9°.

The next step aims to implement *Formula 4.4* in the practical case. Hereafter, to consider a more general scenario, instead of the single probabilities, e.g. $P(A_{NGSO})$, the model will account for Probability Density Functions, as $f(A_{NGSO})$. The PDF that need to be evaluated are $f(A_{NGSO}|A_{GSO})$, $f(A_{NGSO}|\phi)$ and $f(A_{NGSO})$.

The first conditional PDF $f(A_{NGSO}|A_{GSO})$ can be visualized through the intensity plot of *Figure 4.10*, in which each column represents the PDF of the A_{NGSO} conditioned on the particular value of A_{GSO}. To empirically evaluate the conditional probability $f(A_{NGSO}|A_{GSO})$, the simulated data is organized in tuples associating values of A_{GSO} to the corresponding A_{NGSO}. At this point, to reflect the conditioning of A_{GSO}, the tuples are once more divided into sub-groups for different classes of A_{GSO}. The intervals to define the classes of A_{GSO} are chosen with the aim of associating to each class a uniform number of tuples A_{GSO}, A_{NGSO}. The concept of *quantiles* [25], in particular, is implemented to

select the intervals. Quantiles are defined as cut off points for which the Cumulative Distribution Function experiences an increase of a fixed value of probability. *Figure 4.13* depicts the procedure to evaluate the quantiles for the data set of A_{GSO}. For this case, the data set is divided into 11 classes and therefore the vertical jump considered in probability is of $1/11$. As it can be observed, quantile intervals are shorter where the CDF grows steeper, since more points are distributed there, and viceversa. This property guarantees that the classes obtained using quantiles for delimiting the intervals will contain an almost uniform number of values.
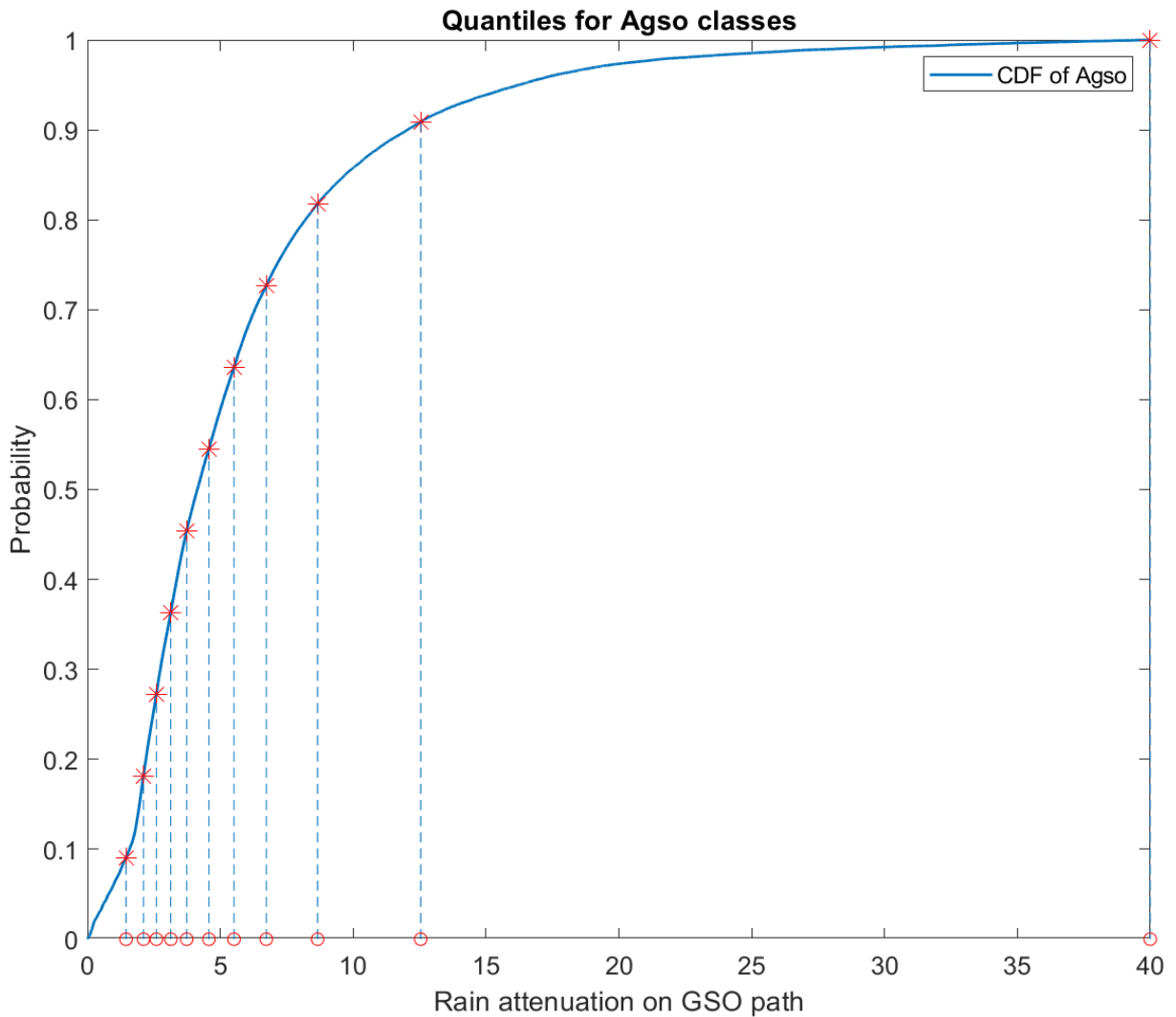
Figure 4.13: Tuples of A_{GSO} and A_{NGSO} for each class of A_{GSO} .

As already stated when describing *Figure 4.10*, the dependence of A_{NGSO} from A_{GSO} is well defined until A_{GSO} remains below about 40 dB, for this reason the data set divided in classes takes into account only the tuples for which A_{GSO} is lower than 40 dB, for finer granularity of the most meaningful data. One final class is evaluated separately to

consider also the values above this threshold, to achieve a complete model. The division in classes is depicted in *Figure 4.14*, where it is important to note that to each A_{GSO} class is associated a mostly uniform number of tuples, with the exception of the last class which, as already explained, was added to complete the model.

{} 12x2 cell	
1	2
1 [0,1.4550]	1104044x2 double
2 [1.4550,2.1121]	1090880x2 double
3 [2.1121,2.5964]	1109605x2 double
4 [2.5964,3.1400]	1093007x2 double
5 [3.1400,3.7376]	1102039x2 double
6 [3.7376,4.5735]	1092633x2 double
7 [4.5735,5.5179]	1105411x2 double
8 [5.5179,6.7318]	1096270x2 double
9 [6.7318,8.6638]	1098369x2 double
10 [8.6638,12.5428]	1100769x2 double
11 [12.5428,39.9952]	1100091x2 double
12 [39.9952,222.7274]	133627x2 double

tuple_gso_ngso{5, 2}		
	1	2
1	3.3734	4.4126
2	3.3734	5.7692
3	3.3734	5.8615
4	3.3734	6.2756
5	3.3734	18.9350
6	3.3734	42.5870
7	3.3734	380.2190
8	3.3734	2.4502
9	3.3734	2.6175
10	3.3734	2.5951
11	3.3734	1.7744
12	3.3734	6.5270
13	3.3734	15.3345
14	3.3734	117.2194
15	3.3734	1.9028
16	3.3734	1.7156
17	3.3734	2.4193
18	3.3734	3.4950
19	3.3734	8.8905
20	3.3734	25.3199
21	3.3734	1.9398

Figure 4.14: Tuples of A_{GSO} and A_{NGSO} for each class of A_{GSO} .

Once the sub-sets of tuples for every class is obtained, it is possible to finally model the conditional Proability Density Function $f(A_{NGSO}/A_{GSO})$, by fitting the statistical distribution for the values of A_{NGSO} contained in each class. To model this PDF, it is necessary to make some assumptions on the possible family distributions that most closely fit the data. Since as demonstrated in *Figure 4.6*, the long-term distribution of A_{NGSO} is very well approximated by a *Burr* distribution, it is reasonable to assume this distribution is a promising starting point to model the data. The *Burr* distribution is defined by three parameters α, c and k. To find the values that these parameters have to assume to best fit the data, it is necessary to operate a maximum likelihood estimation. *Figures 4.15* and *4.16* show how well the Burr distribution fits the Empirical PDF of A_{NGSO} for every class of A_{GSO}.

(a) Classes 0-1.46 dB

(b) Classes 1.462.11 dB

(c) Classes 2.11-2.60 dB

(d) Classes 2.60-3.14 dB

(e) Classes 3.14-3.74 dB

(f) Classes 3.74-4.57 dB
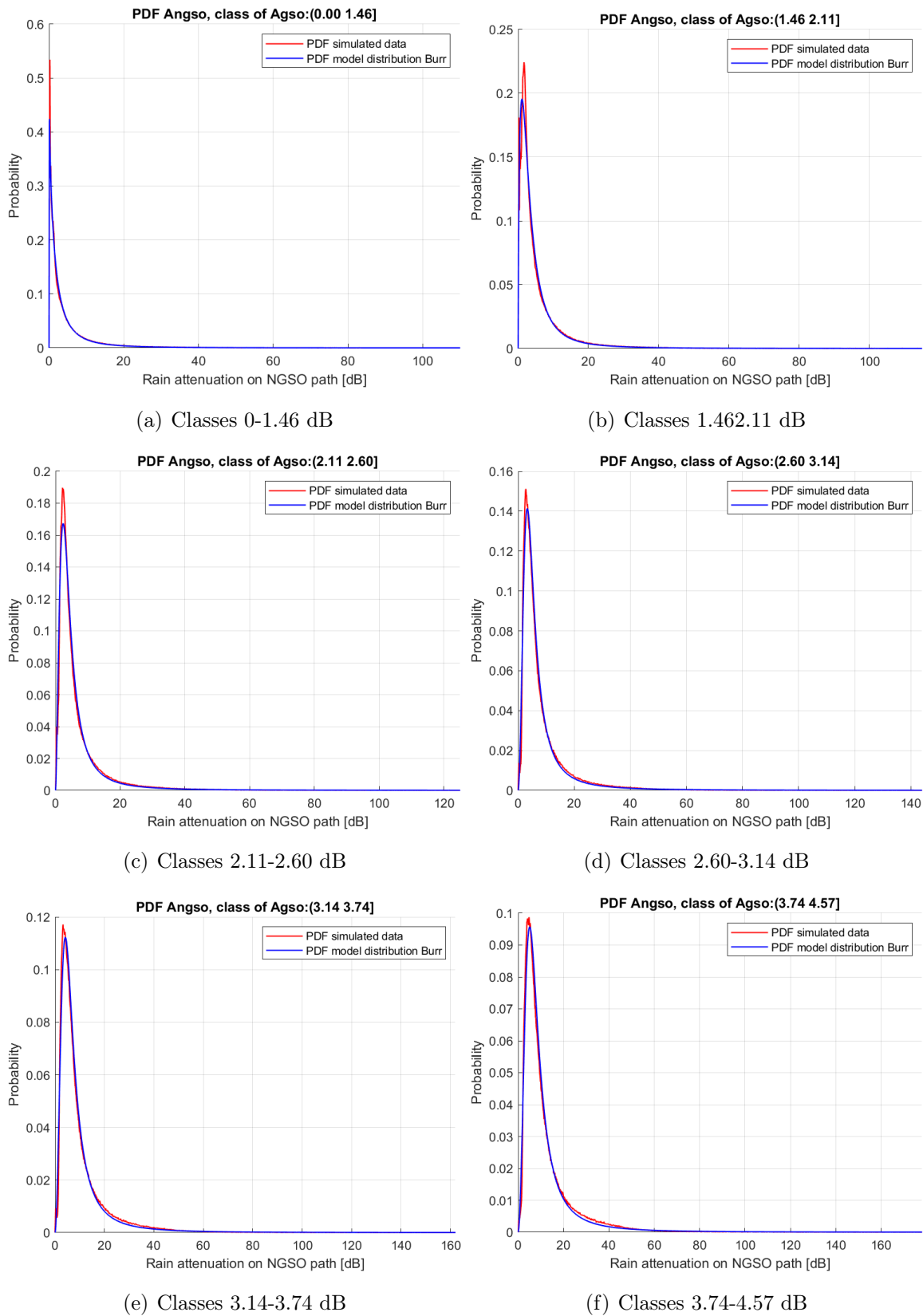
Figure 4.15: PDF fitting of A_{NGSO} for classes of A_{NGSO}: 0 [dB] - 4.57 [dB]
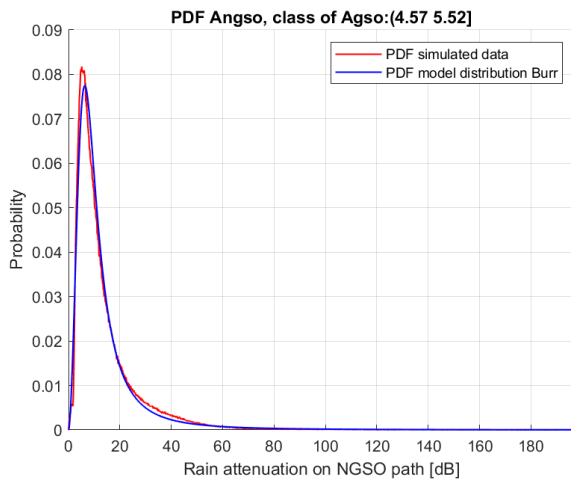
(a) Classes 4.57-5.52 dB
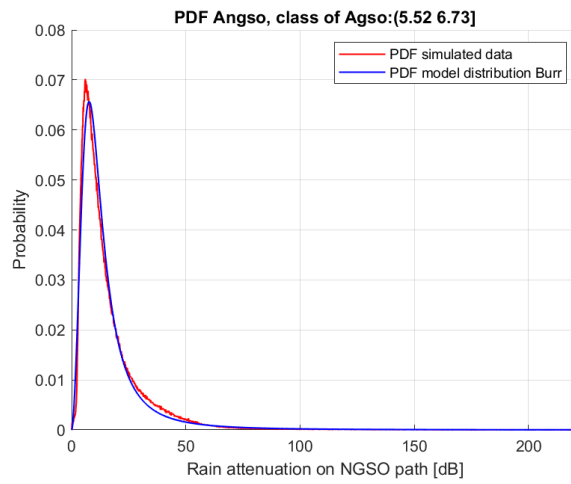
(b) Classes 5.52-6.73 dB
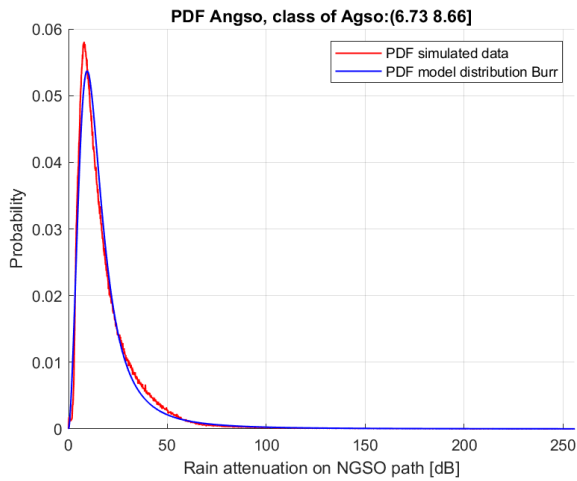
(c) Classes 6.73-8.66 dB
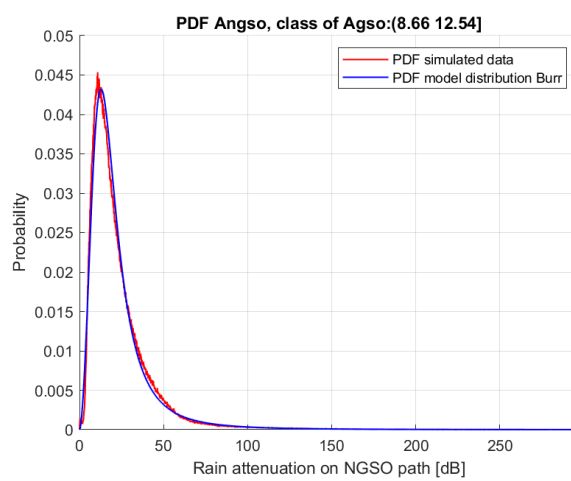
(d) Classes 8.66-12.54 dB
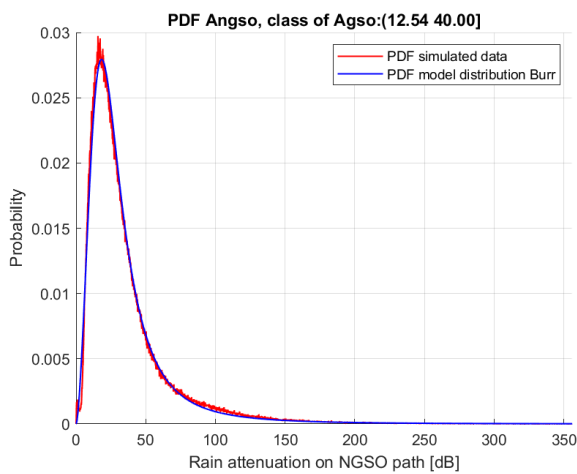
(e) Classes 12.54-40 dB
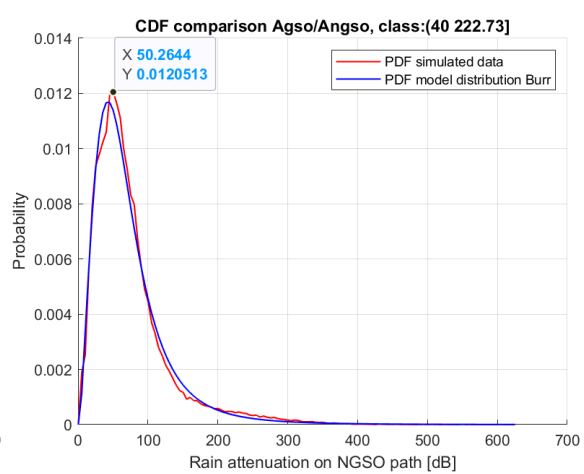
(f) Classes 40- 222.73 dB

Figure 4.16: PDF fitting of A_{NGSO} for classes of A_{NGSO}: 4.57 [dB] - 222.73 [dB]

From the above figures, it it is possible to observe how, for different classes of A_{GSO}, the shape of the PDF of A_{NGSO} changes. In particular, the PDF not only gets wider when A_{GSO} increases, but it also moves to the right, leading to higher values of A_{NGSO}. The last class, corresponding to values of A_{GSO} greater than 40 dB, experiences a peak in probability for rain attenuation on NGSO paths of around 50 dB.

The parameters associated to each class can be visualized in a graph, as illustrated in *Figure 4.17*, in which each parameter is plotted at the middle of the corresponding A_{GSO} class.
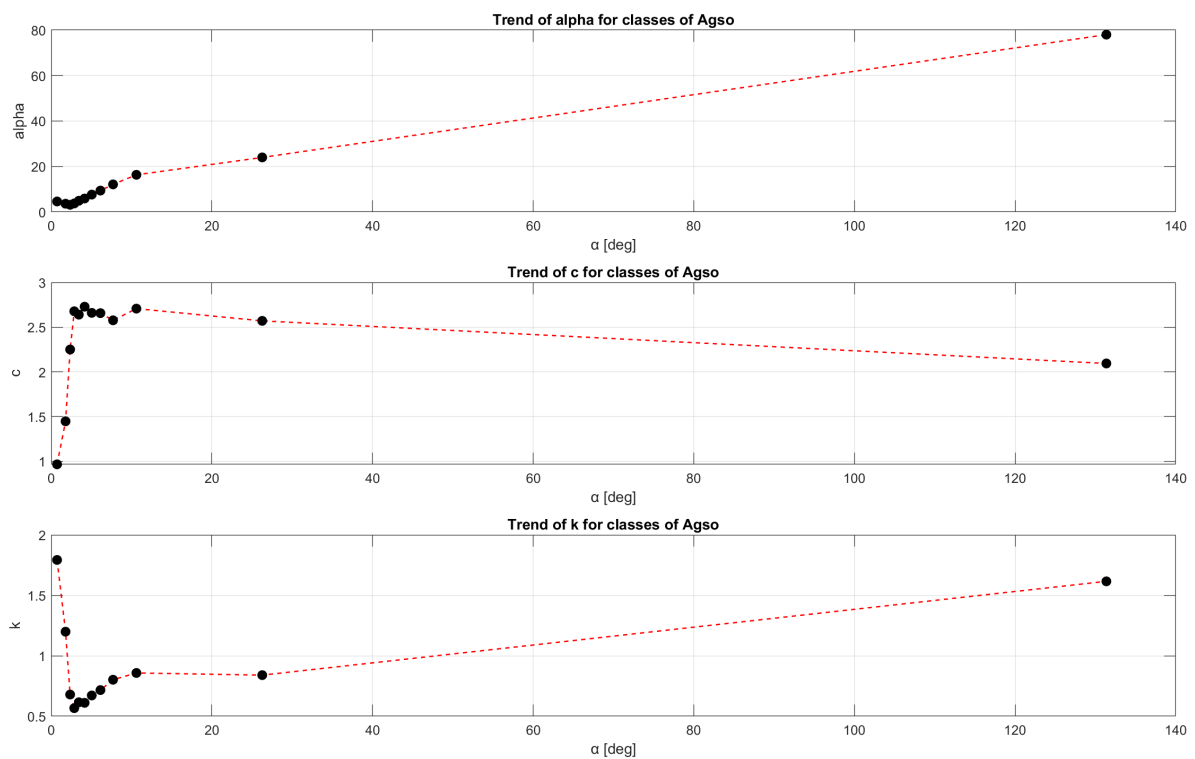
Figure 4.17: Parameters α, c and k of Burr distribution for each A_{GSO} class.

Once the parameters are obtained, the fitting of the distribution is completed and the obtained results can be stored. As can been in *Figure 4.18*, to each of the A_{GSO} classes is associated the specific distribution of the A_{NGSO} conditioned to the value of A_{GSO} of that class. The distribution is stored in a cell containing information on the distribution name and the values of the parameters. Each one of these stored distributions represents the conditional PDF $f(A_{NGSO}|A_{GSO})$ relative to the values of the A_{GSO} class.

Figure 4.18: Tuples of A_{GSO} and A_{NGSO} with associated distribution.

The same procedure is repeated for the set of tuples associating the avoidance angles and the corresponding A_{NGSO}, in order to evaluate the conditional PDF $f(A_{NGSO}|\phi)$. The data are again divided in uniform classes, this time depending on the values of ϕ, as shown in *Figure 4.19*. The best fitting distribution for the PDF of A_{NGSO} is then evaluated for each class of ϕ and the parameters are stored, *Figure 4.20*. Even for this case, the *Burr* distribution proved to be the most fitting for the data.
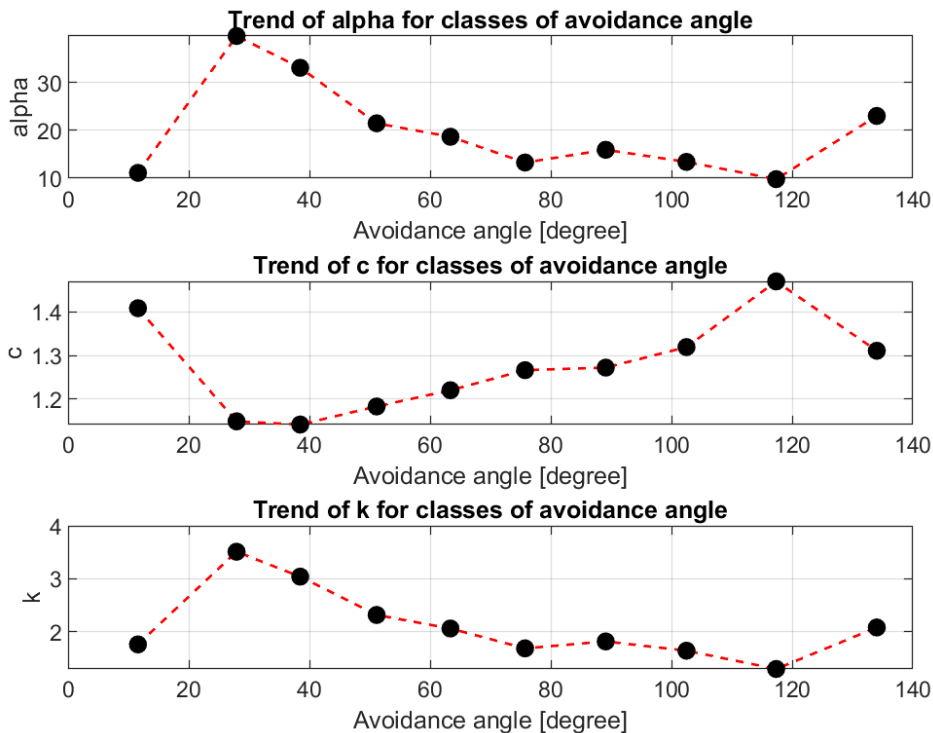
Figure 4.19: Parameters of the PDF relative to each class of avoidance angle.

Figure 4.20: Tuples of avoidance angle ϕ and A_{NGSO} with associated distribution.

Finally, the PDF for the long-term rain attenuation on the NGSO path $f(A_{NGSO})$ is obtained from the *Burr* Probability Distribution Function already described in *Section 4.3*.

Once the model has stored all the Probability Distribution Functions corresponding to each class, the preparation phase is finished and the statistical generation of A_{NGSO} can be carried out. By knowing the considered values for A_{GSO} and ϕ, it is possible to identify the right classes of both conditioning parameters. Once the classes are selected, the right conditional PDF are loaded and it is possible to calculate $\frac{f(A_{NGSO}|A_{GSO})f(A_{NGSO}|\phi)}{f(A_{NGSO})}$ by operating element by element for the same value of A_{NGSO} between the Probability Distribution Functions. The obtained result finally represents the custom PDF $f(A_{NGSO}|A_{GSO},\phi)$, which can be used to generate a random sample distributed according to this PDF by use of the Inverse Transform Sampling method.

4.5.2. Results

Figure 4.21 compares the long-term ECCDF of the rain attenuation affecting the NGSO path with the CCDF of the randomly generated samples through the use of the analytical model 4.4. The model proves to successfully reflect the long-term distribution until the exceedance probability is below to 10^{-3}, which is a particularly appreciable result. Moreover, the modelling of this parameter is also coherent with the information on the rain affecting the GSO path and the avoidance angle associated to the NGSO satellite.
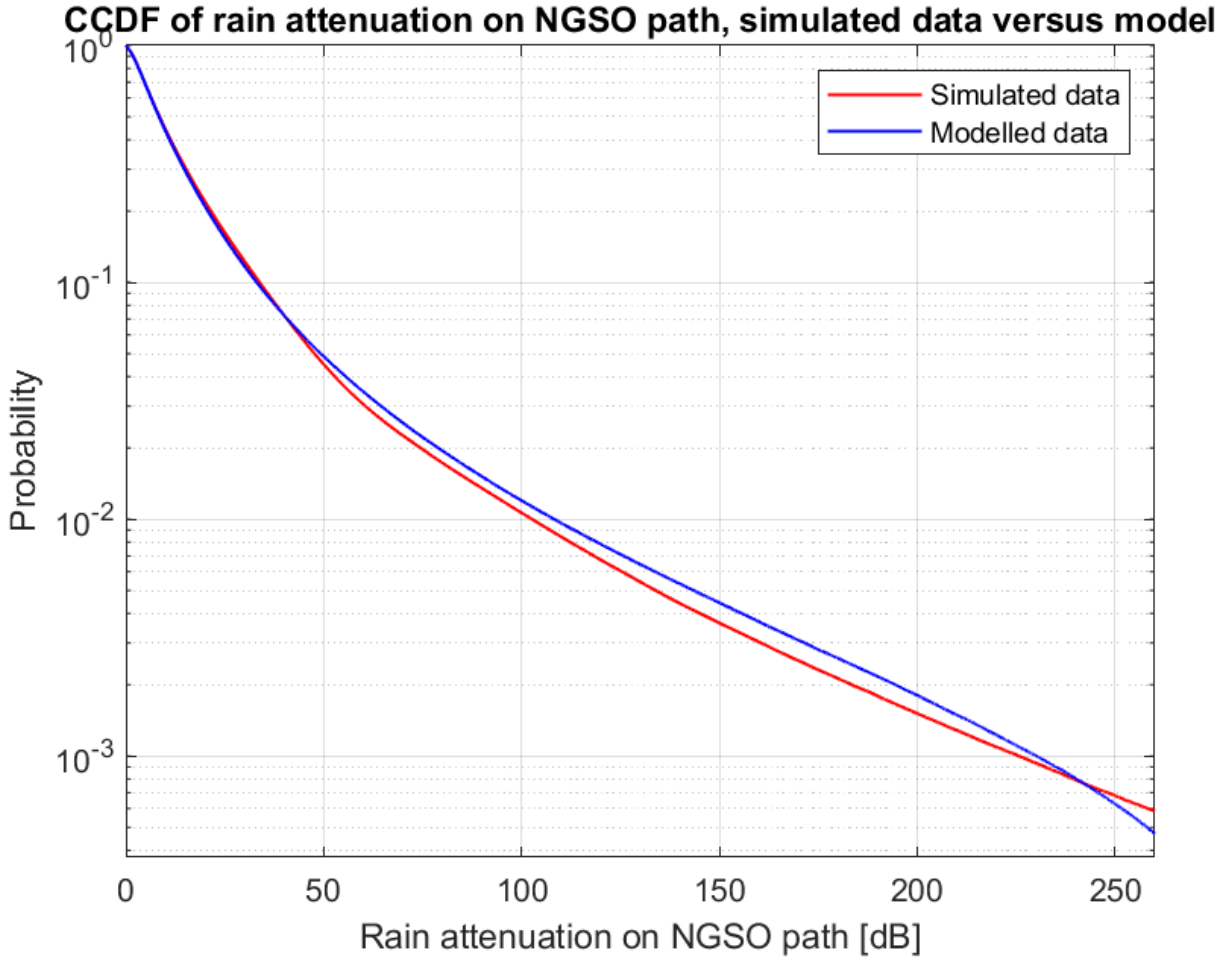
Figure 4.21: CCDF of rain attenuation affecting the NGSO path, empirical versus model.

The latter result can be further compared to a model in which only the information on A_{GSO} is exploited, therefore not resorting to the model (4.4), but simply to the conditional PDF $f(A_{NGSO}|A_{GSO})$: as matter of fact, this is the case obtained if the independence between ANGSO and the avoidance angle is assumed (see equation (4.4)). This comparison is shown in *Figure 4.22*, in which the CCDF relative to A_{NGSO} is compared for the three cases: the parameter is simulated, red line; the parameter is modelled through the conditional PDF $f(A_{NGSO}|A_{GSO})$, green line; the parameter is modelled using *Equation (4.4)*, blue line. It is possible to observe how well the CCDF of the statistical model approximate the original data with respect to a model considering only the dependence on A_{GSO}. This confirms the statistical dependence between the rain attenuation affecting the NGSO path and the avoidance angle. If this was not the case, in fact, the expression (4.4) would simply reduce to $f(A_{NGSO}|A_{GSO})$, since $f(A_{NGSO}|\phi)$ would be equal to $f(A_{NGSO})$ because of the independence and thus it would simplify with the denominator, in (4.4). However, since it was empirically proven that $f(A_{NGSO}|A_{GSO}, \phi)$ and $f(A_{NGSO}|A_{GSO})$ are

characterized by different trends, A_{NGSO} and the avoidance angle ϕ must be correlated to some extent. On the other hand, a much simpler statistical model might be acceptable at the expenses of a slight reduction in the modelling accuracy.
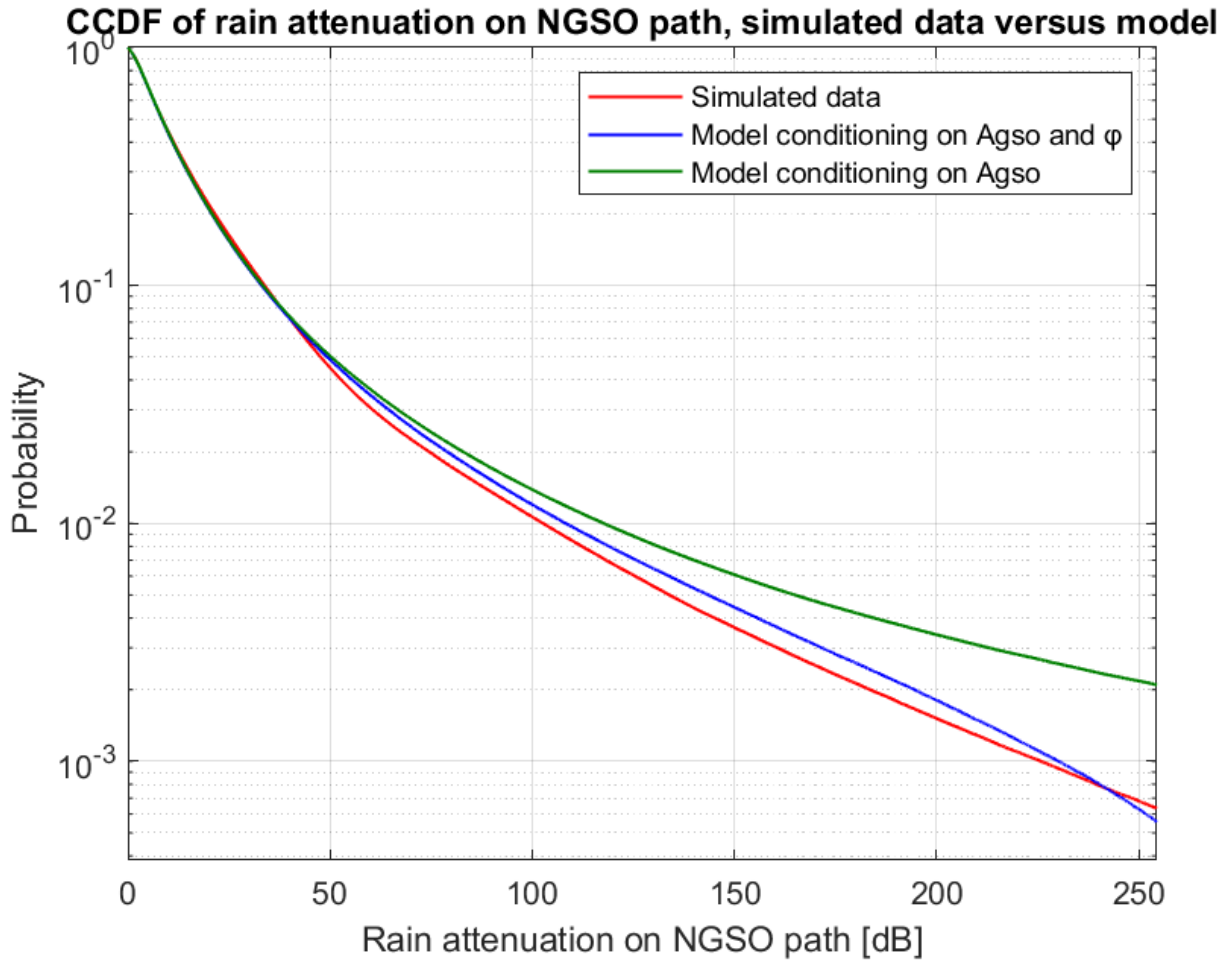
Figure 4.22: CCDF of rain attenuation affecting the NGSO path, empirical versus model.

4.6. Power Budget

This subsection finally presents the power budget obtained through simulations, both for the GSO as well as the NGSO systems, confronting the simulated data with the model. At the end of the chapter, further investigation of the interference caused by the NGSO satellites in the system is also presented, discussing how this analysis greatly supports the system design. It is important to remark, once again, that the presented results are obtained for the case conditioned to non-zero rain attenuation on the links, in order to mainly analyse the performances considering the atmospheric impairment.

4.6.1. Power received from GSO path

Figure 4.23 shows the power received from a GSO satellite, comparing the CCDF for both the simulated data and the modelled case in which the attenuation is randomly generated exploiting the most suitable distribution. In this case, the rain attenuation is generated according to the log-normal distribution already described above. The results are particularly satisfying, the blue line representing the model almost coincide with the red line, which indicates the simulated data. This is an additional proof that the model is correctly functioning, successfully reproducing the properties of the system.
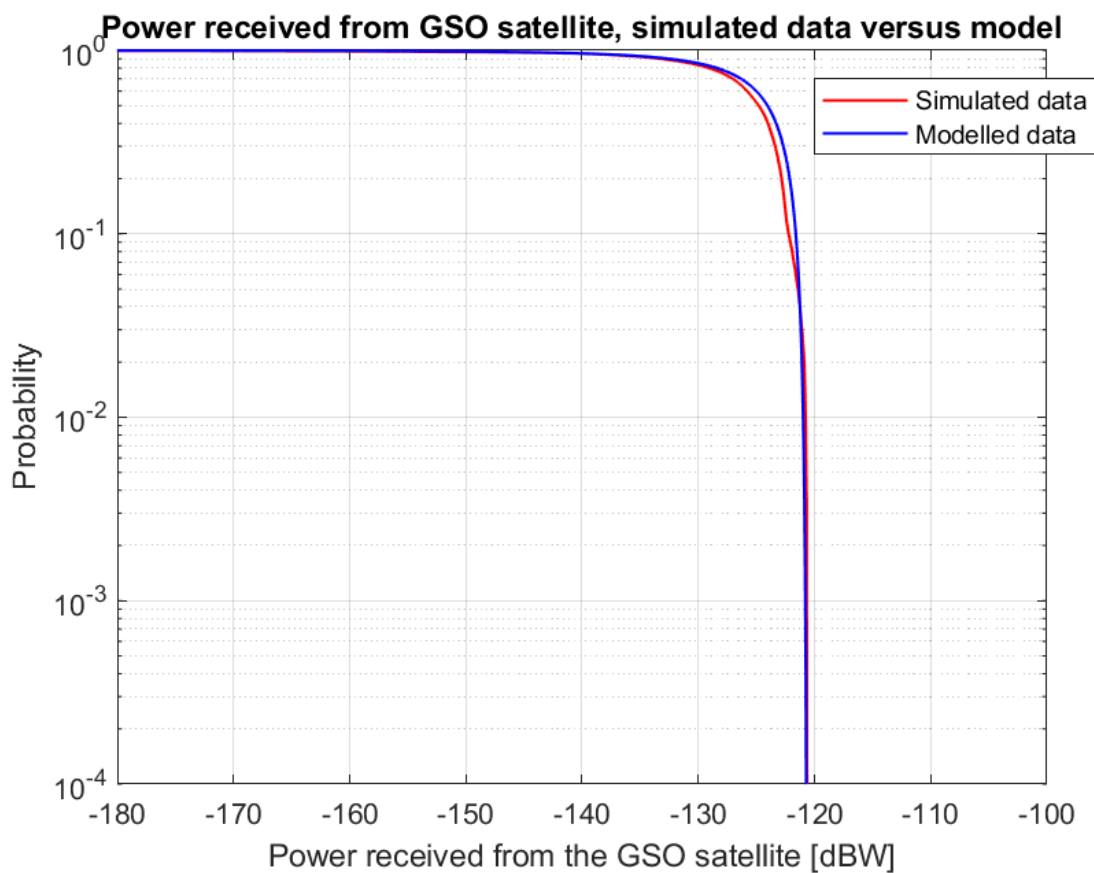
Figure 4.23: Power received from GSO satellite.

4.6.2. Power received from NGSO path

Figure 4.24 compares the Empirical CCDF of the simulated receive power from all NGSO satellites and the CCDF obtained through the model, in which the attenuation due to rain affecting the link is calculated according to the analytical model (4.4). This plot demonstrates that the analytical model is correct as it manages to obtain statistics for the received power very close to the true ones. In fact, the blue line representing the

model practically coincides with the red line indicating the simulated data.

The fact that it is possible to almost perfectly replicate the power received from a NGSO satellite is very important for design purposes, the analytical model can in fact be implemented to effectively analyse the interfering power coming from the aggregation of NGSO space stations.
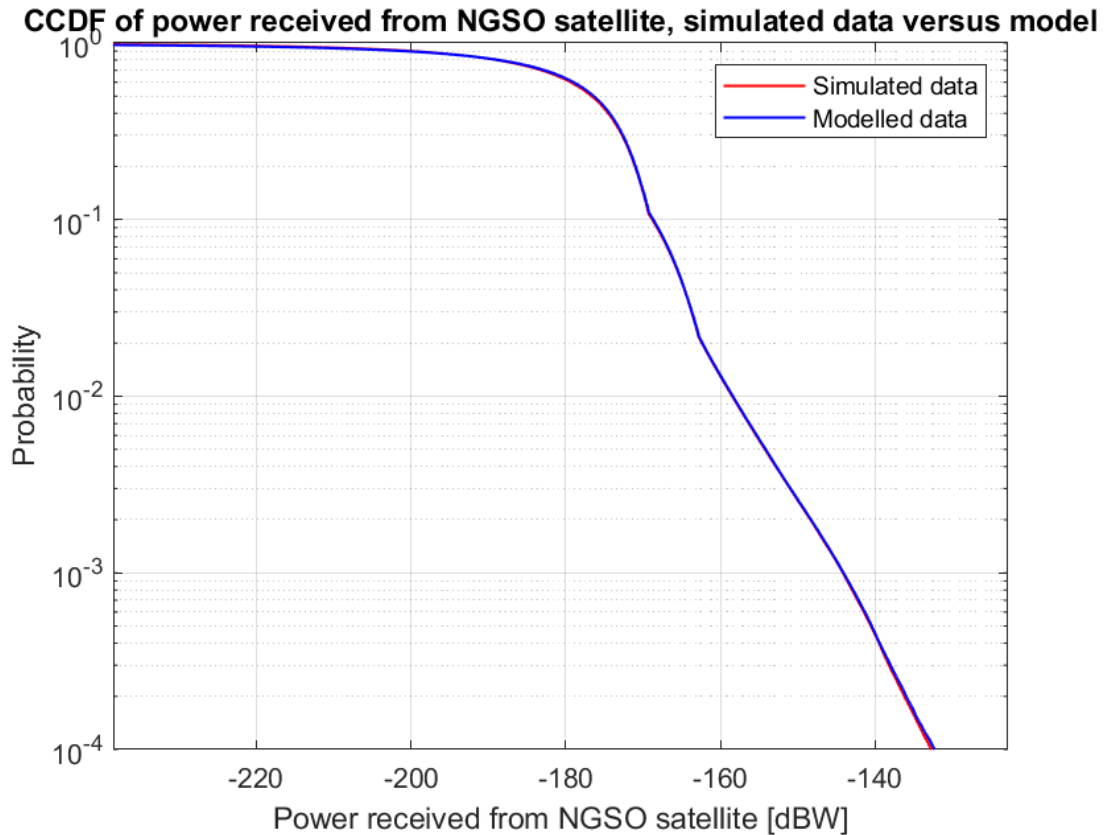
Figure 4.24: Power received from NGSO satellite.

4.6.3. C/I

For the purpose of further analysing the impact of the emissions produced by the aggregation of the NGSO space stations on the GSO fixed-satellite service, another key parameter can be evaluated: the C/I ratio. This parameter is defined as the ratio of the wanted received power, in this case the GSO satellite's, over the interfering one, i.e. the emissions coming from the NGSO spacecrafts. The NGSO satellites contribute singularly in generating interference, depending on how strong their signal is, how many satellites are transmitting and how close to the line of sight they are. Since they are independent signals, their total interfering power can be calculated as the sum in Watt of every single interfering received power. Once this value is obtained, C/I can be calculated as the ratio

between the received power from the GSO satellite and the total interfering power coming from the NGSO satellites. Subsequently, it is reconverted back to dB:

$$C/I = 10\,log_{10}\left(\frac{P_{rx,GSO}[W]}{\sum_{i=1}^{Nco} P_{rx,NGSO,i}[W]}\right) \tag{4.5}$$

where *Nco* indicates the number of transmitting NGSO satellites of the interfering set.

Figure 4.25 and *Figure 4.26* both show the trend of the CCDF of the C/I ratio calculated for the simulated data of the considered scenario. Both the figures evaluate the C/I ratio for different values of *Nco*, for a range from 2^0 to 2^6. Indeed, the *Nco* satellites selected from the interfering set are chosen as the ones characterized by minimum avoidance angles above the threshold α. As expected, the more NGSO satellites are interfering, the more significant will be the total interference power and thus the *C/I* ratio will decrease. The difference between the two plots is the considered value of α, which once again is defined as the threshold for the avoidance angle below which a NGSO satellite should refrain from transmitting. In the first plot α is set to 20°, while in the second it is equal to 2°. The latter in particular is a very extreme case since it considers interfering satellites very close to the line of sight between ground station and GSO satellite. It is noteworthy to observe that reducing the avoidance angle threshold, as expected, strongly affects the *C/I* ratio, in particular the lower α is, the greater will be the interference produced by the NGSO spacecrafts. It is important to remark that the presented results correspond to the scenario and parameters described in *Section 4.1*.
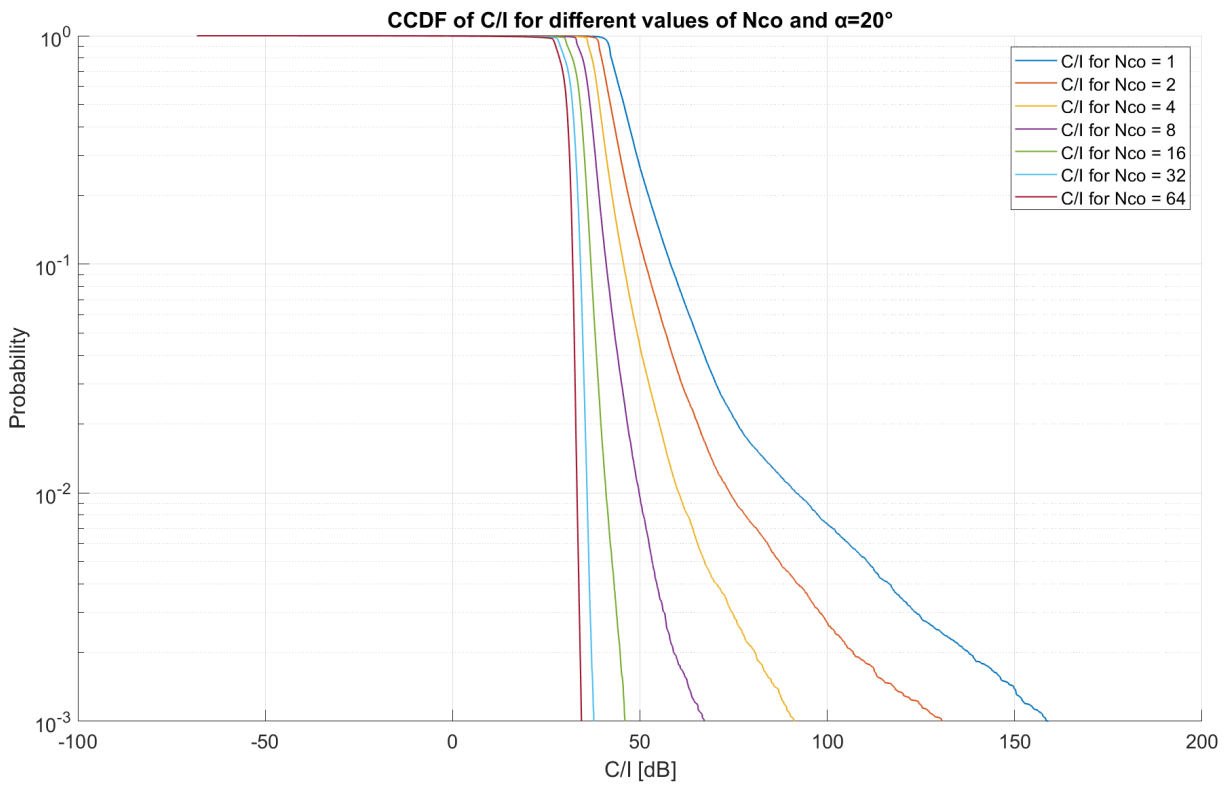
Figure 4.25: CCDF of C/I ratio for Nco ranging from 2^0 to 2^6 and $\alpha = 20°$.
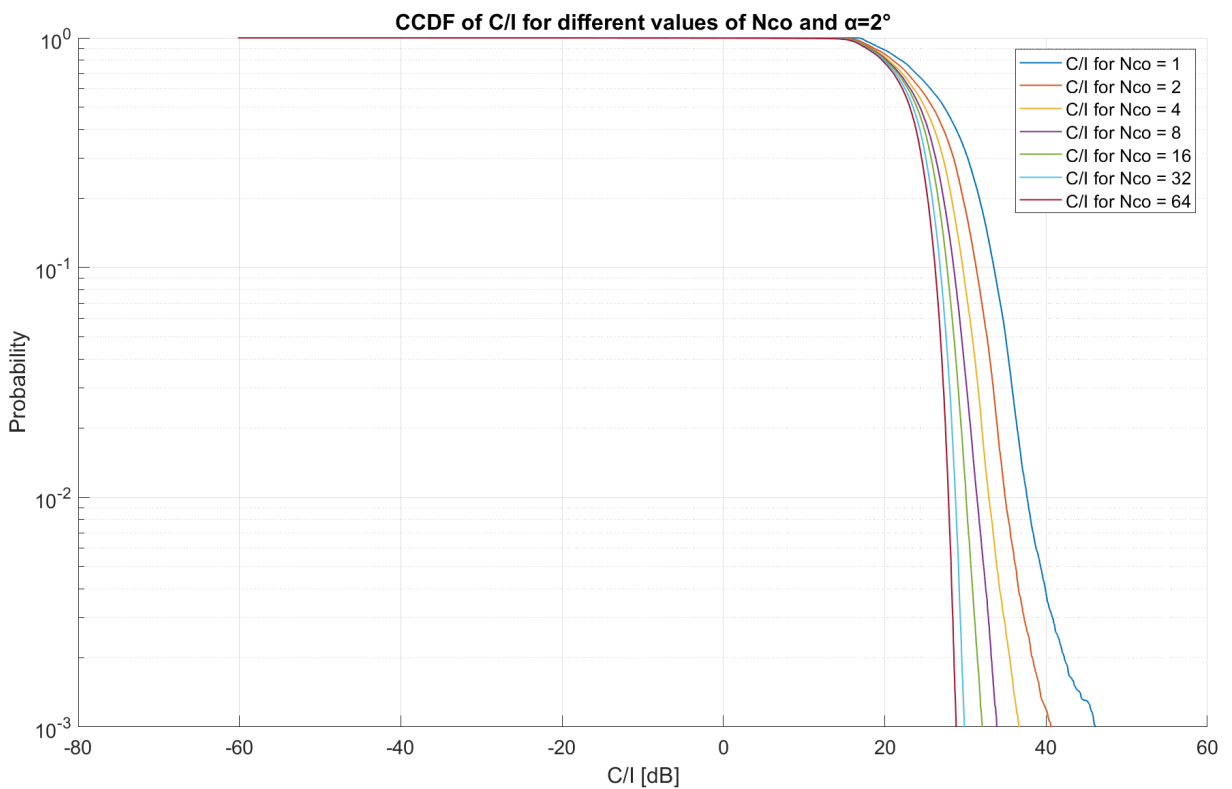
Figure 4.26: CCDF of C/I ratio for Nco ranging from 2^0 to 2^6 and $\alpha = 2°$.

The model presented, exploiting the simulated data, is capable of plotting the CCDF of the ratio C/I by simply tuning the parameters Nco and α. This feature greatly facilitates the design of the system, since it is possible to evaluate the performances and interference by exploiting the same data acquired during the simulation phase.

5 | Conclusions and future developments

The evermore increasing population of NGSO satellites at low orbital altitude is raising awareness over the interference these systems can cause on GSO fixed-satellite services whenever the two systems share, even partially, the same frequency band of operation. NGSO systems are nowadays embracing higher and higher frequencies in order to satisfy the increasing demand for bandwidth. For these frequency bands, however, the radio wave signal is strongly affected by atmospheric impairments, among which rain attenuation proves to be the most impactful. Even though interference mitigation techniques are already being deployed, it is necessary to properly evaluate how much emissions produced by NGSO space stations still persist. The model presented in this thesis allows to analyse a scenario in which a GSO satellite is communicating with a ground station while a constellation of NGSO satellites, operating at the same frequency band, is causing interference to the communication.

The model includes a simulation process which analyses the yearly evolution of the described fixed-satellite service, calculating the power budget of the links between the ground station and the satellites. In order to achieve this result, the simulation calculates the rain attenuation affecting each path by exploiting the 200 km × 200 km rain maps produced by the rain field generator *ST-MultiEXCELL*. Once the power budgets are evaluated, the simulated data collected is stored and organized in tuples associating rain attenuation affecting the path towards the GSO satellite, the rain attenuation on the link towards every NGSO satellites and the corresponding avoidance angles. It is possible to take advantage of these stored parameters for the design of the system by analysing the long term statistics of each one. Moreover, these parameters can be statistically modeled in order to generate new data according to their most fitting distribution as an alternative to additional simulations. The rain attenuation affecting the NGSO path in particular, proved to depend on other system parameters, such as the rain attenuation on the GSO link and the avoidance angle corresponding to the NGSO satellite. In order to coherently model this parameter, the conditional Probability Density Function, conditioned on the

rain attenuation affecting the GSO link and the avoidance angle, is evaluated. Finally, the analysis of the power received from both the GSO and NGSO paths is a powerful tool in order to evaluate the performance of the system, especially to understand how significant the interference caused by the NGSO system can be. Indeed, the model provides a practical method to exploit the simulated data in order to quickly visualize the CCDF of the C/I ratio to evaluate the interference on the GSO communications. The above mentioned plots can also be exploited to tune system parameters such as the number of interfering satellites allowed to transmit in the NGSO constellation *Nco*, as well as the avoidance angle threshold α below which a NGSO satellite must refrain from transmitting.

The presented model considers the rain as the only atmospheric impairment, since it is the most dominant one. Future developments could also include in the simulator phase the evaluation of attenuation due to clouds and gases, as well as the effect of depolarization caused by hydrometeors, in order to investigate a more complete scenario. Furthermore, it would be helpful for the community to study the impact of the emissions caused by NGSO constellations by considering different system parameters, mainly changing the frequency of the transmitted signal and the elevation angle of the ground station link towards the GSO satellite. The presented model can also be exploited to achieve another interesting result by changing the parameters associated to the satellites' transmissions. In this way, it would be possible to evaluate the power budget and the C/I ratio for different values of *EIRP* and gain, to fully understand when the interference coming from the NGSO system becomes critical. This would prove to be vital for the design of the fixed-satellite service. Finally, this work presented only the first order statistics of the obtained parameters, however with further analysis it would be possible to exploit the model also to describe more complex statistics, such as the total time the ground station link is subjected to rain.

Bibliography

[1] Elon Musk. 16th January 2015. *Presentation during SpaceX event*, Fisher Pavillon of Seattle Center, Seattle, WA.

[2] Aldo Paraboni and Michele d'Amico. *Radiopropagazione*. McGraw-Hill, 2009.

[3] Louis J. Ippolito Jr. *Satellite Communications Systems Engineering: Atmospheric Effects, Satellite Link Design and System Performance*. Wiley, 2008.

[4] Roderic L. Olsen, David V. Rogers, and Daniel B. Hodge. *The aR^b Relation in the Calculation of Rain Attenuation. IEEE Transactions on Antennas and Propagation, Vol. AP-26, No. 2*, pages 318–329, March 1978.

[5] ITU-R. *Propagation data and prediction methods required for the design of Earth-space telecommunication systems*. Recommendation P.618-8, 2003.

[6] ITU-R. *Specific attenuation model for rain for use in prediction methods*. Recommendation P.838-38, 2005.

[7] ITU-R. *Rain height model for prediction methods*. Recommendation P.839-4, 2013.

[8] Lorenzo Luini. *Modeling the Space-Time Evolution of Rain Fields. IEEE Antennas Propagation Magazine*, August 2021.

[9] C. Capsoni, F. Fedi, C. Magistroni, A. Paraboni, and A. Pawlina. *Data and theory for a new model of the horizontal structure of rain cells for propagation applications. Radio Science*, 22, No. 3:395–404, May-June 1987.

[10] Lorenzo Luini and Carlo Capsoni. *MultiEXCELL: A New Rain Field Model for Propagation Applications. IEEE Transactions on Antennas and Propagation*, Vol. 22, No. 3, November 2011.

[11] Axel Küpper. *Location Based Services: Fundamentals and Operation*. Wiley, 2005.

[12] Iridium. *Satellites 101: LEO vs. GEO*. `https://www.iridium.com/blog/2018/09/11/satellites-101-leo-vs-geo`, 2018. [Online, accessed 23-June-2022].

[13] Ruoqi Deng, Boya Di, Hongliang Zhang, Linling Kuang, and Lingyang Song. *Ultra-Dense LEO Satellite Constellations: How Many LEO Satellites Do We Need? IEEE Transactions on Wireless Communications*, Vol. 20, No. 3, August 2021.

[14] Encyclopedia Britannica. *SpaceX*. `https://www.britannica.com/topic/SpaceX`, 2022. [Online, accessed 23-June-2022].

[15] FCC. *SpaceX V-Band Non-Geostationary Satellite System: Attachment A, Technical Information to Supplement Schedule S*. Report SAT-LOA-20170301-00027, 2016.

[16] ITU-R. *Final acts WRC-2019*. Article 22, Sharm el-Sheikh, 2019.

[17] ITU-R. *Protection of geostationary fixed-satellite service, broadcasting-satellite service and mobile-satellite service networks from the aggregate interference produced by multiple non-geostationary fixed-satellite service systems in the frequency bands 37.5-39.5 GHz, 39.5-42.5 GHz, 47.2-50.2 GHz and 50.4-51.4 GHz*. Resolution 769 (WRC-19), 2019.

[18] Timur Kadyrov. *Non-geostationary satellite systems and networks*. ITU-R, December 2020. Presentation during 29th World Radiocommunication Seminar, Geneva, Switzerland.

[19] Zafar Fizza. *Analyzing the Impact of GEO Arc Avoidance on LEO Constellation Performance*. Master's thesis, Eidgenössische Technische Hochschule Zürich, 03.2021.

[20] ITU-R. *Application of Article 22 of the Radio Regulations to the protection of geostationary fixed-satellite service and broadcasting-satellite service networks from non-geostationary fixed-satellite service systems in the frequency bands 37.5-39.5 GHz, 39.5-42.5 GHz, 47.2-50.2 GHz and 50.4-51.4 GHz*. Resolution 770, 2019.

[21] ITU-R. *Radiation diagrams for use as design objectives for antennas of earth stations operating with geostationary satellites*. Recommendation P.580-6, 2004.

[22] ITU-R. *Time series synthesis of tropospheric impairments*. Recommendation P.1853-2, 2019.

[23] Matlab. *lognpdf - Lognormal probability density function*. `https://it.mathworks.com/help/stats/lognpdf.html`. [Online, accessed 01-July-2022].

[24] Matlab. *Burr Type XII Distribution*. `https://it.mathworks.com/help/stats/burr-type-xii-distribution.html`. [Online, accessed 01-July-2022].

[25] Matlab. *quantile - Quantiles of data set*. `https://it.mathworks.com/help/matlab/ref/quantile.html`. [Online, accessed 01-July-2022].

List of Figures

List of Tables

List of Symbols

Variable	Description	SI unit
$\boldsymbol{\theta}$	elevation angle	degree
$\boldsymbol{\psi}$	azimuth	degree
$\boldsymbol{\phi}$	avoidance angle	degree
$\boldsymbol{\alpha}$	avoidance angle threshold	degree
$\boldsymbol{A_{GSO}}$	rain attenuation on GSO path	dB
$\boldsymbol{A_{NGSO}}$	rain attenuation on NGSO path	dB
$\boldsymbol{R}$	rain rate	$\frac{mm}{h}$

Acknowledgements

Desidero ringraziare innanzitutto i miei genitori Giovanna e Marco, senza i quali questo fantastico cammino non sarebbe stato possibile, per aver sempre creduto in me, anche più di quanto io stesso abbia mai fatto, e per il supporto che mi ha permesso di superare ogni difficoltà. Un secondo doveroso ringraziamento a mia mamma, per gli ultimi due anni di università a distanza da casa, tra sessioni, progetti e relazioni, il cui sostegno mi ha consentito di tenere sempre la testa alta anche nei periodi più duri.

Un grazie ai miei primi compagni di viaggio, per un'amicizia vera che perdura dai primissimi giorni di università. Ad Agostino e Michael, per le battute, gli scherzi e le innumerevoli ore passate insieme tra lezioni e progetti, senza la loro compagnia affrontare la serietà dell'università non sarebbe stato lo stesso. Ad Emanuele e Alessandro per le svariate giornate e serate passate insieme tra svago e divertimento, ma anche per il supporto morale.

Grazie agli amici che sono arrivati col tempo, conosciuti e mai dimenticati. Ad Alessandro, il pescarese, per la celebre allegria e per essere garanzia di sonore risate. A Giovanni, amico e collega, la cui determinazione mi è stata d'ispirazione per dare sempre il massimo. A Benedetta, amica sincera, sempre disponibile per l'aperitivo di fine giornata per scaricare la tensione e realizzare insieme che effettivamente sì, una soluzione esiste per ogni problema.

Un grande grazie a chi c'è sempre stato, in modo particolare a Silvia, con cui ho condiviso tanti ricordi, sogni, ambizioni, ma soprattutto risate genuine. Grazie per non aver permesso che né il tempo né la distanza intaccassero la nostra amicizia, che rappresenta per me uno dei miei legami più forti e sinceri.

Ringrazio in modo speciale il mio relatore, il Professor Lorenzo Luini, e il mio correlatore, Luis Emiliani, per la disponibilità e la gentilezza che hanno dimostrato nei miei confronti durante il percorso di tesi e per i dati forniti per la realizzazione di questo lavoro. Grazie alle loro guide ed indicazioni sono riuscito a maturare non solo dal punto di vista di studente, ma anche di prossimo ingegnere. Farò tesoro di quest'esperienza e di tutte le competenze apprese.

Infine, tengo a ringraziare il Politecnico di Milano, per aver rappresentato per me un nuovo inizio e tutti i miei professori per le conoscenze che in questi anni mi hanno trasmesso.